Università degli Studi della Tuscia di Viterbo

DEPARTMENT FOR INNOVATION IN BIOLOGICAL, AGRO-FOOD AND FOREST SYSTEMS

PhD course in

SCIENCE, TECHNOLOGIES, AND BIOTECHNOLOGIES FOR SUSTAINABILITY

XXXVI CYCLE

s.s.d BIO/18

Functional Analysis of Genomic Variants Involved in Neurodevelopmental and Neurodegeneration Disorders in Zebrafish *in vivo* Models

PhD Student:

Dott. Graziamaria Paradisi

PhD Coordinator

Prof. Andrea Vannini

Thesis Supervisor

Prof. Giovanni Chillemi

Co-tutor

Dott. Marco Tartaglia

Co-tutor interno

Dott.ssa Antonella Lauri

A.Y. 2023/2024

INDEX

1. INTRODUCTION

1.1 The burden of rare disorders: pediatric encephalopathies affecting brain development and homeostasis

1.1.1 Rare diseases in EU and worldwide: undiagnosed/misdiagnosed patients and lack of therapy

Rare diseases encompass a broad spectrum of heterogeneous disorders affecting circa 1 person per 2.000 in Europe (Nguengang Wakap *et al*., 2020). Eighty percent of cases is linked to gene's functional impairment caused by chromosomic structural or number alterations and mutations in single or multiple genes (Theisen&Shaffer, 2010). In Italy, the prevalence of rare diseases is estimated to be between 2.1-3.5 million people with 1 out of 5 children affected (Federazione Italiana Malattie Rare[1], 2022). These diseases are often chronic, progressive, and degenerative and can cause early death. Currently, over 8.000 rare diseases have been identified, but many of these diseases remain challenging to diagnose accurately due to a lack of knowledge of the molecular pathogenetic mechanisms involved, fundamental to provide better outcomes for pediatric patients, optimize target medical therapies, and for our understanding of the natural history and clinical variability of the diseases (Schieppati *et al*., 2008).

To this general aim, the identification of new putative disease-causing genes and their pathogenetic mechanism can:

1. find out specific disease biomarkers to promote the development of new diagnostic and prenatal screening tests;
2. outline new genotype-phenotype correlations to address the clinical heterogeneity and differentiate these conditions from more common conditions;
3. offer targeted genetic counselling to the families;
4. establish regular prevention programs as well as monitor future-high risk pregnancies.

[1] Federazione Italiana Malattie Rare is part of the National Alliances of Eurordis - Rare Disease Europe, a European organization representing people with rare diseases. It collaborates to ensure the protection of the rights of individuals affected by rare disorders.

In this context, *Bambino Gesù Pediatric Hospital* (Ospedale Pediatrico Bambino Gesù, OPBG) has dedicated healthcare and research activities to rare patients, whose diseases are still orphan of diagnosis. Indeed, OPBG is the largest pediatric institution in Italy that welcomes ~25.000 patients affected by a chronic disorder, mostly of difficult to cure due to their high clinical complexity (OMAR, Osservatorio Malattie Rare[2]). Since 2015, the "*Molecular genetics and functional genomics*" Research Unit led by Dr. Marco Tartaglia, where I developed my PhD work, coordinates a specific research program dedicated to all patients still awaiting for a diagnosis. During these years, the program has led to the identification of several new disease-causing genes and characterization of different genetic disorders previously unknown also with the use of zebrafish model (to cite just few examples: Flex *et al*., 2023; Fasano, Muto, Radio *et al.*, 2022; Motta, Solman *et al*., 2022; Bobone *et al*., 2021; Motta *et al*., 2021; Yuh-Charn Lin, Niceta, Muto *et al.,* 2021; Bauer *et al.,* 2018; Martinelli *et al*., 2018; Flex *et al*., 2016, Sferra *et al*., 2016). Alongside the clinics and the genomic technology applied to diagnostic and research fields, the program encompasses multiple interdisciplinary experimental approaches (*in silico*, biochemical, *in vitro* and *in vivo* models) aimed at the functional and molecular validations of new disease-causing genes and gene variants identified with *high-throughput* genome sequence technology.

1.1.2 Encephalopathies with early onset neurodegeneration affecting motoneurons development and function

The term "*developmental and epileptic encephalopathies*" (DEE) describers a large group of rare and ultra-rare rapidly progressive neurodevelopment disorders, with a frequent onset in infancy or early childhood, characterized by brain development impairment and cerebral dysfunction leading to cognitive disabilities, severe seizure, behavioural disturbances often associated to a delay or a complete loss of motor skills (Nashabat *et al*., 2019). Unfortunately, the causes of DEEs remain unknown in most of the cases. Collectively, these disorders are best characterized by developmental delay, uncontrolled and infrequent seizures or an alteration of the synaptic plasticity or both, affecting adversely brain development (Spoto *et al*., 2022, Sheffer&Liao, 2020). Besides that, a broad emerging spectrum of encephalopathies with aberrant brain development exhibit

[2] https://www.osservatoriomalattierare.it/news/attualita/18336-giornata-mondiale-delle-malattie-rare-circa-25-000-pazienti-seguiti-al-bambino-gesu.

neurodegeneration traits affecting in particular axons and can be associated even to neurodegeneration of the spinal motor neurons (spMNs) already during childhood.

More generally, motor neuron diseases (MND) refer to a group of heterogeneous, chronic, and hereditary neurological disorders characterized by difficulties in walking, feeding and breathing, with early onset (from birth) or in adulthood, and deadly outcome (Teoh *et al*., 2017). These disorders can involve upper motor neurons (UMNs), with the soma localized in the higher regions of the brain imposing commands for movements, or lower motor neurons (LMNs) like brain stem cranial motor nuclei and spinal MNs, or both (Babin *et al*., 2014). All MNDs share common hallmarks: weakness, speech and limbs spasticity due to UMNs dysfunction in the precentral gyrus of the frontal lobe or weakness, attenuated reflexes, twitching and muscle wasting linked to LMNs degeneration in the ventral horn of the spinal cord (Foster&Salajegheh, 2019).

The occurrence of motor neurons (MNs) degeneration can involve two known mechanisms due to differences in somatotopic organization: LMNs degeneration would spread from one side of the spinal cord to the other side of the spinal segment instead for the UMNs the degeneration spreads from the motor cortex area to the neighbour ones (Walhout *et al*., 2018). Recent data suggest that the MNs insult is the result of a derangement of multiple interconnected intracellular processes that have been associated to hereditably genetic mutations in autosomal or X-linked genes impairing for istance:

1. Protein homeostasis (*C9orf72*; Butti *et al*., 2021; Pang&Hu, 2020),
2. RNA metabolism (*FUS*; Assoni *et at*., 2023; *EXOSC3*; Morton *et al*., 2020),
3. Mitochondrial dysfunction and oxidative stress (*SOD1*; Semmler *et al*., 2020),
4. Altered vesicle transport (*ALS2*; Miceli *et al*., 2022),
5. Neurons proliferation/migration (*VRK1*; Vinograd-Byk *et al*., 2015),
6. Cytoskeleton impairment (*TUBB2A*; Sferra *et al*., 2018; Smith *et al*., 2014)

Alterations in one of these events seem to lead to the failure of the motor neuron axon in maintaining its projections and undergo to retraction of the axon itself and in the end to denervation of the target. In combination with the loss of UMNs and supraspinal control, hypertonia and spastic weakness appear often (Arora&Khan, 2023). Most common diseases belonging to this category are the amyotrophic lateral sclerosis (ALS), the spinal muscular atrophy (SMA), the hereditary spastic paraplegia (HSP), the infantile neuroaxonal dystrophy (INAD) and the pontocerebellar hypoplasia (PCH), classified based on the brain's region involved (Mastrangelo, 2019). Considerable overlaps of

clinical and physiopathological characteristics may be observed between these entities, leading to persistent difficulty in establishing a precise diagnosis in some patients and raising controversies about the classification of these disorders. In conclusion, due to their large heterogeneity and the lack of specific disease biomarkers and screening tests, the specific pathophysiology of conditions entailing rare motor neurons degeneration especially in children is still largely unknown, and, besides recent ASO-based (AntiSense Oligonucleotide) approaches in SMA, little or none effective therapies are available (Sivanesan *et al*., 2013).

1.1.3 Next generation sequencing and functional validation *in vitro* and *in vivo*

Sequencing of the human genome in the early 2000s was a revolutionary event in rare disease field, and the establishment of functional genomics approaches that followed have represented a fundamental branch of genomics whose goal is to determine the function of identified candidate genes (and their respective protein products) and possibly pathogenic variants as well as to delineate how different gene functions, interacting each other, are able to regulate different cellular processes (Werner, 2010). Functional genomics studies employ various *in vitro* and *in vivo* approaches that induce or suppress gene expression to identify the molecular pathways in which the encoded protein product is involved and the mechanisms it regulates within the cell/tissue or organism. These approaches are widely used in studies of developmental and evolutionary processes (orthologous gene analysis) as well as during pathological processes (biomedical field) (Marwaha, Knowles, Ashley, 2022). The latter application is essential for understanding the molecular and mechanistic basis of diseases.

The rapid progress of sequencing techniques, now represented by Next Generation Sequencing (NGS) *high-throughput* technology, is effectively enabling the sequencing of genomes, exomes, and transcriptomes of various organisms and the identification of new disease genes and potentially pathogenic genetic variants in patients with genetic disorders in increasingly shorter times, together with a substantial reduction in costs (Buermans *et al*., 2014). In fact, the term NGS refers to a family of methodologies based on the rapid sequencing of clonally arranged clusters of genetic material performed simultaneously on the same sample and on multiple different DNA samples. Although there are several NGS systems, they all share a similar workflow (**Fig. 1**): genomic DNA

is randomly fragmented, ligated with adapters, and hybridized to a support containing DNA baits. Then, amplified by PCR and massively sequenced in parallel (Bamshad *et al*., 2011). The development of this cutting-edge method has allowed for superior diagnostic performance compared to Sanger sequencing, the method that marked the beginning of genomic research in the 1980s (Slatko *et al*., 2018; Bunnik&Le Roche, 2013). Even if the "NGS revolution" has drastically shortened waiting times for a diagnosis in many cases, it has also generated a huge amount of data on potential new disease genes and new potentially pathogenic variants in genes whose function is unknown in vertebrates and therefore requires functional validation.

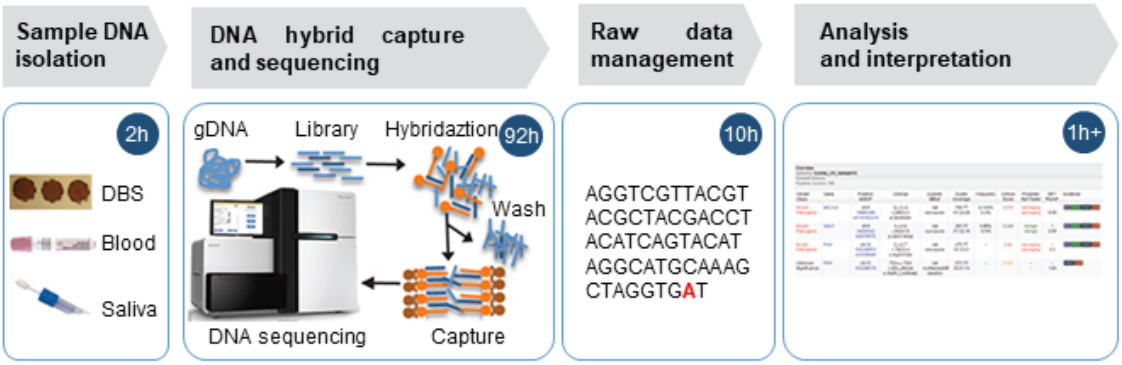

Fig. 1: *Next Generation Sequencing*-based genome sequencing workflow (steps 1-4). Modified from Bhattacharjee *et al*., 2014.

The use of *high-throughput* genome/exome sequencing technologies have significantly changed the way the genetic disorders are now studied, allowing the identification of new disease-causing genes/genetic variants and establishing new genotype-phenotype correlations. However, their pathogenicity must be confirmed with functional studies discussed in paragraph 4.1.3.

In general, understanding how a specific genotype could be translated in a precise phenotype clinically recognizable (genotype-phenotype correlation) requires a functional validation on *in vitro* and *in vivo* models. This is necessary to 1) define the intricate cellular network signalling coordinating the central nervous system developmental program, and 2) screen innovative pharmacological drugs that could be able to contrast or slow down the progression of the disease.

In vitro and in *vivo* approaches used in functional genomics are an integral and essential part of medical genetics studies aimed to characterize the impact on animal physiology (*e.g*., in terms of development, homeostasis, and tissue maintenance) due to mutations

found in patients affecting a wide range of genes. In the biomedical field, basic biological acquisitions derived from *in vitro* and even more so *in vivo* functional models that reproduce animal physiology are essential to allow stratification of patients with genetic diseases necessarily for a differential diagnosis and personalized cares.

One of the still widely used model systems in functional genomics is represented by cell cultures both primary (derived from patient's tissue) and immortalized (mainly commercially available). These are simple, cost-effective, and easily reproducible systems with extremely low costs, which allow for the easy study and isolation of biochemical processes and pathological mechanisms at the molecular level underlying cellular aberrations due to genetic mutations. However, such *in vitro* systems can be sometimes simple representations that cannot resemble complex animal physiology or even tissue or organ levels (Slanzi *et al*., 2020). Moreover, it is not always possible to establish primary cell cultures because of difficult access/sampling (*e.g.*, spinal motor neurons). The implementation of the recent technology for the production of differentiated cells and tissues through IPS (*induced pluripotent stem cells* artificially generated from a terminally differentiated cell) or patient-specific three-dimensional organoids is expanding the possible investigations on *in vitro* systems with relevance in terms of pathophysiology mechanisms (Perez-Lanzon, Kroemer, Maiuri, 2018). However, possible artifacts of these systems due, for example, to long culture and artificial differentiation times may occur.

Functional genomics studies, therefore, benefit from the use of complementary *in vivo* models, both invertebrates (*i.e*., the arthropod *Drosophila melanogaster*, the nematode *Caenorhabditis elegans* and vertebrates *i.e*., frogs of the genus *Xenopus*, teleost fish *Danio rerio*, or classic murine models). Having multiple comparative models and genome sequencing is crucial for understanding the biology of cellular processes involving sets of genes and determining protein factors that led, for example, to the generation of the sophistication of nervous tissue (Domínguez-Oliva *et al*., 2023; Lauri *et al*., 2021). (*Relative advantages, limitations, and amenability to different study approaches between the most used in vivo models for biomedical research will be discussed further in paragraph 1.3.1*).

Both *in vitro* and *in vivo* models are widely used in biomedical research for a wide range of studies aimed to 1) understand the molecular mechanisms regulating different cellular processes (*e.g.* intracellular trafficking, cellular division, cytoskeleton dynamics), 2)

toxicology and pharmacology studies, and 3) cancer research. Despite that, the models are not equivalent and offer a series of advantages/disadvantages schematized in **Table 1**:

***In vitro* model**		***In vivo* model**	
Advantages	**Disadvantages**	**Advantages**	**Disadvantages**
-Simple system from which is possible to isolate specific phenomena -Possibility to control experimental parameters (*e.g.* temperature, pH and CO_2 levels) -Relatively low cost -Not regulated from strict ethical regulations	-Extremely simplified and limited with respect to physiology questions -Difficulties in the reproduction of *in vivo* pathophysiological conditions -Procedural artifacts may occur (*i.e.* cells immortalization) -Human primary cell cultures required to be collected from patients	-Long term studies of biological complex processes -Evolutionary insights into biological processes -Often fast and short developmental program -*In vivo* Drugs/vaccine screening and testing	-Can be very expensive in costs; long and extensive for experimental time -Dedicated housing structures and high qualified personnel required -Ethical strict regulations and compliance standards required -Biological variability among different species

Table 1: List of the principal advantages and disadvantages between *in vitro* and *in vivo* models.

By establishing a working pipeline based on different and complementary multidisciplinary approaches (*in silico, in vitro* and *in vitro*), it is possible to analyse deeper the genetoype-phenotype correlation and the pathogenic mechanism of diseases at different level (*i.e.* whole organism, cellular and subcellular), such stratifying patient's clinics and developing targeted therapies.

At the "*Molecular Genetics and Functional Genomics*" Research Unit in OPBG led by Dr. M. Tartaglia, this strategy has led to the identification and functional validation of many disease genes and genotype-phenotype correlations underlying previously unknown diseases.

Among the studies linked to the work I performed during my PhD using zebrafish and under the supervision of Dr. A. Lauri is worth mentioning:

1. the functional validation of dominant mutants found as *de novo* in a new disease gene, *ARF3* (ADP-ribosylation factor 3; Fasano, Muto, Radio *et al*., 2022) responsible of an ultra-rare epileptic encephalopathy compromising the intracellular trafficking;
2. inherited *LoF* mutations in the tubulin chaperons *TBCD* (tubulin beta cofactor D; Flex *et al*., 2016) and *TBCE* (tubulin beta cofactor E; Sferra *et al*., 2016), for which the generation of *in vivo* zebrafish models was the focus of my PhD thesis (unpublished). My PhD work focused mostly on the second disease, a pediatric MND.

Generally, different mutations in these genes lead to the onset of clinically complex phenotypes altering not only the development and the functioning of the central nervous system but involving also other organs/tissues through pathogenetic mechanisms still not entirely understood.

1.2 Tubulinopathies with early on-set neurodegeneration traits

1.2.1 The function of microtubules (MTs) in neurons and motor system development in vertebrates

Microtubules (MTs), together with actin and intermediate filaments network, represent one of the cytoskeletal components present in all eukaryotic cell types. The development of the central (CNS) and peripheral (PNS) nervous systems rely heavily on cytoskeleton, and MTs as well, functions and alterations in MTs features and dynamicity led to detrimental effects on neural proliferation, migration and connectivity with other cells and with the environment (Sakakibara *et al*., 2013). MTs are linear, polymeric and highly dynamic structures, whose function is crucial for the correct function of many different biological and cellular processes during early embryonic development such as cell division and migration, intracellular trafficking, chromosomal segregation, signal transduction, including proper axon guidance and synapse formations (Gudimchuk&McIntosh, 2021). MTs have intrinsic polarity based on the asymmetry of the α- and β-tubulin heterodimers, the basic building blocks, aligned each other "head-to-tail" forming polymeric filaments called **protofilaments** (**Fig. 2 A and B**). Through lateral interaction, 13 protofilaments in turn are arranged in parallel and associate to form the hollow MT structure precisely (Ø 25 nm) (Kapitein&Hoogenraad, 2015, Nogales *et*

al., 1999). Since tubulin heterodimers are placed in the same orientation "head-to-tail/head-to-tail", the architecture of a microtubule gives its polarity: the *minus end* (the slow-growing end) and the *plus end* (fast-growing end) are capped by α-tubulin and β-tubulin monomers, respectively. MTs are extremely dynamic structures, either existing in a growing state (polymerization) or shrinking state (depolymerization). Within a population of MTs at any point in time, the *plus end* of MTs can rapidly undergo these phases, going from growth to shortening, called (catastrophe), or from shrinkage to growth (rescue). This unique biophysical property, known as "*dynamic instability*", allow MTs to perform essential functions in fundamental cellular processes like cell's division, differentiation, and motility, also to explore the environment and withdraw if it is not suitable and adopting new spatial conformations in response to cellular needs (Roll-Mecak, 2015).

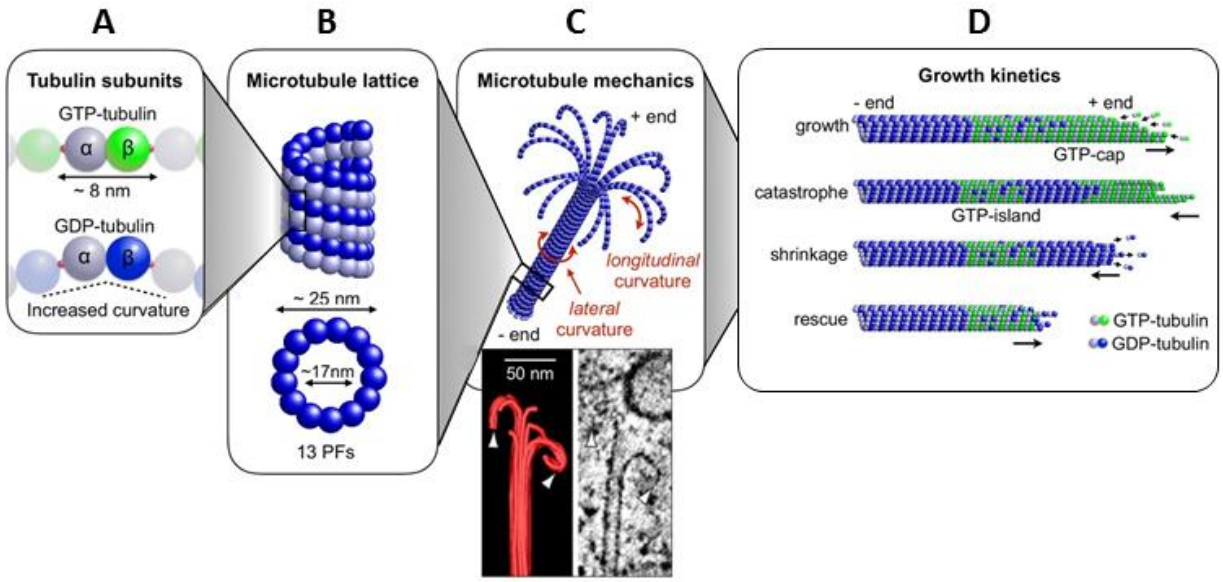

Fig. 2: Diagram connecting structural, biochemical and kinetic aspects of MTs *dynamic instability*. A) α- and β-tubulins heterodimers at different energetic states guanosine-dependent binding (GTP/GDP). **B**) Lateral and transversal arrangement of tubulin dimers composing microtubules. **C**) GTP hydrolysis causes a conformational change in the protofilaments which tend to curve outward from the MT lattice (catastrophe beginning, white arrowhead). **D**) The catastrophe and the shrinking phase could be stopped by remnant GTP-tubulins monomer and MAP proteins (not showed). Modified from Michaels *et al*., 2020.

This process is driven by the presence of two distinct states of MT subunits, GTP- and GDP-bound tubulin dimers that have different structural properties. Cells, and neurons,

which are sustain high metabolism, consume energy to keep the concentration of free tubulin protein bound to carrier guanosine triphosphate (GTP) high above the critical concentration for polymerization, so these subunits are quickly added to the growing *plus end* (growing phase) and form a "cap" which prevents MTs from shrinking. After subunits are incorporated into the MT, only the GTP bound to β-tubulin monomer is hydrolyzed into GDP (Nogales *et al*., 1998). GTP hydrolysis promotes the spontaneous longitudinal curvature along the dimer axis causing GDP-tubulin dimers to be less tightly bound in the MT lattice (**Fig. 2 C**). If this process occurred faster than the adding of new tubulin-GTP dimers, the cap is lost, and the energy stored in dimers released resulting in protofilaments detachment and MTs splaying (catastrophe). However, new tubulin-GTP dimers could be added to the shortening end by promoting the formation of a new cap and MTs re-growing (rescue). Usually, the rescue phase is enforced by the intervention of MAP proteins (*microtubule-associated proteins*) which, by attaching alongside each protofilaments, slow down and reverse MTs shrinkage (Michaels *et al*., 2020; Mitchison&Kirchner, 1984) **(Fig. 2 D**). Since their discovery in the nineties, the structure and the role of MTs have been at the center of biology research as they ensure and participate to the correct development, maintenance, migration, polarization and differentiation of nervous system cells of vertebrates and invertebrates (Prokop, 2020; Brinkley *et al*., 1997).

A typical vertebrate neuron consists of a small soma (situated in the brain, spinal cord, or peripheral ganglion), several dendrites, and a single elongated axon (**Fig. 3 A**). The axon is specialized to transmit information, while the dendrites generally receive the incoming ones: indeed, neurons are highly polarized cells specialized in receiving and interpreting sensory information from the environment and processing it into a sudden and fast response, as an electrochemical action potential, addressed to other neurons or organs (*e.g.* muscles) (Pannese, 2015). Their functional complexity reflects therefore such a structural complexity: neurons have developed an extended cytoplasm specialized to form the axon, which is frequently very long. The axon is unlimited in its growth potential and can traverse great distances within the body: the major expression of this potential is represented by the spinal motor neurons which axons are approximately 1 meter long and allow to reach organs and tissues targeted (*e.g.* skeletrical muscles) even extremely far from the exit point of the spinal cord horn. For these reasons, neurons and motor neurons in particular require a robust intracellular signaling network based on the active and anterograde transport of different molecules (*e.g.* neuropeptides, neurotransmitters) and organelles (*e.g.* mitochondria, *cargo* in general) from the synapse to the soma/dendrites,

and *vice versa*, depending on the dynamicity of microtubules and its associated-motor proteins (**Fig. 3 B**) (Hirokawa *et al*., 2010). In addition, in all neurons classes MTs network formed at the basis of the cellular soma somato-dendritic "filter", called axon initial segment (AIS), which avoids detrimental *cargos* to go back to the soma. Therefore, developing neurons depend on the stochastically dynamic nature of the MTs in order to remodel their shape, proliferate and migrate, as well as other pivotal processes during different phases of neural development as:

1. Neurites formation and axon specification (Kuijpers *et al*., 2011),
2. Axon elongation and branching (Dent *et al*., 2011; Yu *et al*., 2000),
3. Dendritogenesis and synaptogenesis (Rao *et al*., 2017; Jaworski *et al*, 2009).

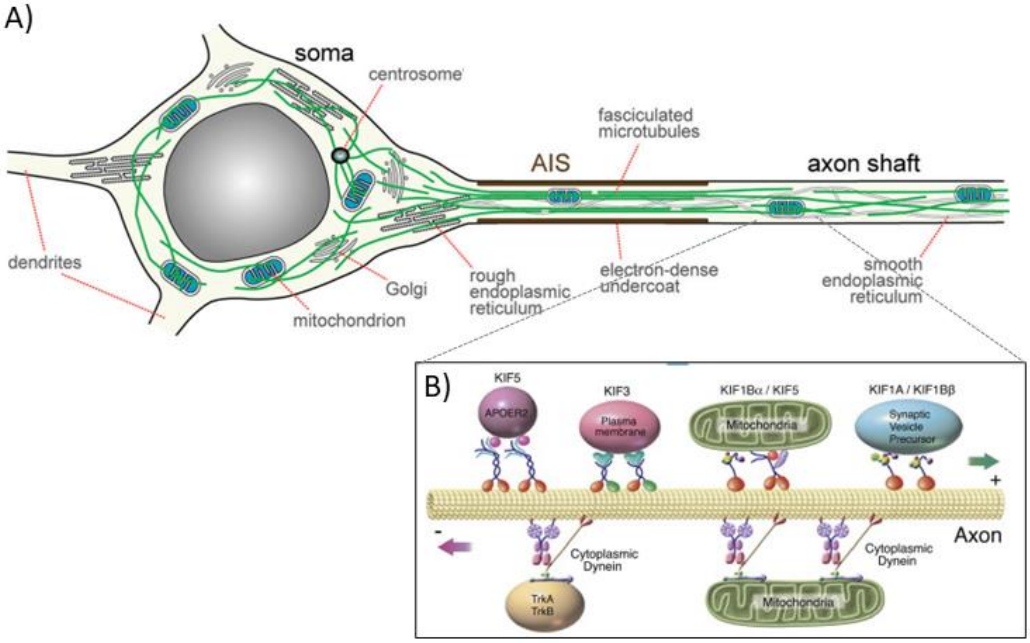

Fig. 3: Representative structure of a neuron and the bidirectional intracellular trafficking transport. A) Soma and proximal axon representative of a neurite. In the soma, microtubules (MTs, in light green) are diffusely organized but start to fasciculate, at the basis of the cell body, by forming the axon initial segment (AIS) which acts like a filter preventing Golgi apparatus and rough endoplasmatic reticulum organelles entering the axon shaft. B) Inset showing kinesin and dynein motor proteins interacting with *cargos* (*e.i* mitochondria, neurotransmitter's vesicles) and presiding to their axonal transport along microtubules towards the *plus* and *minus end* respectively. In short-range transport, such as in the pre- and post-synapses and filopodia, the molecular motor functions are guaranteed by the myosin family proteins. *AIS*, axon initial segment. Modified from Prokop, 2020 (panel A)) and Hirokawa *et al*, 2010 (panel B)).

Intracellular transport is fundamental for neuronal morphogenesis, function, and survival particularly for MNs, high-specialized cell controlling a variety of downstream muscles (*e.g.* skeletrical, visceral) and organs (*e.g.* brachial arches) together with are involved in the performance of complex movements such as walking or swimming, breathing, and feeding. MNs are divided into two categories, upper MNs (UMNs) and lower MNs (LMNs), according to 1) the location of their soma, 2) targets and 3) type of neurotransmitters used to the electrochemical response (**Table 2**) (Stifani, 2014).

	Upper MNs (UMNs)	*Lower MNs (LMNs)*
Position	Cerebral cortex	Brainstem Spinal cord
Neurotransmitter	Glutamate	Acetylcholine
Target	Inside the CNS	Outside CNS (*i.e.* muscles)

Table 2: Comparison of different features between vertebrate upper and lower MNs. From Stifani, 2014.

Across phylogeny, MN system represent a remarkably component of the neuronal circuitry, counting different subtypes, able to convey commands from the processing centers located in the central nervous system (CNS) to the effector muscles in the periphery (Catela&Kratsios, 2021). In invertebrate organisms such as *Drosophila* and *C.elegans*, the spMNs are generated from a restricted set of progenitor cells located in the ventral nerve cord (equivalent to vertebrate spinal cord) (Landgraf *et al*., 2006), and in the worm in particular the entire cell lineage is defined at single-cell resolution (Kerk *et* al., 2017). In *C.elegans* MNs specification fate and the subtype is defined by *unc-3* gene expression with a precise combinations of effector genes (**Fig. 4 A**). In *Drosophila*, neuronal progenitors are specified by a cascade of sequentially expressed transcriptional factors (TFs), such as Hunchback (Hb), Kruppel (Kr), Pou domain protein (Pdm), Castor (Cas), Grainyhead (Grh), Sevenup (Svp) and Distal antenna (Dan), and under the influence of the activation or repression of these inductive signals (morphogens) each

neuroblast (NB) will give rise to a Ganglion Mother Cells (GMC) which, in turn, will give rise to glia cells and neurons, including MNs (**Fig. 4 B**).

On the other hand, vertebrate spinal MNs arise from neuronal progenitors distributed in a specific region of the ventral neural tube (**Fig. 4 C**) (Catela&Kratsios, 2021). A large body of evidence is available especially from mammals, but basic processes are conserved also in other vertebrates. Indeed, the dorso-ventral patterning and the generation of distinct progenitor domains depend on morphogens deriving from axial midline cells of the notochord and the floor plate at the ventral neural tube. The morphogen *Sonic Hedgehog* (Shh) is secreted by floor plate cells and the notochord and establishes a ventral to dorsal decreasing threshold concentration responsible for the specific subtype motor neuronal specification fate. On contrary, at the dorsal neural tube, *Bone Morphogenetic Protein* (BMP) and *Wingless*/*Integrated* (Wnt) molecules are secreted from the roof plate to generate a dorsal to ventral decreasing gradient. These anti-parallel morphogen gradients define the initial progenitor domains along the dorso-ventral axis of the neural tube (Avilés *et al*., 2013).

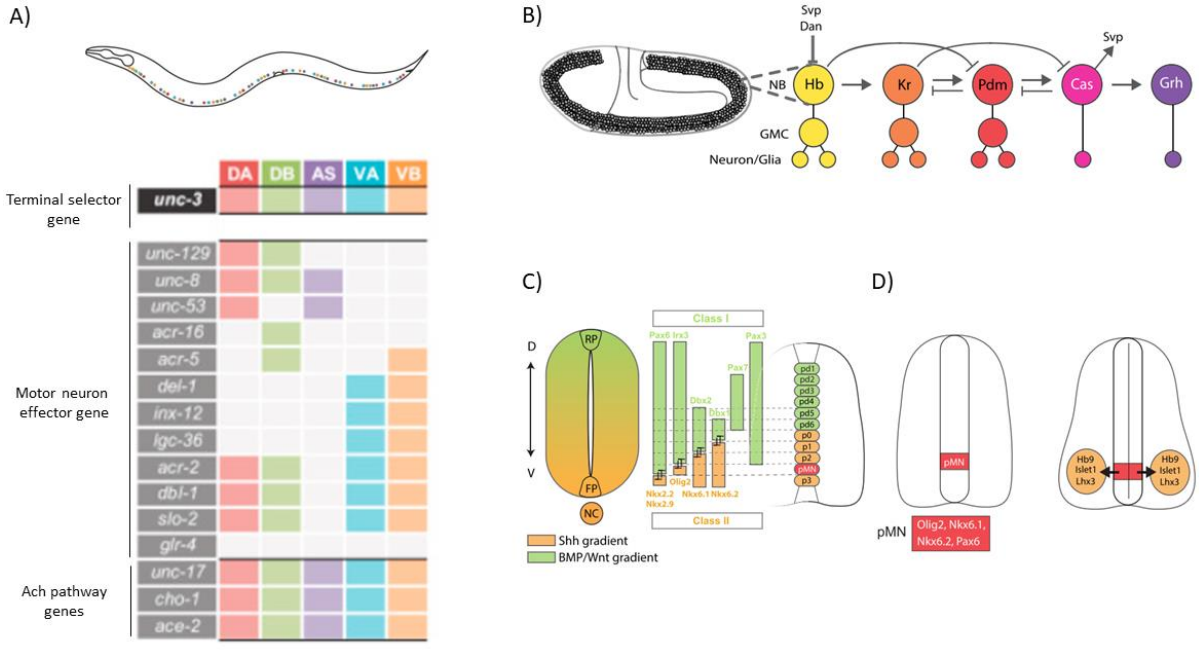

Fig. 4: Specification of MN progenitor cells fate in A) *C.elegans*, B) *Drosophila* embryos ventral nerve cord and C-D) in vertebrate spinal cord. A) In table are listed the unique combinations of *unc-3* with effector genes and defining the five cholinergic motor neuron classes (DA, DB, AS, VA and VB) highlighted in different colors. Abbreviations: DA, dorsal A class motor neuron (embryonically); DB, dorsal B class motor neuron (embryonically); AS, class AS neurons (post-embryonically); VA, ventral A class motor

neuron (post-embryonically); VB, ventral B class motor neuron (post-embryonically). **B**) In *Drosophila*, embryonic neuroblast's (NB) identity is determined by the cross-regulated expression of a number of transcriptional factors (TFs) which will define the diversity NB-derived cell types. Abbreviations: Hb, Hunchback; Kr, Kruppel; Pdm, Pou domain protein; Cas, Castor; Grh, Grainyhead; Svp, Sevenup; Dan, Distal antenna, GMC, ganglion mother cell. **C**) Overlapping expression of TFs induced by Sonic Hedgehog (Shh) defines the MN progenitor domains. **D**) Then, after their migration to the ventral spinal cord horns, MNs start to express a subset of specific TFs essential for the acquisition of the MN's fate. Abbreviations: BMP, Bone Morphogenetic Protein; Wnt, Wingless/Integrated; pd1-pd6, dorsal neuron progenitors; p0-p3, ventral interneuron progenitors; pMN, ventral motor neuron progenitor. Images modified from Kerk *et al*., 2017 (panel A) and Catela&Kratsios, 2021 (panel B, C and D).

In detail, the antiparallel concentration gradient of these three morphogens triggers the expression of TFs that define the boundaries and identities of each neural progenitor cells (pd1-6, p0-3, pMN). While Class I factors (Pax3, Pax6, Pax7, Irx3, Dbx1, Dbx2) are repressed by Shh, Class II factors (Nkx2.2, Nkx2.9, Nkx6.1, Nkx6.2, Olig2) are activated by Shh. In later steps, the integration of the cross-repressive activity between Class I and II TFs delineated the boundaries between the MN (pMN) and interneuron progenitor domains (p0-p3). A fundamental difference between invertebrates and vertebrates is that, in the latter, all MNs in the spinal cord are clonally derived from the same pool of progenitor cells that express the same combination of TFs such as Olig2, Nkx6.1, Nkx6.2 and Pax6 (Gouti *et al*., 2015). Once MNs progenitors are generated in the vertebrate spinal cord, cells exit from the cell cycle and the transcription of specific TFs, such as Olig1, Olig2 and neurogenin2, promote the activation of the molecular program to MN identity and repressing simultaneously the interneuron fate. Then, neurogenin2 guided the acquisition of motor neuron fate in two ways: first, by interacting with retinoic acid (RA) receptors it induced chromatin arrangements that allow the activation of genes defining a "generic" MN identity. Then, neurogenin2 together with Olig2 activated the transcription of the post-mitotic MNs homeodomain Hb9 gene, also known as mnx1. In mice and zebrafish is well-known that the function of Hb9 (mnx) is essential for the acquisition of MN features and the suppression of genes involved in V2a interneuron type development. In the absence of Hb9 indeed, MNs switch to the interneuron fate displaying aberrant migration patterns and losing the expression of Islet1, the earliest marker of developing motor neurons (Seredick *et al*., 2012; *Arber et al*., 1999). Once activated, Islet1 formed a complex together with the LIM homeodomain protein 3 (Lim3/Lhx3) and the LIM domain binding 1 (LDB1/NLI) factor which is essential for the maintenance of MN

identity. In zebrafish, all MNs initially express Islet1 and Lhx3 and the loss of Lhx3 during the embryonic stages of motor system formation, primary MNs showed aberrant and hybrid morphological and molecular features of both MNs and interneurons (Seredick *et al*., 2014). In *C. elegans* it was shown that the orthologs of Islet1 and Lhx3 are able to interact and form a complex, suggesting the ancient origin of MN's determination mechanism (Bhati *et al*., 2017). Following the initial acquisition of their general fate, spMNs differentiate once more to adopt highly specific identities reflecting their respective muscles targets. SpMNs specification in fact follow a spatial-temporal gradient of several proteins such as FGF (*fibroblast growth factor*) and TGFβ (*transforming growth factor beta*) along the dorso-ventral and rostro-caudal axes which determined, in concentration-depending manner, MNs arising located ventrally and rostrally earlier in neurogenesis (Stifani, 2014). These proteins induce the expression of transcriptional factors of *homeobox* HOX family whose patterning will induce the columnar organization of the spMNS along the rostro-caudal axis (D'Elia&Dasen, 2018). Despite, as mentioned, teleost and tetrapods share basic common features in MNs early developmental programs, it is interestingly to note that in fish the axial columnar groups diversification of spMNs in brachial, thoracic and lumbar organization is missing (D'Elia&Dasen, 2018; Babin *et al*., 2014); however it could be appreciated that zebrafish axial MNs are functionally organized along the dorsoventral axis of the spinal cord according to the recruitment of distinct type of muscle required to support swimming activities (**Fig. 5**).

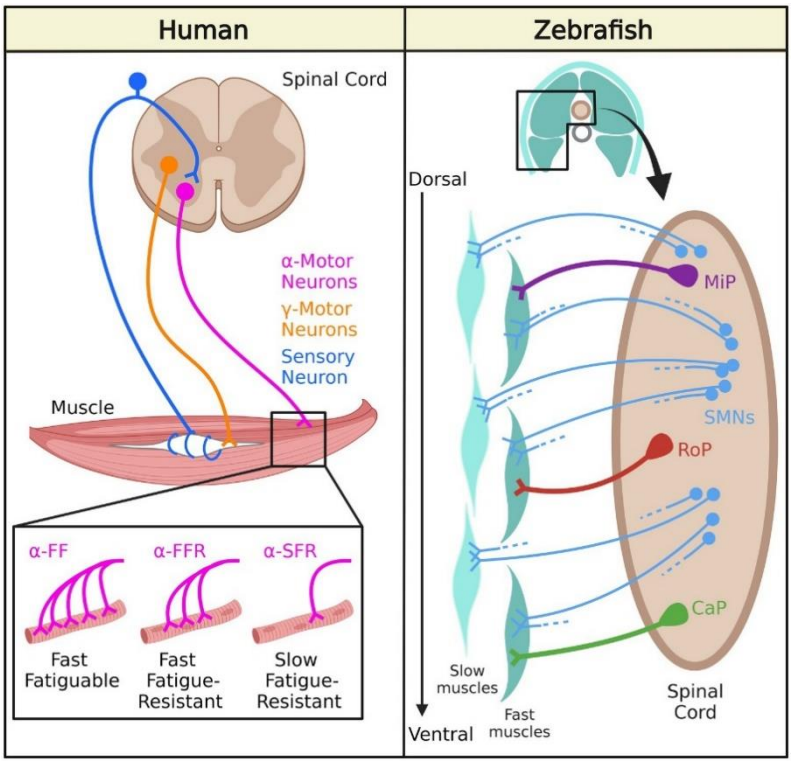

Fig. 5: Spinal motor neurons system organization in human and zebrafish. In mammals, lower motor neurons as spMNs are classified according to their morphology and target innervation as α-MNs and γ-MNs. The former innervates extrafusal muscle fibers responsible for skeletal movements and, based on the contractile properties of their motor unit targets, classified in: fast-twitch fatigable (α-FF), fast-twitch fatigue resistant (α-FFR) and slow-twitch fatigue resistant (α-SFR). γ-MNs innervate intrafusal fibers of the muscle spindle regulating its activity in response to stretch. In zebrafish, MiP PMNs innervate dorsal fast muscles, CaP PMNs innervate ventral muscles and RoP PMNs the fibers in between. SMNs instead innervate both types of muscle. From Singh&Patten, 2022.

In addition, the muscle spindle proprioceptive sensory receptors involved in the transmission of muscle's stretching informations to the CNS are absent in adult fish and recently it has been discovered a novel spinal proprioceptor organ, represented by a specialized class of late born spMNs functioning as mechanosensitive neurons to optimize efficient locomotion (Picton *et al.*, 2021). Fundamentals of zebrafish neuromuscular system development and muscles innervation will be discussed in paragraph 1.3.3.

1.2.2 Tubulin post-translational modifications and "*dynamic instability*" in health and disease

Neurons receive information from the environment and rely on their axons to transmit them to other neurons or muscles and to reach their targets the axon must be robust and plastic, fast in remodel itself following the reception of external stimuli. The αβ-tubulin dimers consist in a compact folded main "core" involved in the MTs lattice interactions with protruding C-terminal external tails undergoing to **post-translation modifications** (PTMs), a group of biochemical modifications which tuned the biophysical properties of MTs and their interactions with cellular effectors without affecting the active polymerization sites (Roll-Mecak, 2015; Verhey&Gaertig, 2007). Tubulins and MTs are subject to evolutionarily conserved and developmentally regulated PTMs that can be divide into two categories, "stabilizing" and "destabilizing", the most important are (**Fig. 6**):

- Addition/removal of one tyrosine residue from α-tubulin (destabilizing/stabilizing, both reversible);
- Removal of the penultimate glutamate residue (Δ2-tubulin, highly stabilizing and not reversible).
- Acetylation of the α-tubulin (stabilizing);
- Poly-glutamylation of α- and β-tubulin (stabilizing);
- Phosphorylation of β-tubulin (destabilizing). The function of this post-translational modification remains uncertain; however, in *Drosophila* hypomorphic mutant Minibrain/DYRK1a it has been showed that the haploinsufficiency of the related-encoded serin-threonine protein kinase prevents the phosphorylation of β-tubulin highly conserved serine 172 residue (S172; Caudron *et al*., 2010; Fourest-Lieuvin *et al*., 2006) and leading to an increase of branches length of the larval peripheral sensory class III neurons (Ori-McKenney *et al*., 2016).

Discovered in the '70, detyrosination/tyrosination cycle is the major PTM regulating the MTs dynamic instability: Peris *et al*. (2006) has shown that the difference in stability between Tyr-tubulin and Detyr-tubulin (or also known as Glu-tubulin) is not due to the intrinsic changes in the biophysical features of the MTs polymers but to the MTs regulators modalities of recruitment, which might even contribute to the mechanism

underlying many neurodegeneration disorders. It seems that PTMs of tubulins impose a "code" on the MTs that is red by different microtubules-related proteins showing preferential affinities for MTs domains enriched of deficient in certain modifications. As an example, the motor protein kinesin-1 seem to prefer MTs rich in detyrosinated and acetylated tubulins, while kinesins 5 and 13 prefer tyrosinated tubulin (Kahn *et al*., 2015; Sirajuddin *et al*., 2014; Yu *et al*., 2015). Within a neuron cell, MTs exist in variable lengths and can be both stable and dynamic and influenced by all the mentioned above tubulin's PTMs (Dubey *et* al., 2015). MTs dynamics and the proportion between these two pools have the potential to influence a wide variety of cellular processes (*i.e.* neuronal polarity and morphology, transporting *cargos* and neurotransmitters) and alterations in the ratio of stable/shrinking MTs may contribute to disease progression, as observed in Amyotrophic Lateral Sclerosis (ALS) and Hereditary Spastic Paraplegia (HSP) were MT's stability reduction and hyper-stabilization seem to lead to neurodegeneration respectively (Clark *et al*., 2016; Tarrade *et al*., 2006).

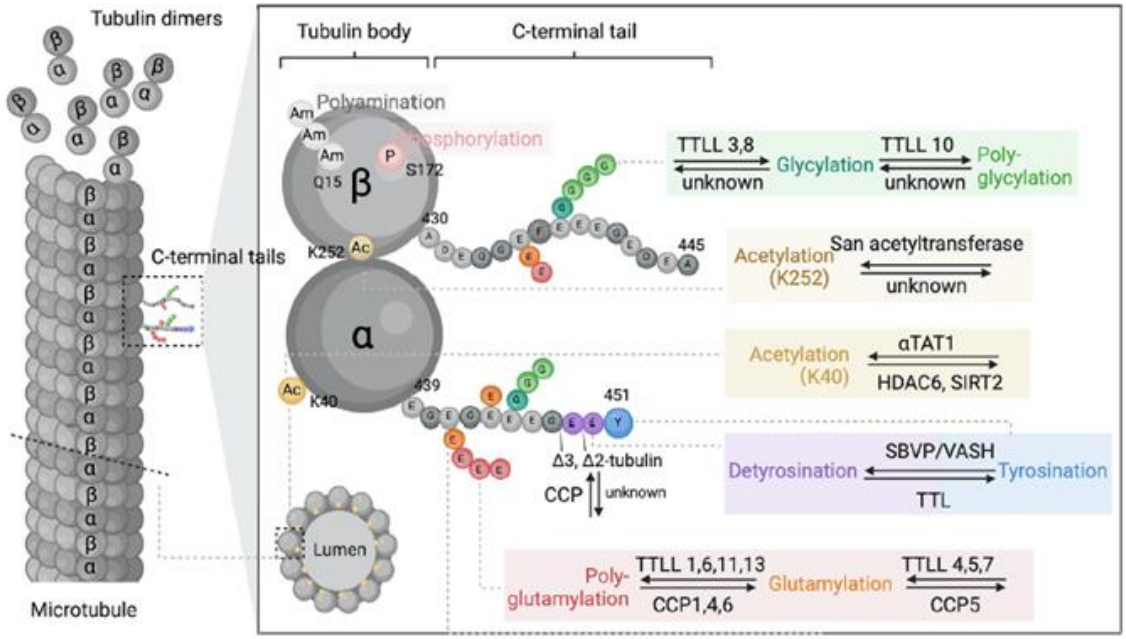

Fig. 6: Microtubules and tubulin post-translational modifications. MTs are assembled from "head-to-tail" orientated αβ-tubulin heterodimers protruding their C-terminal amino acid tails on the external surface of the filament. PTMs occurred at specific sites of the tubulin main "core", such as acetylation (Ac), phosphorylation (P), and polyamination (Am), or within the C-terminal tails as detyrosination/tyrosination. From Liu *et al*., 2022.

Given the essential functions carried out by MTs in neurons, it was proposed that a large number of neurodegenerative disorders depend on MTs and their associated proteins dysfunction (**Fig. 7**). The best documented MTs-loss disease is Tauopathy, a neurodegenerative disorder in which it appears that aberrant phosphorylation of Tau protein led to its aggregation in neurofibrillary tangles and dissociation from growing MTs. The latter, become unstable and probably more sensible to microtubules-severing proteins such as Katanin and Spastin, heterodimeric ATPase enzymes involved in tubulin dimers release from the *plus end* of the main MTs shaft and from the branching respectively, regulating MTs number and length in neuronal cytoplasm (Matamoros&Baas, 2016). Normally, severing activity generates short MTs allowing to efficiently transport, remodel and facilitating the axonal growth.

Mutations in the gene encoding for MTs-severing Katanin protein leads to a dysregulated catastrophe of the MTs and initiates the "dying-back" of the axon, a common feature observed in several neurodegenerative disorders (Yaron&Schuldiner, 2016; Dubey *et al*., 2015; Wood *et al*., 2006). In addition, an increasing number of neuronal branching is observed. On contrary, LoF of Spastin protein, responsible for Hereditary Spastic Paraplegia disorders, resulted in a local accumulation of detyrosinated stable MTs and a reduction of dynamicity at the *plus end* along the main shaft acting as a trigger for a progressive degeneration of the corticospinal tract of the lower limbs (Dubey *et al*., 2015).

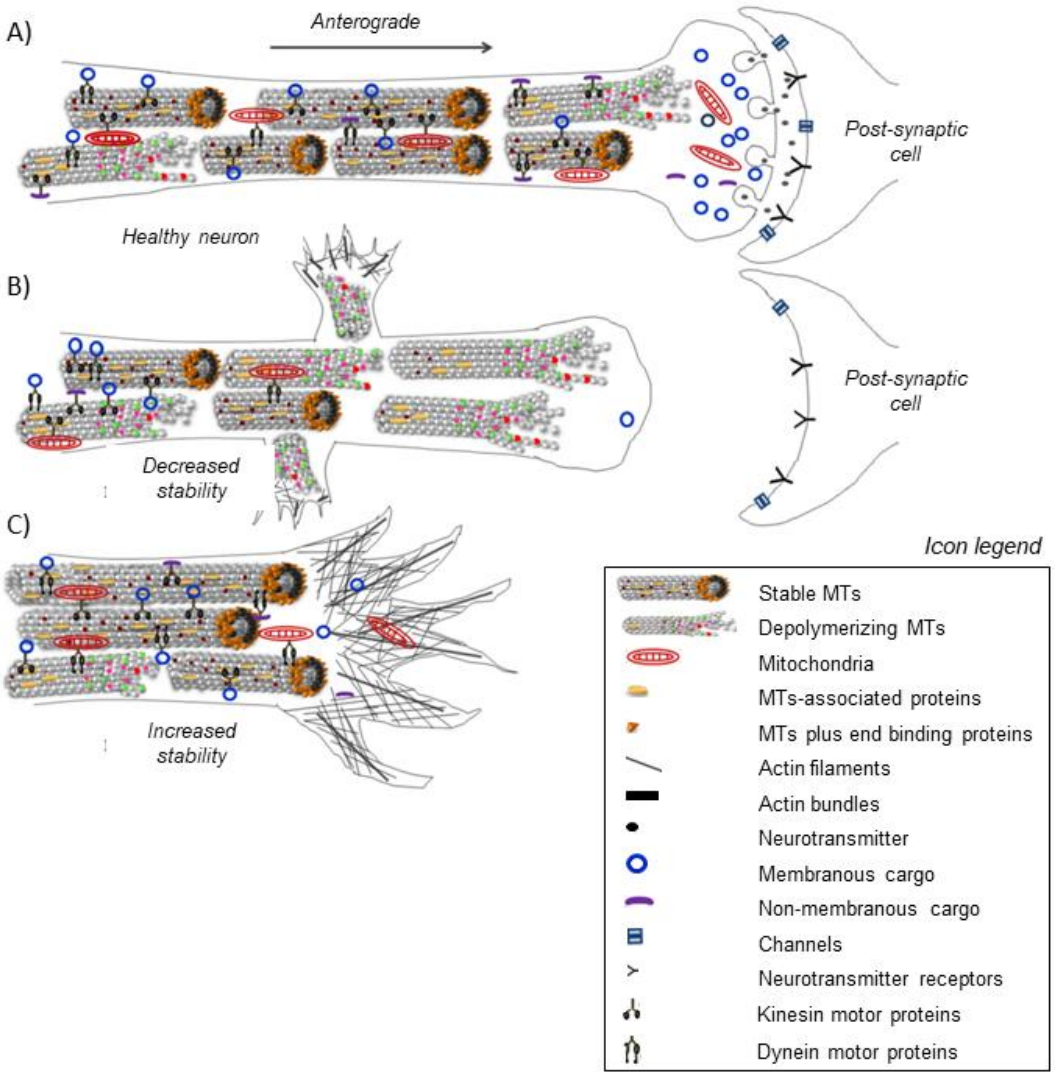

Fig. 7: Alterations in stable and dynamic MTs proportion affect neuronal structure and functions. A) Healthy neurons have a balance mix of short and long, stable and shrinking MTs regulating cellular processes, from axonal transport to cargos release at the presynaptic terminal button. **B)** Increased number of depolymerized, unstable MTs species normally leads to excessive neuronal branching, synapses collapse and reduction of the axonal transport (dying-back neuropathy). **C)** Hyperstable MTs increased the diameter of the neurite axon, inhibit its outgrowth and the neuronal branching. Modified from Dubey *et al*., 2015.

MTs in neurons have a variety of distinct functions that are coordinated within the same MTs cytoskeleton and could differed from the near one (Matamoros&Baas, 2016). The different composition in tubulin type plays a distinct role and their disfunction can contribute to neurodegenerative diseases. Different genes encode for tubulin isotypes differing each other for the presence of specific amino acid residues at the C-terminus tails (Maillard *et al*., 2023; Romaniello *et al*., 2018). Of note, mutations in these genes such as *TUBA1A, TUBG1, TUBB2B, TUBB3, TUBB2A* and *TUBB5* have been associated

to a wide broad spectrum of genetic disorders collectively called **tubulin-related cortical dysgenesis** or **tubulinopathies** (Bahi-Buisson&Maillard, 2016). In this context, pediatric patients with mutations in *TUBB2A*, *TBCD* and *TBCE* were recently identified at OPBG. LoF mutations in these genes, encoding tubulin and tubulin chaperons lead to the onset of complex phenotype involving the nervous system and sometimes other organs through pathological mechanisms still not completely understood (**Fig. 8**) (Sferra *et al*., 2018; Flex *et al*., 2016; Sferra *et al.,* 2016). Missense mutation in β-tubulin neuro-specific isotype II *TUBB2A* (*tubulin beta 2A*) (Sferra *et al*., 2018) determines aberrant axonal transport and morphological alteration in mitotic spindle assembly that seem to lead to dysfunctional mitotic cellular division having a strong impact on brain neurogenesis and neurite axon development. *In vitro* functional studies have evidenced that LoF mutations in *TBCD* and *TBCE* genes altered MTs dynamic instability leading to neurodegeneration in opposite manners (increasing or decreasing tubulin polymerization), as discussed below.

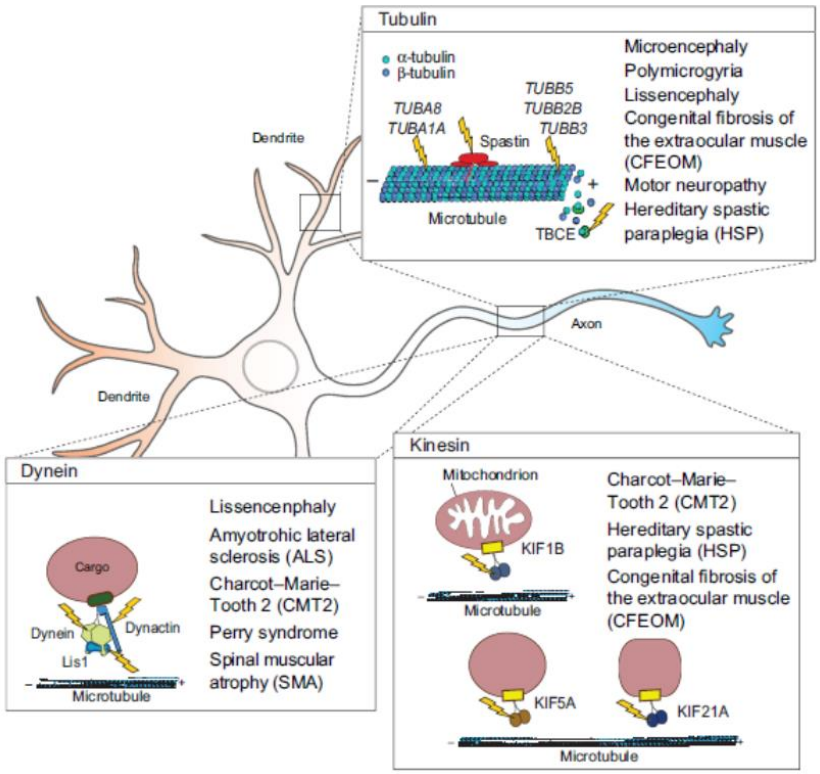

Fig. 8: Representative schematics of neuronal diseases linked to axonal transport defects induced by genetic mutation in genes encoding for tubulin isotypes and/or MTs-associated motor proteins. From Franker *et al*., 2013.

1.2.3. Tubulin chaperons TBCD and TBCE and their loss of function mutations in infantile neurodevelopmental disease with neurodegeneration

As mentioned, LoF and hypomorphic mutations in *TBCD* and *TBCE* genes have been recently linked to a new neurodevelopmental disorder with early signs of neurodegeneration. Severe patients with microcephaly and cortical atrophy have been reported. In addition, patients that seems to be apparently "normal" at birth, can lose major developmental and motor milestones within few months/years and exhibit additional clinical features such as spastic paraplegia or tetraplegia, seizures, intellectual disabilities and hypotonia (Caputo *et al*., 2023; Chen *et al*., 2021; Liao *et al*., 2020; Tian *et al*., 2019; Grønborg *et al*., 2018; Zhang *et al*., 2018; Ikeda *et al*., 2017 Pode-Shakked *et al*., 2017; Edvardson *et al*., 2016; Flex *et al*., 2016; Sferra *et al*., 2016). The genes involved encode for two of the five tubulin chaperon proteins composing the cytosolic chaperonin complex, called *tubulin-binding complex* (TBC), which interacting differentially with α- and β-tubulin, control and regulate MTs folding.

In detail, TBCD protein is the biggest protein (length: 1192 amino acid residues) of the TBC complex and, together with importin-β and GTPase ARL2 proteins, interacts directly with β-tubulin protein by establishing the correct maintenance of growth and organization of cytoskeletal MTs and mitotic spindles formation from the MTOC (microtubule organizing center) complex, a subcellular structure enucleating MTs from the centrosome (Chen *et al*., 2021), and also guides the axonal transport of mitochondria in neurons. This quaternary structure forms an intermediate scaffold onto which α-tubulin is added, facilitated by TBCE and TBCB cofactors. Not much is known on the structure of TBCD. The protein is mainly composed of *Armadillo* and HEAT-repeated motifs (**Fig. 9**). The latter is a repeated structural motif characterized by the presence of antiparallel α-helix in pairs stacked into a consecutive array and responsible for protein-protein interactions (Chen *et al*., 2021; Grynberg *et al*., 2003). *Armadillo* repeats, also involved in protein-protein interactions, are located at the N-terminal and differs from the HEAT motifs for the presence of two addition short helix followed by two longer helices (Grynberg *et al*., 2003; Groves&Barford, 1999). The C-terminal domain seems implicated in the large TBC complex.

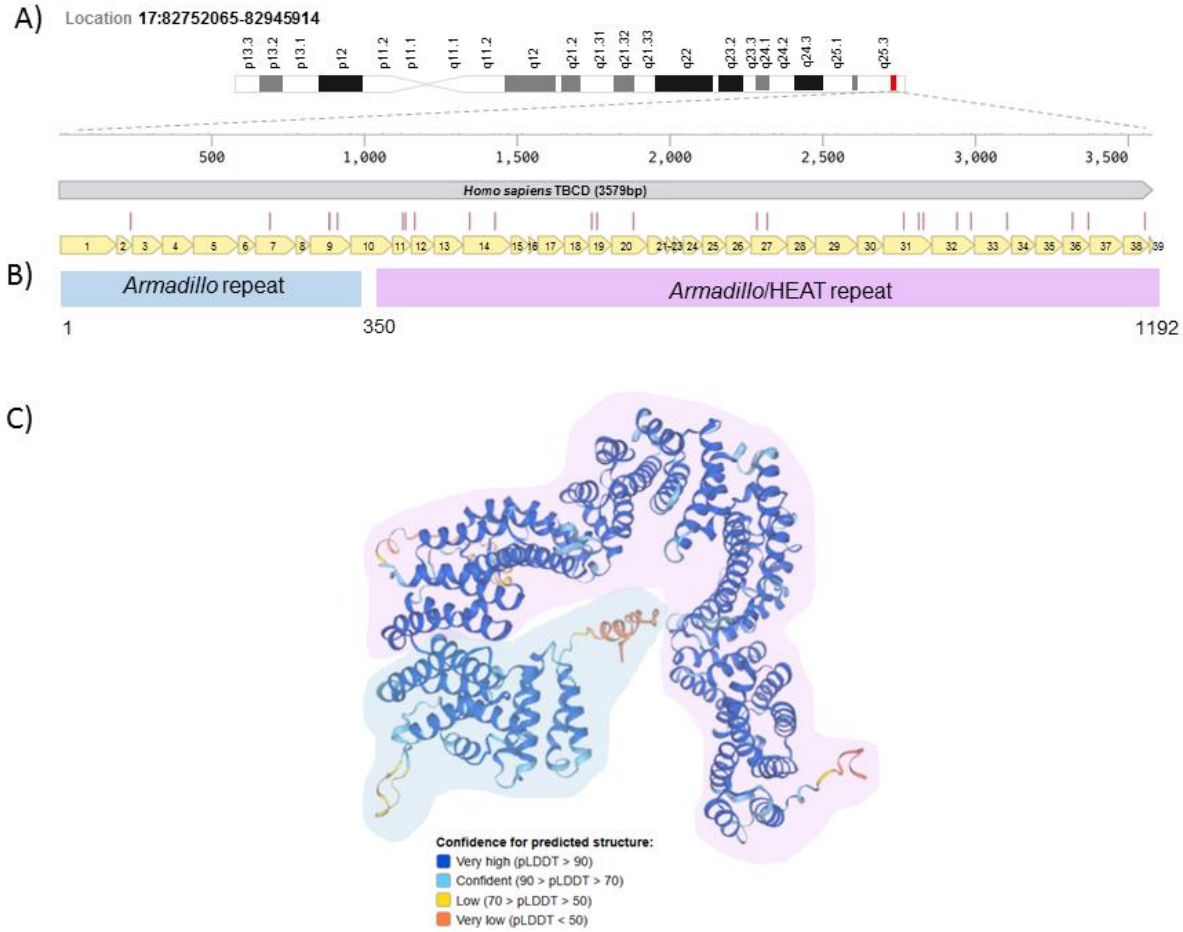
A)
Location 17:82752065-82945914
p13.3 p13.2 p13.1 p12 p11.2 p11.1 q11.1 q11.2 q12 q21.2 q21.31 q21.32 q21.33 q22 q23.2 q23.3 q24.1 q24.2 q24.3 q25.1 q25.3
500 1,000 1,500 2,000 2,500 3,000 3,500
Homo sapiens TBCD (3579bp)
1 2 3 4 5 6 7 8 9 10 11 12 13 14 15 16 17 18 19 20 21 23 24 25 26 27 28 29 30 31 32 33 34 35 36 37 38 39
B)
Armadillo repeat
Armadillo/HEAT repeat
1
350
1192
C)
Confidence for predicted structure:
Very high (pLDDT > 90)
Confident (90 > pLDDT > 70)
Low (70 > pLDDT > 50)
Very low (pLDDT < 50)

D)

Genetic condition	Allele 1	Allele 2	Amino acid substitution	Reference
homozigous	c.881G>A	c.881G>A	R294G	Caputo *et al.*, 2023
compound heterozigous	c.1340C>T	c.817+2T>C	A447V	Chen *et al.*, 2021
compound heterozogous	c.881G>A	c.22801C>A	R294Q	Liao *et al.*, 2020
compound heterozigous	c.230A>G	c.907C>T	H77R, R303 *	Tian *et al.*, 2019
compound heterozigous	c.2953C>T	c.3550C>T	R979C, Q1184 *	Tian *et al.*, 2019
homozigous	3099C>G	3099C>G	N1033K	Grønborg *et al.*, 2018
compound heterozygous	230A>G	deletions of exons 28 to 39	H77R	Zhang *et al.*, 2018
homozigous	c.2825G>A	c.2825G>A	R942Q	Ikeda *et al.*, 2017
compound heterozygous	c.2981C>T,	c.3313G>A	T994M, V1105M	Flex *et al.*, 2016
compound heterozygous	c.1876G>A	c.1130G>A	A626T, R377G	Flex *et al.*, 2016
compound heterozygous	c.771+1_771+10del	c.1121C>T	T374M	Flex *et al.*, 2016
compound heterozygous	c.686T>G,	c.3365C>T	L229R, P1122L	Flex *et al.*, 2016
compound heterozygous	c.1564-12C>G (splicing)	C.2314C>T	R772C	Miyake *et al.*, 2016
compound heterozygous	c.1160T>G	c.2761G>A	M387R; A921T	Miyake *et al.*, 2016
compound heterozygous	c.2280C>A	c.3365C>T	Y760 *; P1122L	Miyake *et al.*, 2016
homozigous	c.2810C>G	c.2810C>G	P937R	Miyake *et al.*, 2016
homozigous	c.1757C>T	c.1757C>T	A586V	Edvardson *et al.*, *2016*
homozigous	c.1423G>A	c.1423G>A	A475T	Pode-Shakked *et al.*, 2016; Edvardson *et al.*, 2016
compound heterozigous	c.1757C>T	c.3192-2A>G	A586V	Pode-Shakked *et al.*, 2016
compound heterozigous	c.3365C>T	c.1739G>A	P1122L, R580Q	Pode-Shakked *et al.*, 2016

Fig. 9: Structural organization and functional domains of TBCD protein. A) Genomic location of human *TBCD* gene on chromosome 17 (genomic sequence length: 3579 bps). **B**) Representation of *TBCD* exon sequence (39 exons). Pink pipes indicate genomic mutations collected from past literatures reported in the table in C). **C**) TBCD 3D structure and domains *Armadillo* repeats and *Armadillo*/HEAT motif

highlighted in light blue and pink respectively and **D**) the subset of the known list of all *TBCD* patient's mutations causative of neurodevelopment/neurodegenerative disorder. 3D protein structure prediction from Alphafold project, version 2 and modified from https://www.proteinatlas.org/ENSG00000141556-TBCD/structure.

The post-CCT chaperon TBCE is involved, together with TBCB protein, in α-tubulin folding and degradation that is essential for controlling the cell tubulin dynamics and turnover. αβ-tubulin dissociation from the MTs main shaft is efficient only when TBCE and TBCB are both present in the mix; indeed, TBCB alone is unable to dissociate tubulin heterodimers while TBCE alone seems able to. TBCE protein (length: 527 amino acid residues) is structured in three domains (**Fig. 10**):

1. The *cytoskeleton-associated protein glycine-rich* (CAP-Gly), is a sequence made of 80 amino acids at the N-terminal, highly conserved from yeast to human, involved specifically in binding the EEY motif at C-terminal of α-tubulin. The interaction is crucial to regulate tubulin folding and dissociation;
2. The *ubiquitin-like domain* (UBL) consisting in five-stranded mixed β-sheet grasping one α-helix, is the characteristic fold shared by all ubiquitin and ubiquitin-like proteins. However, TBCE UBL domain is 5 amino acid residues shorter than ubiquitin and missing of the glycine residues responsible for the covalent bond with target protein lysine residues required for ubiquitylation;
3. The *leucine-rich repeats* (LRR) are 9 tandemly arranged protein-ligand interaction motif highly conserved from prokaryotes to eukaryotes. Each repeat is 19–29 amino acids long and has a well-conserved N-terminal stretch of 9–12 amino acids made of hydrophobic residues (usually leucine) forming a β-strand. The arrangement of multiple repeats in tandem generates a horseshoe-shaped solenoidal structure (Sferra *et al*., 2016; Serna *et al*., 2015; Dolan *et al*., 2007).

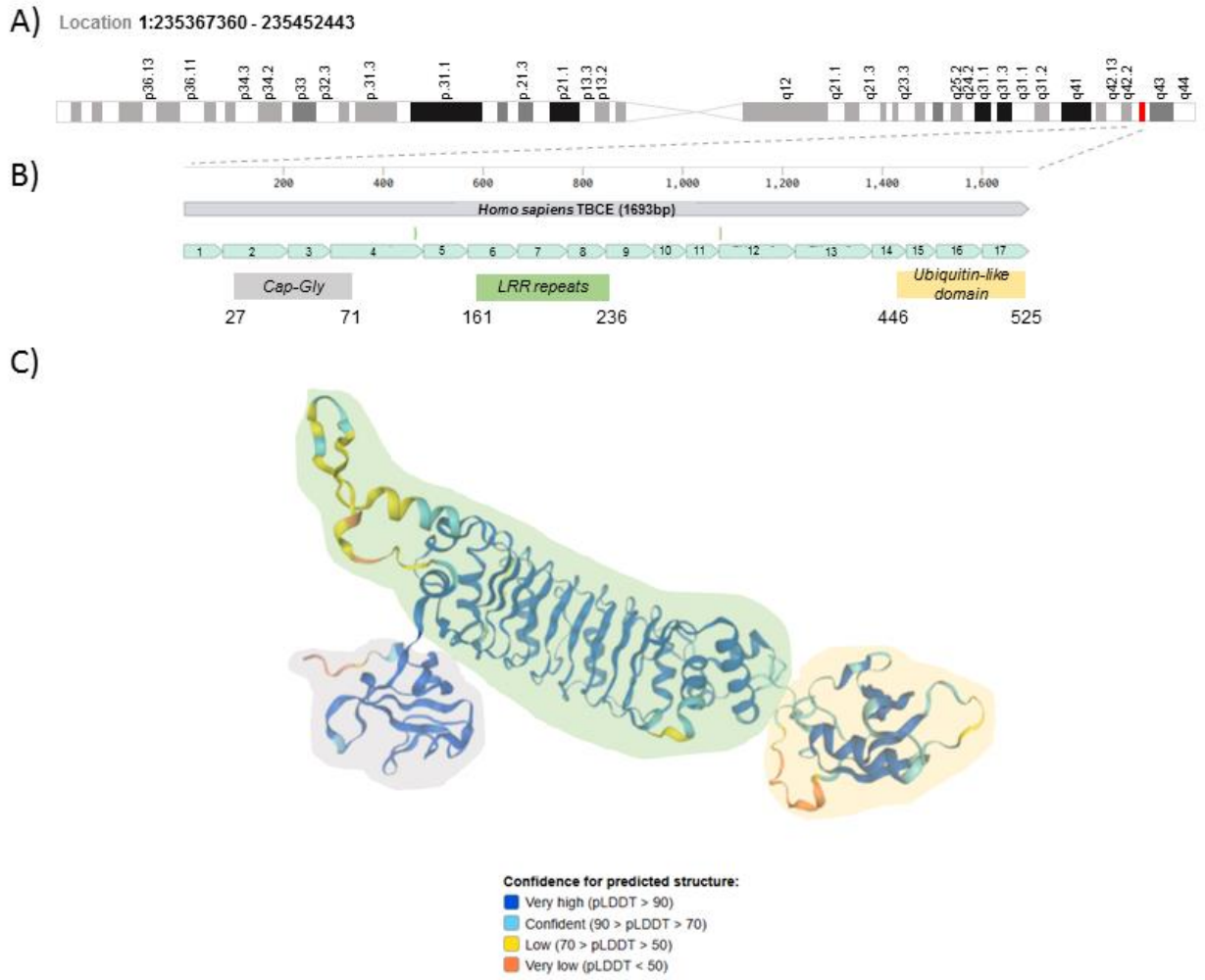

D)

Genetic condition	Allele 1	Allele 2	Amino acid substitution	Reference
Homozigous	c.463T>A	c.463T>A	p.I55N	Sferra *et al.*, 2016
Compound Het	c.463T>A	c.1076delC	p.I55N; p.L1076*	Sferra *et al.*, 2016

Fig. 10: Structural organization and functional domains of TBCE protein. A) Genomic location of human *TBCE* gene on chromosome 1 (genomic sequence length: 1693 bps). **B**) Representation of *TBCE* exon sequence (17 exons). Green pipes indicate genomic mutations collected from past literatures reported in the table in C). **C**) 3D structure of TBCE protein with CAP-Gly motif (light grey), LRR leucine tandem repeats (green) and UBL domain (light orange) respectively. **D**) The list of all *TBCE* patient's mutations causative of neurodevelopment/neurodegenerative disorder. 3D protein structure prediction from Alphafold project, version 2 and modified from https://www.proteinatlas.org/ENSG00000284770-TBCE/structure.

Based on genetic and biochemical studies it has been proposed that overall TBCD and TBCE form a supercomplex important for MT dynamics, however the mechanism of action, especially in vertebrates, is poorly understood (Nithianantham *et al*., 2015). A stepwise αβ-tubulin biogenesis and degradation seems to be regulated through the TBC complex (**Fig. 11**): briefly, α- and β-tubulin monomers are bond by TBCA and TBCB and, after their folding, tubulins are hands off to TBCE and TBCD respectively forming an activator multicomplex. After, ARL2 GTPase is recruited and stimulated to hydrolyze GTP in GDP allowing the MTs assembly and disassembly (Nithianantham *et al*., 2015).

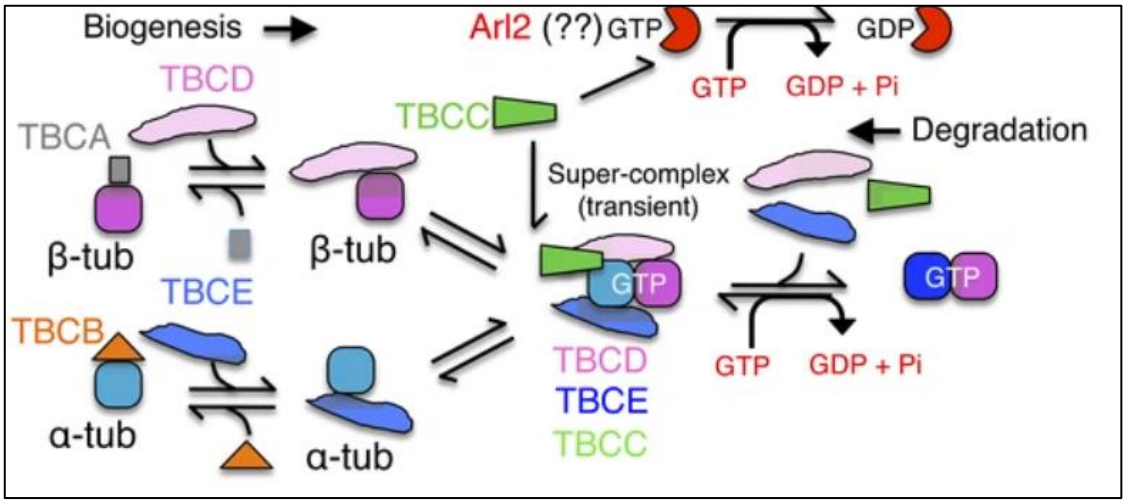

Fig. 11: Diagram showing the molecular dynamics of biogenesis/degradation of MTs mediated by tubulin chaperon cofactors (TBCA, TBCB, TBCC, TBCD and TBCE) and ARL2 GTPase. From Nithianantham *et al.,* 2015.

The maintenance of tubulin dimers pool by the TBC proteins seems essential for MTs dynamics and synaptogenesis and their loss or overexpression are both lethal in many eukaryotic organisms (*i.e. Drosophila*, *S. cerevisiae and pombe*, mammals). Similarly, *tbce* mutants of *Arabidopsis* have defective MTs, leading to lethality (Jin *et al*., 2009; Martin *et al*., 2002; Steinborn *et al*., 2002). In humans, *in vitro* functional analysis on fibroblast's patients-derived cells of the missense mutations in *TBCD* and *TBCE* have highlighted abnormal MTs behavior in both cases although it seems occurring with a different pathogenic mechanism: *TBCD* LoF seems to determine an increasing MTs polymerization and stability whereas hypomorfic mutations in *TBCE* causes reduced

polymerization with a consequent abnormal morphology of the mitotic spindle (Flex *et al*., 2016; Sferra *et al*., 2016). The effect of hyper-stable and highly unstable MTs has already been seen in neurodegenerative disorders (Sferra *et al*., 2020; Sau *et al*., 2011) but it is not known which are the effects of this altered organization of cytoskeletal MTs on homeostasis, proliferation and migration of neuronal precursors in the physiological context of a developing living vertebrate organisms. Therefore, studies aimed at verifying *in vivo* system are crucial for understanding the impact of altered MTs dynamics on the innervation and synaptogenesis processes.

1.3 *In vivo* models to study cellular and functional defects of motor neurons diseases

1.3.1. *In vivo* models used to study nervous system development: mouse, zebrafish and fly fruit

As discussed in paragraph 1.1.3, *in vivo* models are crucial for understanding the pathogenetic mechanisms of human diseases. The possibility of using such models as representative systems, especially in the pediatric context, is mainly linked to the fact that often aberrant proteins produced in patients with genetic mutations are evolutionarily conserved and involved in the maintenance of essential cellular functions, whose basic characteristics are themselves highly conserved (*e.g.*, intracellular trafficking control, cell cycle (Fasano, Muto, Radio, 2022), DNA repair, cytoskeleton dynamics (Flex *et al*., 2016; Sferra *et al*., 2016)). In fact, at least the "core" processes related to early embryonic development programs appear to be homologous among distant species on the evolutionary tree, and there is strong gene synteny and functional conservation among various animal phyla (Holland *et al*., 2020; Matsubara *et al.*, 2016; Holland, 2009).

The vertebrate models *Danio rerio* (zebrafish) and mouse have an orthology level with the human genome of about 71% and 80%, respectively, and cellular differentiation, embryogenesis, and systemic physiology processes have key mechanisms that, beyond the differences mainly due to speciation, are mainly conserved among these species. Based on the cellular and developmental processes in which the genes under investigation are involved, *Drosophila* and *C.elegans* can be successfully employed as models not only for comparative studies but also for understanding human pathologies. For instance, recent studies carried out on the fly fruit showed that LoF mutations in the highly

conserved *ankle2* gene prevent the encoded protein from regulating the asymmetric neuroblasts division, resulting in mutants displaying defects in the development of the nervous system leading to microcephaly, a feature observed in pediatric patients (Thomas *et al.,* 2022; Link *et al*., 2019; Yamamoto *et al*., 2014). Similarly, *C.elegans* models of missense mutations of the *cdc42* gene, encoding a GTPase involved in many crucial cellular functions, caused a growth delay and morphological abnormalities of varying degrees in the nematode (Martinelli *et al*., 2018). The observed phenotypes are in line with the clinics of patients, recreating a simple but faithful model of some cellular and molecular traits typical of the Noonan syndrome, a heterogeneous developmental disorder caused by the deregulation of the RAS pathway at various levels (in RAS itself, its interactors, or upstream pathways; Zenker *et al*., 2022; Tartaglia *et al*., 2011).

Although invertebrate organisms such as the fly fruits and nematode worms shared many similarities with human at the molecular level, their physiology is very different and strongly limit their use as disease model for study neurodegenerative disorders. On contrary, fish and rodents are widely use in neuroscience and biomedical research to investigate on molecular, biological and pathological mechanisms underlying human diseases. Recently, Fasano, Muto and Radio (2022) described a new disease gene, *ARF3* (ADP-ribosylation factor 3), encoding for a small GTP-ase involved in *trans*-Golgi trafficking control and responsible of an infantile encephalopathy, in which affected patients displayed microcephaly, intellectual delay, epilepsy and skeletal abnormalities already reported and noted to this kind of disorder (El Ghouzzi&Boncompain, 2022; Ain *et al*., 2021; Rasika *et al*., 2019). Interestingly, zebrafish mutants expressing *ARF3* human mutations generated in our laboratory resembled the human phenotype and shown microcephaly and severe skeletrical abnormalities remarkably. *In* vitro and *in vivo* models supported the evidence that the expression of *hARF3* pathogenic variants disrupt Golgi apparatus morphology, vesicles formation, and alter cargo recycling through the endosomal compartment. Moreover, a preliminary evaluation carried out on the fish (to which I contribute during my PhD) suggested the involvement of ARF3 protein in regulating neuron precursor's cell division. Although, the emergence of Golgi apparatus stress may contribute significantly to cortical impairments eliciting microcephaly (Passemard *et al*., 2019, Létard *et al*., 2018), the mechanisms underlying aberrant neuron progenitor's replication is still under investigation.

The mouse model (*Mus musculus*) is the leading organism to model neurodevelopmental and neurodegenerative disorders due to its 1) high level of syntheny and orthology conservation with human genome, and 2) several neuroanatomical and brain functional similarities between the species (Damianidou *et al*., 2022). For instance, mice are the most common species used to model amyotrophic lateral sclerosis (ALS), a rare neurodegenerative disorder affecting the peripheral nervous system (both upper and lower MNs) and characterized by neuromuscular junction denervation, motor endplate resizing and loss of terminal Schwann cells. On contrary, the absence of upper motor neurons limited the use of zebrafish to model ALS (Alhindi, Boehm, Chaytow, 2022; Morrice, Gregory-Evans, Shaw, 2018).

Despite each model offers a wide range of specific advantages in usage, they are affected by limitations as well, that should be experimentally considered (summarized in **Table 3**):

	Model organisms			
	Invertebrates		**Vertebrates**	
	Drosophila	***C.elegans***	**Zebrafish**	**Mouse**
General features				
Animal facility management and breeding/maintenance of the strain lines	Economic	Economic	Moderately expensive	Expensive
Availability of genetically modified organism lines	+	+++	+++	+++
Anatomical similarities	-	-	+	++
Genetic/molecular similarities	+	+	++	+++
Evolutionary conservation of the biological processes	+	+	++	+++
Reproduction	+++	+++	++	+
Embriogenesis	4-5 days (external)	3 days (external)	5 days (external)	21 days (*in-utero*)
Life expectancy	2 weeks	2-3 weeks	2-3 years	1-2 years

Bioethical implications (D.L. 4/03/2014 n°26; Directive n°2010/63/UE)	Absent	Absent	Present	Present
Genetic engineering tools and neuro-functional assays				
Transgenesis	++	++	++	++
CRISPR-Cas9 technology	+	+++	+++	+++
In vivo transient genetic manipulation	++	++	+++	+
In vivo microscopic investigations	++	++	+++	+
Mass pharmacological screenings	++	++	+++	-
Behavioural assays	++	++	+++	+++

Table 3: Comparison between *in vivo* models used in biomedical research. The models are assessed for their relative benefits, limitations, and amenability to different study approaches. Legend: (+) sufficient/partially suitable; (++) good; (+++) very good/best.

1.3.2. Main features of the model organism zebrafish (*Danio rerio)*

The model organism used for the characterization and evaluation of the effects of pathogenetic variants in *TBCD* and *TBCE* genes on the neurogenesis is the small freshwater teleost fish *Danio rerio*, or well-known as zebrafish, belonging to *Cyprinidae* family. Zebrafish is endemic to the Northen-Easter India countries and commonly inhabits streams, slow-moving or stagnant water bodies, including rice fields (Engeszer *et al*., 2017; Hamilton, 1822). The zebrafish is so called due to five horizontal blue stripes on the side of the body extending to the end of the caudal fin. Adult male and female specimens are dimorphic (**Fig. 12**): the former is fusiform and laterally compressed with a slight yellow cast ventrally; the latter on contrary has a bigger, whitish belly and silvery livery. Zebrafish can grow to 2.5 cm in length (up to 4 cm in captivity) with a lifespan around two to three years, which could be extended to five years under ideal conditions (Spence *et al*., 2008). Females can spawn every 2-3 days and the high fecundity, together with the external fertilization, allows to obtain a consistent number of embryos which, at

least within the 24 hpf, remain optically transparent and observable through the chorion, an acellular polypeptide structure surrounding mature teleost eggs (Bonsignorio *et al*., 1996).

Fig. 12: Zebrafish A) female and B) male specimens. Modified from Parichy, 2015.

Embryonic development is extremely fast and within 24 hpf the body plan is perfectly formed and muscles, cardiovascular and nervous system are visible and appreciable under a dissecting microscope. Within 3 dpf, embryos come out of the chorion becoming autonomous in food seeking and swimming. Zebrafish embryogenesis is extremely fast and divided into seven broad periods (**Fig. 13**) (Kimmel *et al*., 1995):

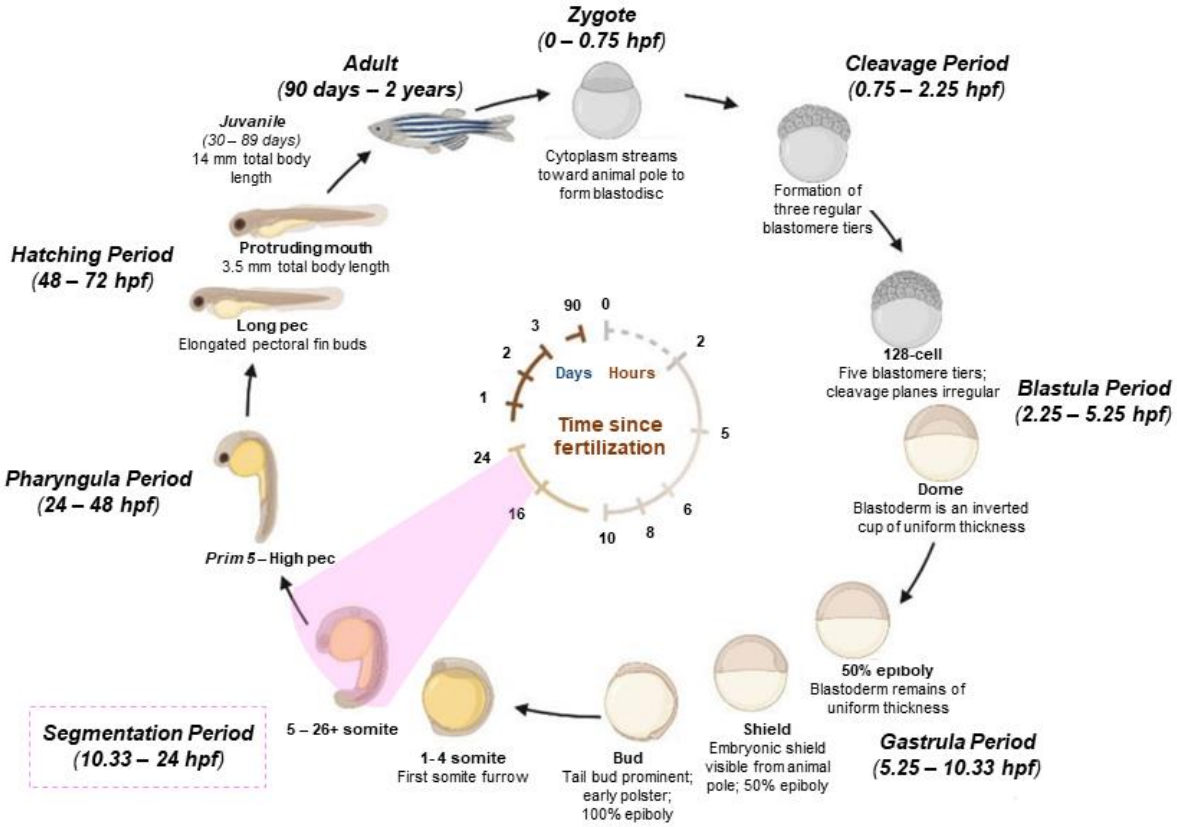

Fig. 13: *Danio rerio* (zebrafish) life cycle. In pink is shown the critical time window (16-24hpf) of the segmentation period during which neurogenesis and MNs differentiation begin. Modified from Coppola *et al*., 2023.

- **Zygote period** (**0 hpf**): this phase starts from the fertilization event until the first cleavage occurs (~40 minutes). Fertilization also actives cytoskeletal actin filaments determining non-yolky cytoplasm toward the animal pole on whose apical summit the blastodisc begins to segregate;
- **Cleavage period** (**0.75-2 hpf**): blastomeres divide synchronal at about 15 minutes intervals. The division is meroblastic, and cells are interconnected by cytosolic bridges. For this reason, synthetic mRNA injected are distributed equally within the entire embryo;
- **Blastula period** (**2-5 hpf**): the blastodisc takes the appearance of ball-like. During this period the embryo enters in mid-blastula transition (zygotic genome is activated and gastrulation cell movements started), the yolk syncytial layer is formed, and epiboly begins.
- **Gastrula period** **(5-10 hpf**): gastrulation begins and the morphogenetic cell movements of involution, convergence and extension take place leading to

formation of embryonic sheets (mesoderm, endo- and ectoderm). During this phase, also the three body axes (dorso-ventral, antero-posterior, and medial-lateral) are distinguishable.

- **<u>Segmentation period</u>** (**10-24 hpf**): is so called because represent the phase in which the segmentation of the nervous system and motor neurons differentiation begin and the rudiments of the primary organs become visible. The first step in vertebrate's nervous system development is the specification of the neuroectoderm. This process is called 'neural induction' and initiates at the onset of gastrulation, with the forming mesodermal layer which involutes and comes into contact with the overlying ectoderm (Schmidt, Strähle, Scholpp, 2013). In a BMP-induced Notch-dependent and Wnt-dependent "waves" manner in a rostro-caudal gradient of FGF, the paraxial mesoderm organizes into primitive segmented somite (metameric structure giving rise to the muscles) pairs either side of the forming neural tube, in a head to tail direction along the entire length of the embryo (Ruggeri *et al*., 2013). Contemporary, neural crest cells (NCC) from the neural tube migrate along the rostro-caudal direction and differentiate into several cell types that serve various functions depending on the location that they ultimately migrate to and mainly classified into: cranial, trunk and vagal/cardiac neural crest cells (Rocha *et al*., 2019) (**Fig. 14**).

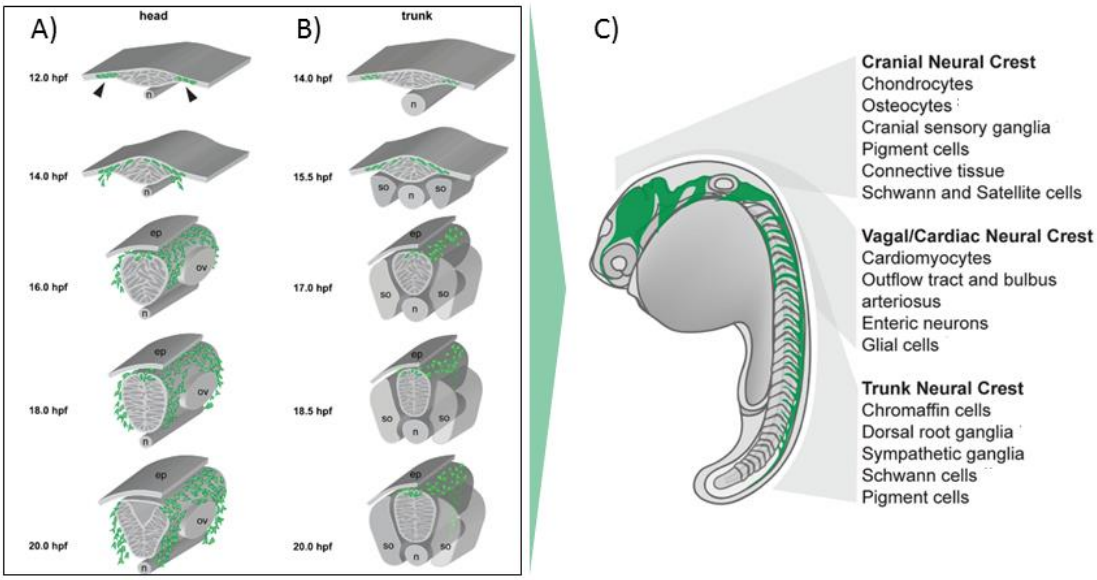

Fig. 14: Zebrafish neurulation and neural crest cells (NCC) migration pathways. A) Cranial and **B**) trunk neurulation and NCC migrations (in green) at different stages of zebrafish embryonic

development. **C**) NCC regionalization and tissue derivates in the 22 hpf zebrafish embryo. Abbreviation: n, notochord; ep, epidermis; ov, otic vesicle; s, somite. Modified from Rocha *et al*., 2019.

After the neuronal induction promoted by diffusible factor such as Noggin and Chordin (which prevent BMP expression in the future dorsal region), neural fate determination begin, thanks to the expression of Sox protein family (*i.e.* Sox2) in the region between the ventral-caudal cluster of the mid-brain and the presumptive neurons of anterior rhombomeres, and required to active genes implicated in the primary neurogenesis like *HuC/D* (also known as Elav 3/4, a RNA-binding protein involved in neuronal differentiation) and *neurog1* (neurogenin 1, a transcriptional factor enhancing and regulating the expression of those genes promoting the neurogenesis) (Schmidt *et al*., 2013). These induce the expression of *neuroD*, a transcriptional factor crucial for neuronal differentiation and maturation which marks the beginning of secondary neurogenesis, an additional step in brain development program currents only in fish (Chitnis *et al*., 1998) (**Fig. 15**). During this phase, primary spMNs formation is appreciable and, in the end, they will exit from a spinal cord segment and grow across the medial surface of one myotomal muscle following a specific trajectory (Panzer *et al*., 2005). Fundamental aspects of zebrafish motor system development will be discussed deeper in paragraph 1.3.3.

- **Pharyngula period** (**24-48hpf**): The period name focuses attention on the primordia of the pharyngeal arches, present but at early times difficult to distinguish individually. The embryo shows evidently bilateral symmetry structures organization, a well-developed notochord, expanded nervous systems and discernible somites. Body movements are still irregular and not controlled.
- **Hatching period** (**48-72 hpf**): the embryo comes out of the chorion signing the end of the embryonic development and becomes a larva able to swim freely and all the anatomical structures are fully established (Kimmel *et al*., 2015).

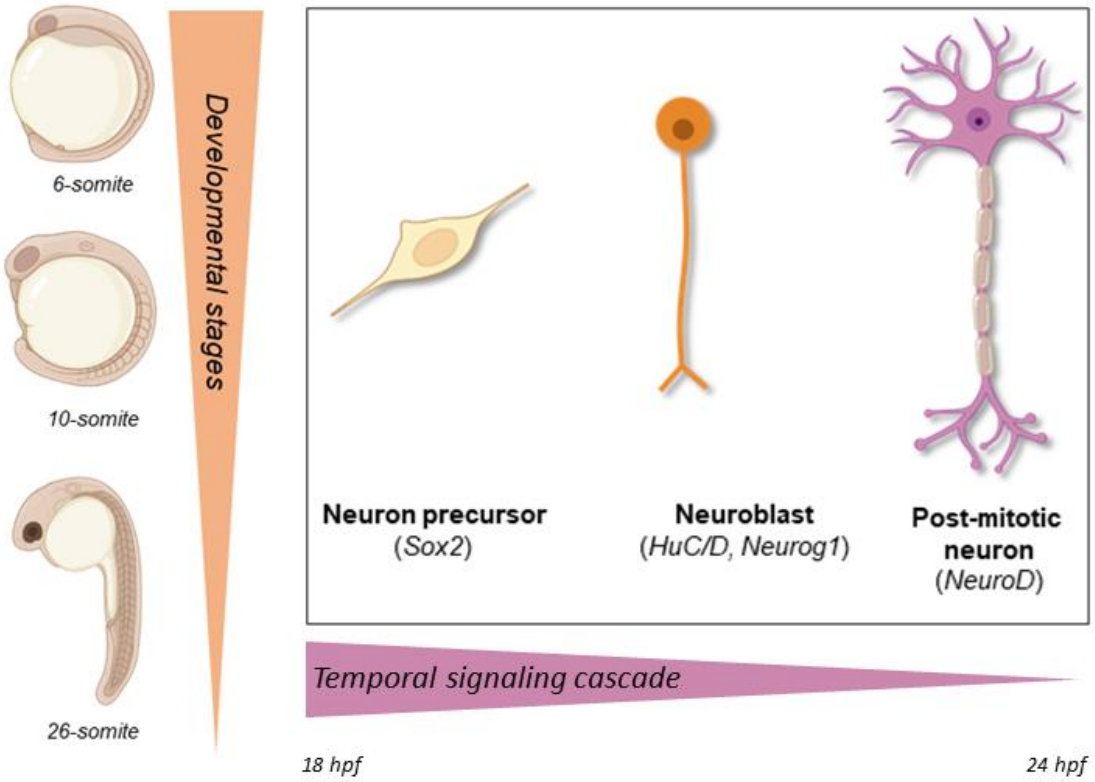

Fig. 15: **Diagram of simplified primary neurogenesis signaling cascade in zebrafish embryo from 16-24 hpf.** Icon source from Biorender.

Given the transparency of the embryos, especially in the earliest stages of embryogenesis, morphological changes occurring both in physiological and disease conditions can be easily evaluable and the gene expression pattern quantified with histochemical techniques on fixed and stained embryonic tissue such *whole mount* (full embryo/larvae) or sections (Ferguson&Shive, 2019; Santos *et al*., 2018). Other special features are contributing to the widespread use of zebrafish for disease modelling: 1) easy maintenance and management of zebrafish colonies in a small amount of space, 2) short generation time and sexual maturity reaching at the third month of the development (Ali *et al*., 2011). Although zebrafish is commonly used as study model for screening new drugs, evolutionary and comparative genetics studies, in recent years it has convincingly demonstrated its usefulness potential to study vertebrate gene functions and increasingly human genetic disorders involving the development of the nervous system and to improve new diagnostic and therapeutic approaches (Patton *et al*., 2021; Babin et al., 2014). Indeed, full sequencing of zebrafish genome revealed that ~71% of all human proteins

and ~80% of disease-causing gene have an ortholog in zebrafish: even if they have evolutionarily separated more than 300 million years ago, humans and teleost fish shared several syntenic genomic region which allow the zebrafish to be an excellent connection bridge between invertebrate and vertebrates. In addition, given the two *whole genome duplication* rounds, taken place in teleost fish, the generation of paralogues gene copies have resulted into their subfunctionalization or neofunctionalization allowing the emergence of specific phenotypes when one of these is mutated (Sandve *et al*., 2018; Braasch *et al*., 2016).

1.3.3. Motoneurons development and muscle innervation in zebrafish embryos and larvae

Movement is the most common final output of nervous system (NS) activity and is essential for a broad range of animals' behaviors as feeding, breathing, swimming, procreating, escaping and survival. All these locomotor activities are generated by a complicate network of neurons known as central pattern generators (CPGs), located in the ventral nerve cord of invertebrates and in vertebrate's spinal cord (Grillner&El Manira, 2020). As discussed in paragraphs 1.1.3 and 1.3.1, animal models of human MNDs, mostly rodents, but also the fruit fly (*Drosophila melanogaster*) and the nematode (*C. elegans*), have been used in attempts to understand the neurobiological basis of MNDs and predict successful treatment strategies (Holmes *et al*., 2022; Bakkar *et al*., 2021; Tay *et al*., 2021; Ikenaka, Tsukada, Giles *et al*., 2019; Da Costa *et al*., 2014; Keil *et al*., 2014). Zebrafish is a vertebrate with a similar overall nervous system organization to humans and represents a powerful experimental model for studying neurogenic disorders and spinal cord or lower-level MNDs, due to the high conservation of genes implicated in neurodegenerative diseases and physiological processes involved in nervous system morphogenesis and maintenance (Bashirzade *et al*., 2022; Bandmann&Burton, 2010). In addition, in non-mammalians vertebrate like teleost fish, the NS is easily accessible for in-depht analysis of the neuronal circuit that on contrary cannot be achived in mammals.

Zebrafish spMNs are commonly divided into primary and secondary MNs classified based on their axonal trajectory and muscles innervation (Menelaou&McLean, 2012) (**Fig. 16**):

1. *caudal (CaP) primary motor neurons,* innervating the ventral trunk musculature;

2. *middle (MiP) primary motor neuron*, innervating the dorsal trunk musculature;
3. *rostral (RoP) primary motor neuron*, innervating the muscle fibers in between. They can be further divided in ventrally (vRoP) and dorsally (dRoP) projecting RoP MNs;
4. *variable (VaP) primary motor neuron*, innervating muscles in between MiP and RoP.

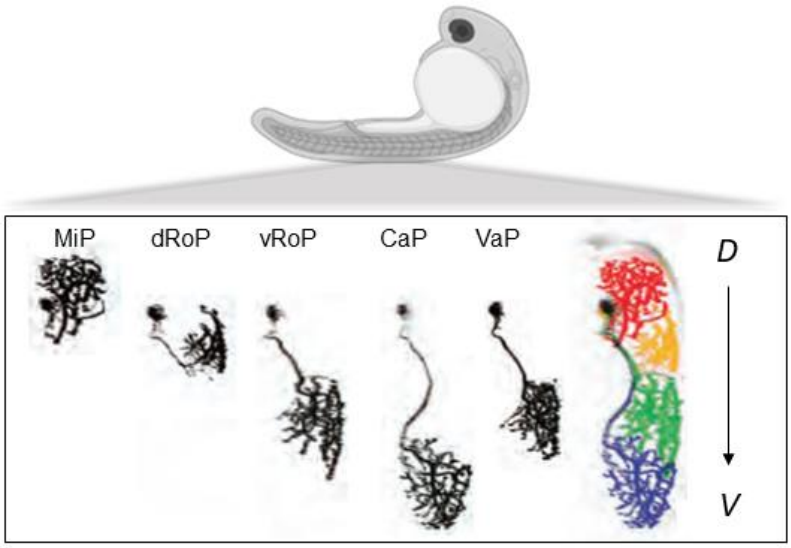

Fig. 16: Schematic illustrating zebrafish PMNs distribution in traverse view. Primary motor neurons and their innervation of epaxial (dorsal) and hypaxial (ventral) musculature. MiP, middle primary; dRoP, rostral primary, dorsally projection; vRoP, rostral primary, ventrally projection; CaP, caudal primary; VaP, variable primary. The distinct types delineate four epaxial and hypaxial muscle groups (color coded). Modified from Bello-Rojas *et al*., 2019. Icon source: Biorender.

Primary MNs (PMNs) appear during the gastrula period and undergo axogenesis since ~16 hpf, a process allowing to extend their neurite to the muscle targets by following trajectories delineated by specific molecules cues (Ye *et al*., 2019). On contrary, secondary MNs (SMNs), located more ventrally in the spinal motor column, born during the later stage of zebrafish embryogenic development and start extending their axon around 22-23 hpf by following the path established by PMNs (Menelaou&Svoboda, 2008). During embryonic development each differentiating neuron sends out their protruding axon which most distal portion, called the growth cone, is an extremely dynamic structure containing a network of not stabilized cytoskeletal MTs which leads the axon to quickly response to environmental changes and migrate to its target (Bashaw&Klein, 2010). Axon extension is permitted to the highly unstable MTs

encapsulated by the lamellipodia of the growth cone which by remodeling cytoskeletal MTs and actin filaments under the influence of specific signals, steered themselves as finger-like projections (filopodia) allowing such the exploration of the surrounding environment (Suter *et al*., 1998). This pathfinding process known as axonal guidance started at 16-24 hpf after that the axon of each PMNs grown along a common pathway, lateral to the notochord (a rod-like structure, located ventrally to the neural tube, providing mechanical and signaling cues to the developing vertebrate embryo), and reached the choice point at which the trajectories of each PMNs diverge according to their classification (Panzer *et al*., 2005). After a pause at the choice point, then they proceeded to innervate the medial surface of one myotomal fast muscle fibers (**Fig. 17 A** and **B**). Subsequently, axons branched extensively to innervate more lateral muscle fibers. Approximately 5 hours later, also SMNs extended their axons and reached their target represented by the most ventral fast muscle fibers (**Fig. 18**).

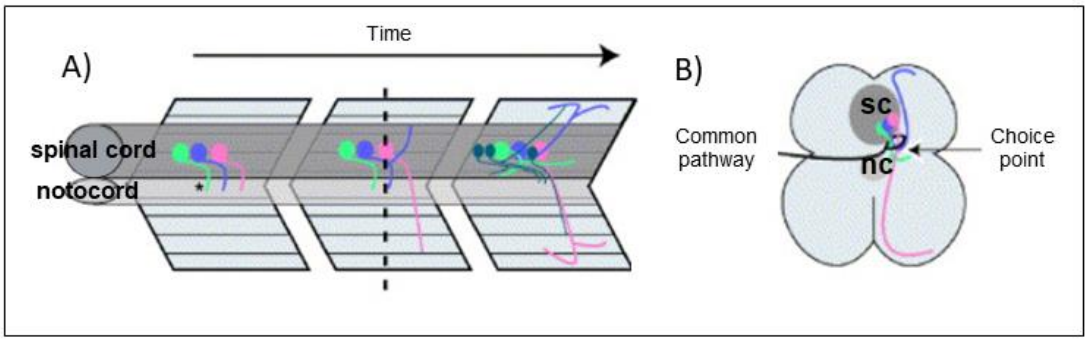

Fig 17: Schematic summary of the topography and muscles innervation of trunk spMNs in a zebrafish embryo. **A**) Timing routs traveled by each PMNs (CaPs, pink; MiP, blue; RoP, green) in a single myotomal segment. **B**) Cross-section of 24 hpf embryo shows the common pathway, choice point, and the projections of MiP and CaP PMNs. Images in panel (A) and (B) modified from Panzer *et al*., 2005.

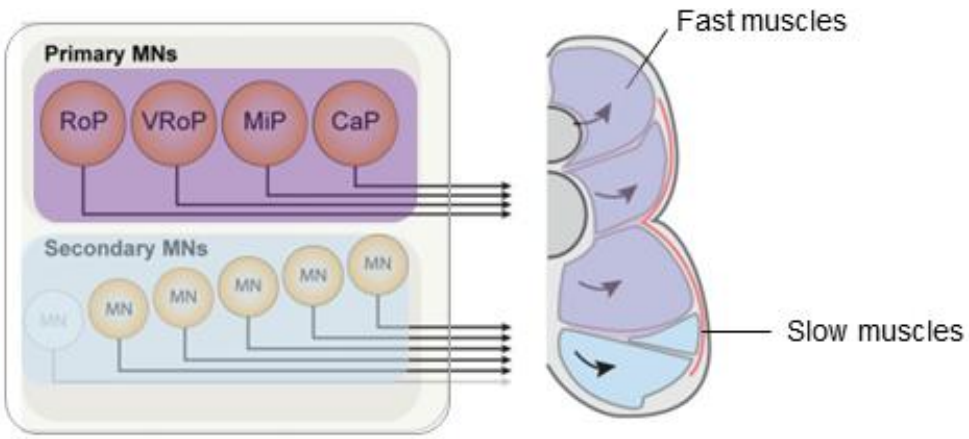

Fig 18: Additional schematics showing trunk sections with spMNs innervation in a zebrafish embryo. PMNs (purple) and SMNs (cyan) network innervation in zebrafish embryo/larvae. Modified from Berg *et al*., 2018.

Since Sperry proposed the chemoaffinity hypothesis (Sperry, 1962), which paved the way to find out the axon guidance molecules (AGMs), a series of genetic and biochemical screening identified a number of proteins which could actively attract or repel axons and, later, it was demonstrated their evolutionary conservation among invertebrates and vertebrates (Chilton, 2006; Tessier-Lavigne&Goodman, 1996). Thanks to a number of molecules, through the axonal guidance within 28 hpf each PMNs have reached its proper territory in the myotome and highly functional neuromuscular synapses, called neuromuscular junctions (NMJs), started forming closed to the choice point and then are formed adjacent to muscle pioneers fibers. NMJ represents a special type of synapse that mediate communication between the terminal end of a motor nerve and muscle cell and is composed by three main parts (Omar, Marwaha, Bollu, 2023) (**Fig. 19**):

1. a presynaptic terminal, rich in voltage-gated calcium channels and SNAP family proteins (*e.g.* syntaxins and synaptosomal-associated proteins) which mediate, together with synaptic vesicle proteins (*e.g.* synaptotagmins and synaptobrevins), the docking and fusion of synaptic vesicles (SV) with the nerve terminal's membrane following the arrival of an action potential. Each SV stores over 5000 molecules of acetylcholine (ACh) neurotransmitter that will be release into the synaptic cleft;
2. a synaptic cleft, the space between the nerve terminal and the plasma membrane of muscle. ACh released in the site interact with nicotinic ACh receptors (AChR) on the motor endplate;

3. a motor endplate (the post-synaptic element of NMJs), represented by the thickened portion of the muscle sarcolemma folded into depressions coated of AChRs. After the binding of neurotransmitter, sodium channels opened and the influx generates the endplate potential transmitted to the muscle membrane.

By 48 hpf, motor axons have extended lateral branches to create more NMJ contacts with multiple muscle fibers while the main axon shaft innervated the myosepta (a thin connective fascia separating myotomes from each other). At 72 hpf, motor axons have innervated the full extent of the lateral myosepta, and branching and NMJ number have extremely increased and exhibit a complex pattern organization and morphology (Panzer *et al*., 2005).

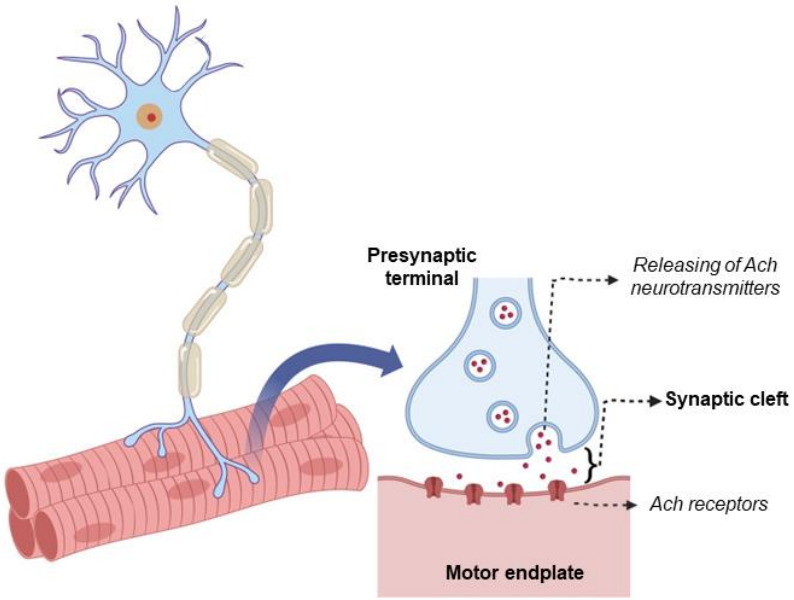

Fig. 19: Diagram of vertebrate neuromuscular junction structure. Modified from Singh&Patten, 2022.

In young zebrafish larvae and in adults (> 5dpf), motor neuron innervation becomes an intricate network of different MNs distributed along the length of each muscle fiber which are innervated by one PMNs and several MNs. On slow muscle fibers, NMJ appeared as small puncta while NMJ of the fast fibers appeared bigger. In addition, different interneurons (INs) cell populations, as the V2a interneurons, are required to support such high frequency behaviours through a fine-tuned alternation of vigorous (*i.e.* swimming or escape) versus slow movements (McLean and Fetcho, 2009).

1.3.4. Available tools to study neurological processes in zebrafish models of human motoneurons diseases

As mentioned, zebrafish is a fast expanding and powerful model system for studying vertebrate developmental biology, especially nervous system, providing multiple significant advantages over mammalian organisms such as mice (Sertori *et al*., 2016). The embryonic development is external, rapid and visually accessible; breeding females can lead to 50 to 100 eggs per mating providing available offspring which is crucial for genetic studies and experiments demanding large sample sizes (Veldman&Lin, 2008). Considering the potential and limitations of this organism (see paragraph 1.3.1), several advanced approaches of functional genomic (and precisely genetic engineering) offer the possibility to study unknown human gene's function and molecular mechanisms both in physiological and pathogenetic contexts in this vertebrate model. These include:

1. **Generation of transient knock-down (KD) mutant lines**: the microinjection of synthetic oligonucleotides antisense to endogenous mRNA (morpholino, MO) or synthetic mRNAs (mutagenized or not) into embryos at the single cell stage, is useful for evaluating the impact of ortholog genes reduction and overexpression on cell functionality during the early stages of model organism's embryonic development. This genetic manipulation technique is commonly used to investigate the function of a particular gene in the etiology of neurodevelopmental disorders. Gene expression can be downregulated in two different manners: 1) by avoiding the recognition of ATG start codon with the 40S ribosome subunit, such blocking protein translation effectively, 2) or interfering with the splicing process which could cause the DNA sequence's frame shift. However, in both cases the effect induced by MO or mRNA is temporary and dilutes rapidly over time (3-5 days in the first case; 2-3 in the second) limiting the temporal window in which is possible to appreciate late onset phenotypes. Teleost ancestors experienced a double round of whole-genome duplication events resulting in neofunctionalization/subfunctionalization of the paralogs that could mask mutant's phenotypes (or it could be present but with less severity as expected). This issue is extended also to stable knockout mutants (Stainier *et al*., 2017; Bill *et al*., 2009).
2. **Stable transgenic lines**: transgenesis approach has been developed to generate stable mutant lines and fluorescently labeled cell populations that can be studied

in disease models by introducing foreign small or large DNA fragments capable of expressing one or more gene of interest or to disrupt endogenous gene expression pattern. The integration of transgenes such as reporters into the genome enables to study tissutal/cellular changes *in vivo* occurring during the embryonic development by tracing the presence of the fluorescent protein encoded by the reporter transgene in the target cell. For instance, transgenic lines for neuronal lineage are widely used to trace neuron's sub-population (*e.g.* post-mitotic neurons and neuronal precursors) permitting to investigate and decipher the neuronal network development and interactions modalities (Kemmler *et al*., 2023). The most common system exploited for the generation of transgenic lines in zebrafish is the transposon system Tol2 consisting of two components, a transposon-donor plasmid carrying the construct to insert into the genome (and flanked by Tol2 specific-recombinant sites) and the synthetic mRNA encoding the transposase. Once microinjected into fertilized eggs, the Tol2 construct is excised from the donor plasmid and integrated into the genome also of the germ lineage during the embryonic development and transmitted to the next generation (Kawakami *et al*., 2016). In addition, the transgenesis can be paired with spatial-temporally controlled gene expression to investigate cell-type specific gene function within a molecular pathway in physiological condition using the bipartite system *UAS/Gal4* derived from the yeast. Briefly, Gal4 is a transcriptional factor (TF) which activates transcription of its target genes by binding to a specific *cis*-regulatory site called *Upstream Activating Sequence* (UAS). The two components of the system are carried in separate parental fish lines: in the driver line *gal4* gene is under the control of a tissue-specific promoter (*e.g. mnx1*) while in *UAS* responder line the gene of interest (*e.g.* fluorescent protein such as RFP, *red fluorescent protein*) in under *UAS* element control (Helpern *et al*., 2008). This system was implemented by Dr. F. Del Bene (Institut de La Vision, Paris) for the establishment of the transgenic fish line (*Tg*:(mnxGal4:HSP70/10UAS:lynRFP)) that I take advantage to study aberrant zebrafish MNs development in *tbce* transient model for my PhD thesis.

3. **CRISPR-Cas9 genome editing**: CRISPRs (*Clustered Regularly Interspaced Short Palindromic Repeat*) are palindromic repeated sequences interspersed in the genome of many bacteria and archaea, separated each other by DNA spacer sequences generated after bacteriophage's infection. Together with the different

Cas9 genes located in the same locus, thus it represents an RNA-mediative immune system adaptation which functions to protect the host cell (Xu&Zhanjun, 2020; Jinek *et al*., 2012). The RNA-guided endonuclease Cas9 induced a targeted double-strand DNA break (DBS) with the help of guide RNAs (gRNA), small ~20 bps (base pairs) synthetic nucleotide RNA, complementary to the genomic target sequence that have to be modified. In order to recognize and modify the target sequence, are required 1) the fully absence of mismatches between gRNAs and target, 2) the target sequence must be unique in the genome and 3) preceded by 3 nucleotide length PAM sequence (*Protospacer Adjacent Motif*, generally NGG sequence) necessary for the cleavage. During these years, PAM-less Cas-9 endonuclease have been engineered to increase the chance to reach more efficiently a subset of sequences hard to "hit" and never interested by previous genome editing technology such TALENs (*Nuclease Transcription Activator-like Effector*) (Walton *et al*., 2020). DNA cleavage can be repaired by the DNA repair cellular machinery repaired with the conservative Homologous Directed Repair (HDR) process which efficiency is unfavored than *Non-Homologous End-Joining* (NHEJ), especially in the early stages of embryonic development whose cells go from cell cycle's S-phase to M-phase rapidly and bypassing the cellular checkpoints that regulate the DNA structural integrity. Unfortunately, NHED is an error-prone repair machinery, and it is well established that it introduces small insertions/deletions (InDels) at the cleavage sites (Brinkman *et al*., 2018). Therefore, NHED method is widely used in zebrafish to introduce insertions and deletions. Genome editing (included CRISPR-Cas9 technology) can have limitations: 1) presence of off targets unintentionally contributing to the phenotype, 2) injected embryos are mosaics for the mutations in G0 and is necessary to cross these founders several times up to second/third generation to obtain a homogenous genetic background.

4. **Immunofluorescence assays (IF)**: belonging to the immunohistochemistry techniques, IF is a highly specific method based on an antigen-antibody immune reaction, used for the sub-cellular detection of proteins of interest present in the tissue or cells to be examined. To detect protein expression, the biological sample is incubated with an antibody specific to the protein of interest; the antibody may be coupled with a fluorophore (direct IF) or has to be detected by a secondary antibody conjugated to a fluorophore (indirect IF) and produced in a different

animal specimen from the one in which the primary has been produced (Joshi&Yu, 2017). This method is commonly used in zebrafish, for which have been implemented a conspicuous number of protocols based on the embryonic/larval stages and to the antigen of interest, for the evaluation of complementary spatio-temporal informations on gene expression pattern on fixed tissue or on whole embryos (Santos, Monteiro, Luzio, 2018). As all biochemical techniques, IF results hindered by limitation such as 1) photobleaching, a phenomenon preventing the optimal excitation of the fluorophore over the time due to its interaction with reactive oxygen species generated during confocal acquisition, 2) autofluorescence emitted by biological structures (*e.g.* the yolk in zebrafish embryos) resulting in a low signal-to-noise ratio and 3) non-specific staining (Santos, Monteiro, Luzio, 2018).

5. **Confocal imaging and super resolution microscopy**: collectively, microscopy techniques allow the microscopic observation of cellular preparations or whole fixed and living embryos, through which is possible to study morphological alterations (Weber&Koster, 2013). This method relies on the possibility to label cellular structures with one or multiple fluorophores, a molecule that can be excited to emit light, usually in the visible range, which is then captured by a photomultiplier that converts photons to electrical signal elaborated subsequently by a software. Fluorescent probes, such as synthetic vital dyes, antibodies conjugated with fluorophores, and the fluorescent proteins cell-type-specific expression in transgenic lines are widely used to investigate and trace cellular and molecular alterations occurring during the embryogenesis, in different background (*i.e. wild type* versus mutant) (Ko *et al*., 2011). The main advantage of optical microscopy is its noninvasive nature, as compared with other such as electronic ones. However, optical microscopy is limited in its spatial resolution: described by Ernst Karl Abbe, this limit assumed that the smallest resolvable distance between two points may never be smaller than the half the wavelength on the imaging light. This imply that the resolution of an image depends on the diameter of the light bundle, such the numerical aperture of the lens, and smaller beams will excite one fluorophore one per time creating high-resolved image (Lauterbach, 2012). However, in accordance to Abbe's law, laser beam can't be concentrated in a diameter less than 150 nm. The diffraction limit was considered unbreakable for long time until in the last two decades optical super resolution

techniques were developed. During the third year of my PhD internship at the Pediatric Hospital Bambino Gesù, I had the opportunity to learn more about STED (*STimulated Emission Depletion,* Abberior GmbH) *super resolution* microscopy whose functioning is used as exemplified model of this technology. The rational consisting in the illumination all fluorophores in a diameter of 150 nm and the decreasing of the number of active molecules at the same time with the scope to deactivate all the fluorophores external to a circle of 50 nm (4 time smaller than the excitation beam) actually obtaining the same effect if using a hypothetic laser with small diameter. To this aim, were implemented 1) specific objectives and lens with high numerical aperture and 2) double laser beams system. Briefly, superimposed on the normal excitation beam but concentric with it, an emptying donut-shape beam (at different wavelength with zero intensity in the center) moves along the surface of the sample and induce the deactivation of illuminated fluorophores thought a process called "stimulated emission collectively, microscopy techniques allow the microscopic observation of cellular preparations or whole fixed and living embryos, through which is possible to study morphological alterations (Weber&Koster, 2013). This method relies on the possibility to label cellular structures with one or multiple fluorophores, a molecule that can be excited to emit light, usually in the visible range, which is then captured by a photomultiplier that converts photons to electrical signal elaborated subsequently by a software. Fluorescent probes, such as synthetic vital dyes, antibodies conjugated with fluorophores, and the fluorescent proteins cell-type-specific expression in transgenic lines are widely used to investigate and trace cellular and molecular alterations occurring during the embryogenesis, in different background (*i.e. wild type* versus mutant) (Ko *et al*., 2011). The main advantage of optical microscopy is its noninvasive nature, as compared with other such as electronic ones. However, optical microscopy is limited in its spatial resolution: described by Ernst Karl Abbe, this limit assumed that the smallest resolvable distance between two points may never be smaller than the half the wavelength on the imaging light. This imply that the resolution of an image depends on the diameter of the light bundle, such the numerical aperture of the lens, and smaller beams will excite one fluorophore one per time creating high-resolved image (Lauterbach, 2012). However, in accordance to Abbe's law, laser beam can't be concentrated in a diameter less than 150 nm. The diffraction limit

was considered unbreakable for long time until in the last two decades optical super resolution techniques were developed. During the third year of my PhD internship at the Pediatric Hospital Bambino Gesù, I had the opportunity to learn more about STED (*STimulated Emission Depletion*, Abberior GmbH) *super resolution* microscopy whose functioning is used as exemplified model of this technology (Microscopy facility, under the guidance of Dr. A. Lauri). The rational consisting in the illumination all fluorophores in a diameter of 150 nm and the decreasing of the number of active molecules at the same time with the scope to deactivate all the fluorophores external to a circle of 50 nm (4 time smaller than the excitation beam) actually obtaining the same effect if using a hypothetic laser with small diameter. To this aim, were implemented 1) specific objectives and lens with high numerical aperture and 2) double laser beams system. Briefly, superimposed on the normal excitation beam but concentric with it, an emptying donut-shape beam (at different wavelength with zero intensity in the center) moves along the surface of the sample and induce the deactivation of illuminated fluorophores thought a process called "stimulated emission" with the result that only the molecules included in the donut-hole will emit fluorescence signals (Nieto-Garai *et al*., 2022; Roymahapatra&Sinha, 2014) (**Fig. 20**).

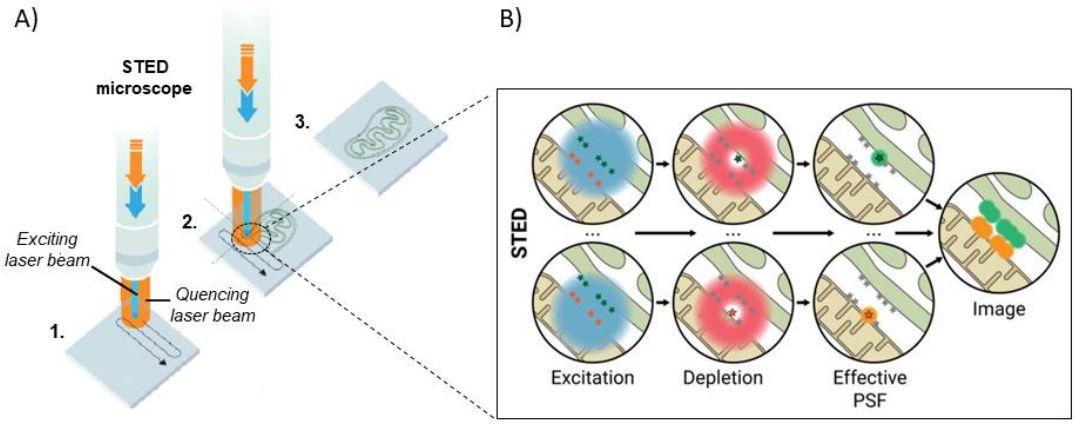

Fig. 20: Schematic representation of the principle of STED super resolution microscopy. A) In STED microscopy, annular laser beam quenches all fluorescence, except that in a nanometre-sized volume (1). The laser beam scan over the sample. Since scientists know exactly where the beam hits the sample, they can use that information to render the image a much higher resolution (2). The final image gets a resolution that is much greater than 200 nm. **B**) After a giving point is excited with the exciting beam (blue laser), a second high-intensity donut-shaped beam (red) is used to deplete all the fluorophores in the overlapping

zone. Only fluorophores in the centre of the donut (green and orange spots) will emit fluorescence. Image in panel (A) modified from Roymahapatra&Sinha, 2014; image in panel (B) modified from Nieto-Garai et al., 2022.

In summary, all the features listed so far make the zebrafish an excellent model organism to study human neurodevelopmental and neurodegenerative disorders, a broad group of conditions usually rare and clinically heterogeneous impairing the plasticity of the nervous system and behaviour of affected pediatric patients leading to intellectual disability, developmental delay, loss of motor-milestones, and limbs spasticity (Chia *et al*., 2022; Vaz *et al*., 2019). Last, to date, different zebrafish model for neurodevelopmental and neurodegenerative disorders carrying specific mutation in disease-causing genes are available; a subset of the main examples of zebrafish models of motor neuron diseases (MNDs) are listed in **Table 4**:

Known genetic alterations	Representative zebrafish model
Amyotrophic lateral sclerosis (ALS)	
C9ORF72 (#614260) ***SOD1 (#14750)*** ***TARDBP (#612069)*** ***FUS (#137070)***	• **Stable *C9orf72* LoF zebrafish model** (Butti *et al*., 2021): fish display motor defects, muscle atrophy, motor neuron loss and mortality in early larval and adult stages • **5'UTR and ATG start codon MO-mediated *C9orf72* KD in zebrafish** (Ciura *et al*., 2013): embryos show axonal motor neurons degeneration • **Stable model of *sod1* generated with TILLING engineering** (Da Costa *et al*., 2014): larvae/adults specimens display aberrant NMJs and a reduction in spMNs • **KO *tdp-43* zebrafish model** (Bose *et al*., 2019): mutants displayed gross

	morphological defects, early lethality, reduced locomotor function, aberrant NMJs architecture. • **MO-mediated *fus* LoF and R521H missense mutation gain of function models in zebrafish** (Kabashi *et al*., 2011): embryos showed locomotor defects and abnormal MNs projections.
Spinal muscular atrophy (SMA)	
SMN 1 (#600354) ***SMN 2 (#602595)***	• **Stable *smnΔ$^{1-14}$ and smnA6T^{ind27}*** (Tay *et al.*, 2021): smnA6T^{ind27} showed MNs loss and locomotor deficits later than the early-onset smnΔ$^{1-14}$ model. Also muscles morphology is altered. • **Stable miRNA-mediated KD *smn1* in zebrafish embryos** (Giacomotto *et al*., 2015): embryos expressing miRNA against *smn1* 3'UTR exhibit neuron abnormalities (short axons, abnormal branching, presence of pathfinding errors). • **ATG MO-mediate SMA zebrafish model** (McWhorter *et al*., 2003): Reduced smn protein levels in the developing embryo results in motor axon–specific truncations and branches, independent of motoneuron cell death.
Hereditary Spastic Paraplegia (HSP)	
	• **MO-mediated *spastin* (*spg4)* model** (Wood *et al*., 2006): morphants showed dramatic defects in motor axon outgrowth and NMJs impairment.

SPASTIN (#604277) ***ATLASTIN (#606439)*** ***KIF5A (#602821)*** ***ATAXIN 3 (#607047)***	• **MO-mediated *atl1* model** (Fassier *et al*., 2010): increased branching of spMNs and reduction larval mobility. • **Stable mutant kif5a model** (Campbell *et al*., 2015): embryos display sensory motor deficits, peripheral neuropathy, degeneration of sensory axon. • **Stable ataxin3-84Q mutant** (Watchon *et al*., 2017): larvae showed decreased MNs axonal length and deficient locomotion activities.

Table 4: A subset of growing list of motor neurons disorders (MNDs) and representative examples of MNDs-causing genes modelled in the vertebrate zebrafish model.

2. AIMS OF THE THESIS

My PhD project was part of a wider program at OPBG aimed at diagnosing and dissecting pathogenic mechanisms in orphan patients, primarily carried out by "Molecular Genetics and Functional Genomics" Research Unit. Specifically, I focused on the investigation of the functional impact of LoF of *TBCD* and *TBCE* genes caused by recently discovered missense variants, on motor neurons development, using *Danio rerio* (zebrafish) as *in vivo* model (**Fig. 21**).

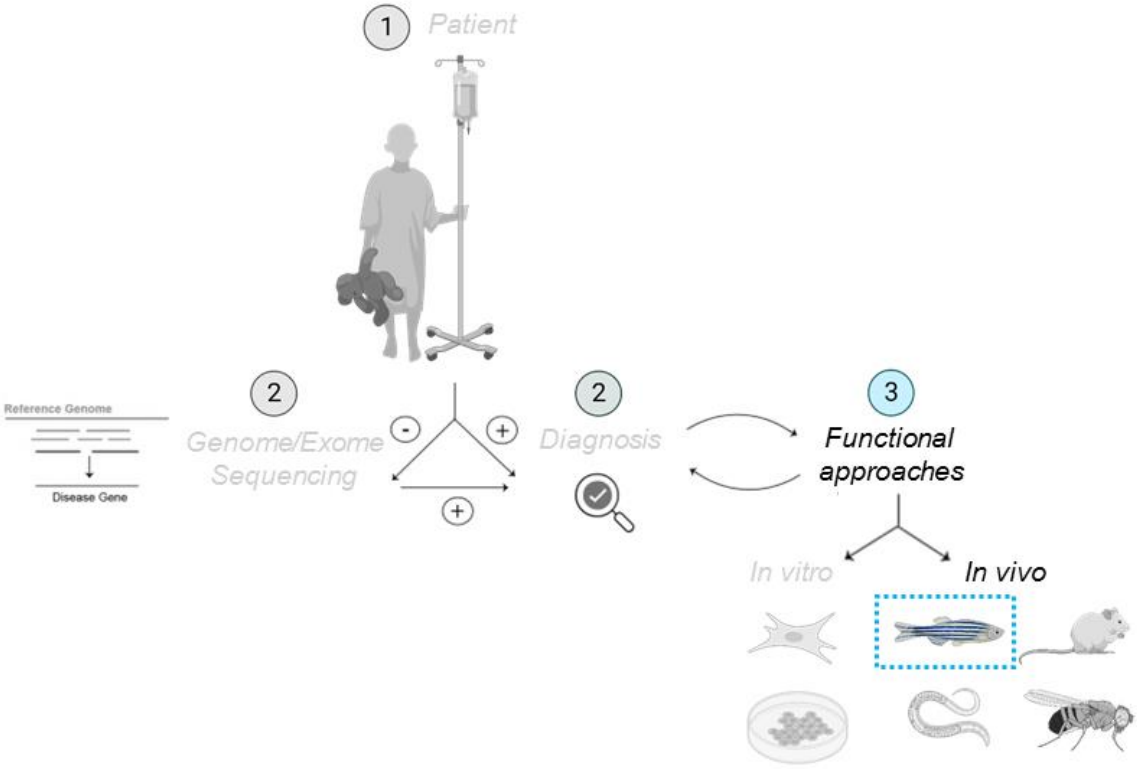

Fig. 21: **Schematic representation of the main focus of my PhD work**. The image is a representation of the general experimental workflow for the research and validation of new variants and causative-disease genes involved in undiagnosed rare disorders. The images are numbered to indicate the different steps of the workflow, starting from patient's clinical assessment up to the *in* vitro/*in vivo* validation. During my PhD project, I contribute to the point (3) with the scope to use zebrafish models (cyan rectangle) to investigate the impacts of *TBCD* and *TBCE* LoF mutations found in patients with complex encephalopathy showing motoneurons disease. Modified from Marwaha *et al*., 2022.

The initial characterization of zebrafish's orthologue genes was followed by experiments designed to generate transient models of *TBCD* and *TBCE* LoF and investigate motor

neurons morphology during development and initiate investigation of microtubules dynamics. The initial characterization of zebrafish's orthologue genes was followed by experiments designed to generate transient models of TBCD and TBCE LoF and investigate motor neurons morphology during development and initiate investigation of microtubules dynamics. To this aim, I have assessed *tbcd* and *tbce* morphant fish (animals treated with morpholino antisense oligonucleotides which temporally knockdown the gene expression by interfering with endogenous mRNA translation or splicing) and *tbcd* G0 crispant fish (crispants are "generation G0" CRISPR-Cas9 engineered organisms with stable genomic modifications such as deletions, insertions and substitutions of single nucleotides and/or entire gene portions within the genome enabling the gene function permanently. These modifications can be transmitted by next generations G1 up to G3). In details:

1. **Evaluation of TBCD and TBCE proteins in the orthologues species** via comparative analysis of 1) amino acids sequences, 2) protein domains and 3) protein sequence alignments using on-line free tools such as *Ensembl*, ExPasy Motif Scan, and *Clustal Omega* respectively. Following, I assessed the temporal expression of TBCD and TBCE proteins in zebrafish embryos collected at different developmental stages through semi-qualitative PCR (RT-PCR).
2. **Quantification of spMNs defects induced by decreasing dosages of TBCD and TBCE proteins** in transient and *tbcd* stable G0 crispant zebrafish model of disease. In details, alterations of motor neurons innervation patterns (*e.g.*, length of motor neurons formed, arborization, neuromuscular junctions, cytoskeleton morphology), proliferation and death rate in late spinal cord motor neurons were analyzed through confocal *imaging* and immunofluorescence (IHC) techniques.
3. **Preliminary investigation on microtubules increased stability as possible molecular mechanism of disease** assessed in early *tbcd* G0 crispant mutants using *super resolution* microscopy and IHC techniques.

Stable G3 KO mutants generation is currently ongoing by expert personnel to allow future longitudinal studies and pharmacological experimentation of MT destabilizing/stabilizing molecules, already promising for the treatment of various adult neurodegenerative diseases.

3. MATERIALS AND METHODS

3.1 Zebrafish husbandry

Danio rerio breeding and experimentation was performed in the OPBG fish animal facility under the guidance of specialized personnel. All animal experiments described in my PhD thesis, including both the housing and care of animals, were conducted in fish before the free feeding stage (5 days post fertilization) in accordance with ARRIVE guidelines (https://arriveguidelines.org) and 26/2014 regulation on animal experiments internally approved by the Italian Ministry of Health.

Adult zebrafish are kept in a water-circulating system (Tecniplast) under controlled conditions of light/dark cycle (14:10), water temperature (28 °C), osmolarity (350–400 μS) and pH (6.8–7.2) that ensure animal welfare (Westerfield, 2000). Fish are daily fed with dry and live food and paired when sexually matured to obtain eggs. Zebrafish embryos are kept in embryo medium under controlled temperature (28°C) and light-dark cycle (14:10) till use (live imaging or fixation).

3.1.1 Zebrafish breeding and embryos collecting

All experiments on live fish were conducted by experienced personnel resulting from fish mating occurring when a male and a female are housed in a special mating tank consisting in two separate compartments divided by a partition (**Fig. 22**).

Fig. 22: **Example of breeding tank**. From Tecniplast website.

Females have clearly visible big abdomen while males are slim and darker. After removing the partition, fish mating occurs and eggs dropped at the bottom of the tank through a grid are externally fertilized by sperm released in the water. After mating event, embryos are normally collected in Petri dishes, cultured in embryo medium containing (5M NaCl, 1M KCl, 1M $CaCl_2$, 1M $MgSO_4$) to prevent contamination and under controlled conditions. For each experiment described in my PhD thesis, embryos below 5dpf were collected at desired developmental stage according to Kimmel *et al*. (1995) classification (**Fig. 23**).

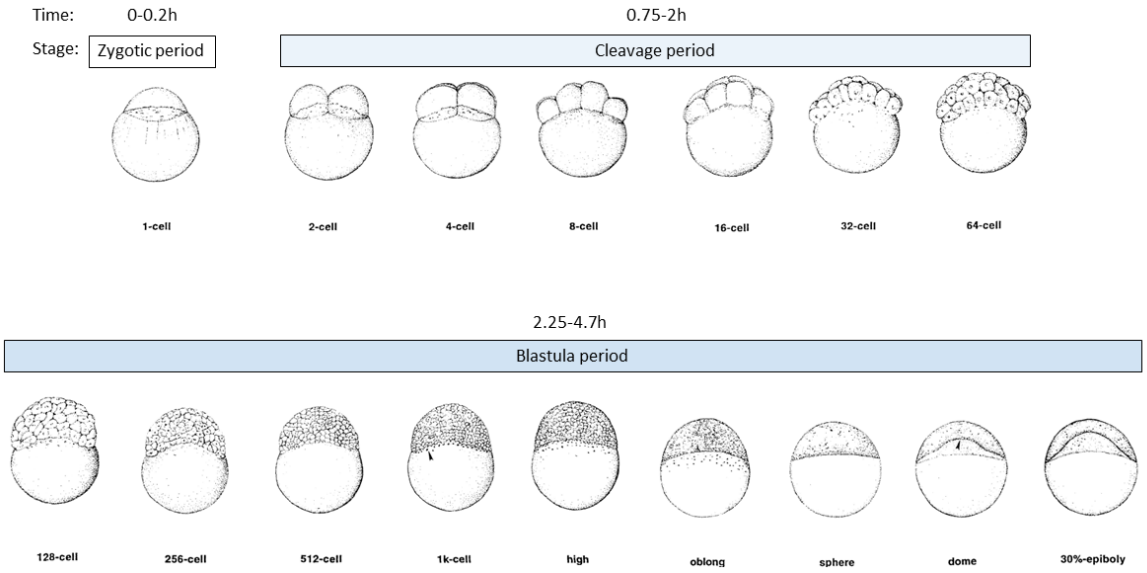

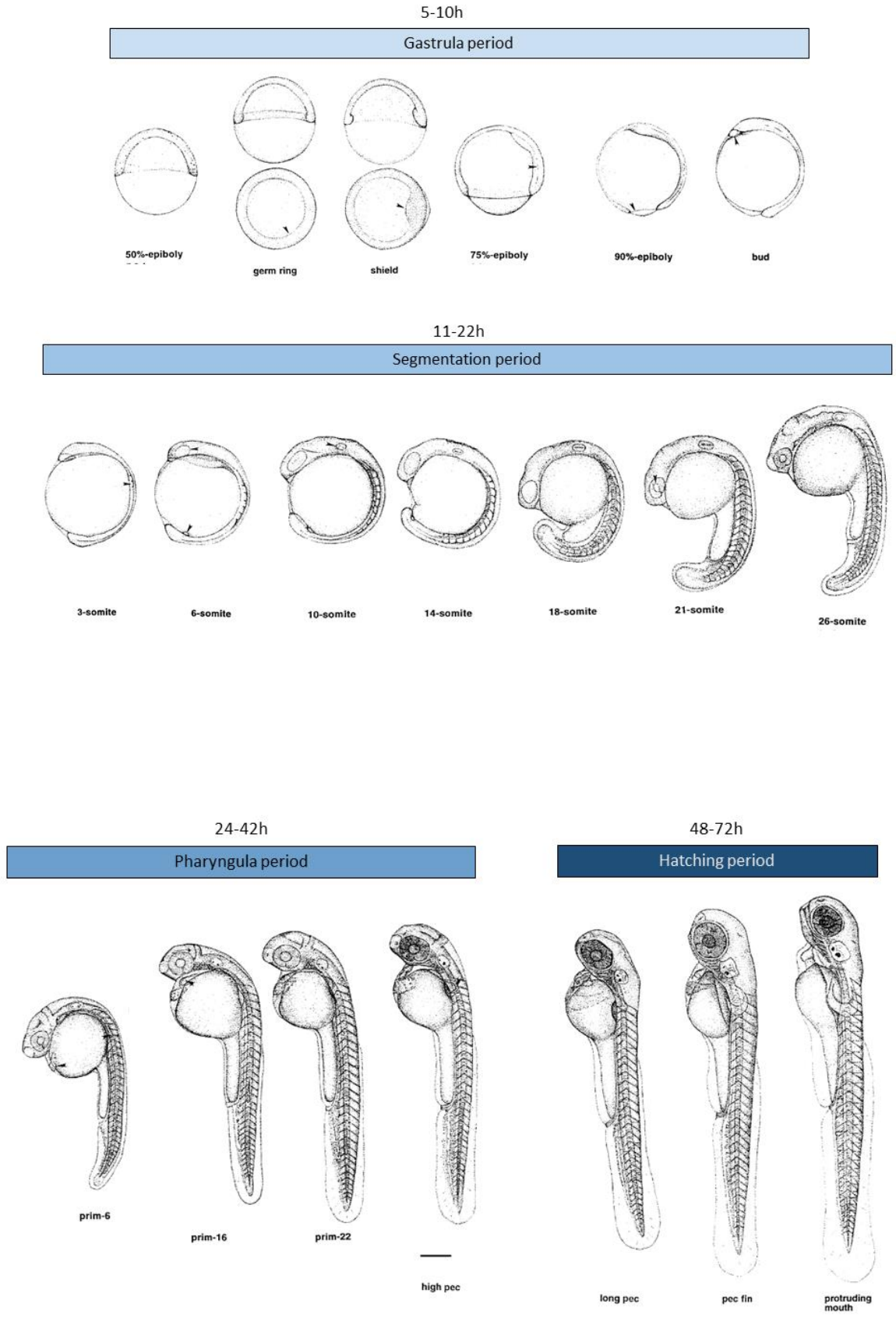

Fig. 23: **Schematic temporal diagram of zebrafish development** (modified from Kimmel *et al*., 1995).

3.2 RNA extraction from zebrafish embryos and morpholino validation

3.2.1 Sample collection for gene expression analysis, RNA extraction and cDNA synthesis

For the gene expression analysis of *tbcd* RNA transcripts during development, whole zebrafish embryos were collected at developmental stages from 2.5 to 96 hpf (*hours post fertilization*), and the tissue was stored at -80°C.

RNA extraction was performed using *TRIzol Reagent* (ThermoFisher) according to manufacturer's protocol. Briefly, embryos were homogenized in 500µl of TRIzol followed by the addition of 100µl of chloroform. Lysates were vortexed, incubated at R.T. and centrifuged for 15' at 4°C. Supernatants were collected, mixed 1:1 with phenol-acid chloroform and centrifuged at 4°C. Resultant supernatants were mixed with isopropanol (2 volumes), sodium acetate (1/10 volume, pH 5.2) and glycogen. Lysates were incubated at -20°C for at least and centrifugated at maximum speed. Next, RNA pellets were washed with cold EtOH 70%/H_2O DEPC, centrifuged for 5' and resuspended in H_2O DEPC. Total RNA was quantified by *Tecan Infinity M Plex* (i-Control 2.0 program) spectrophotometer and RNA quality (RIN) was assessed by Bioanalyzer RNA 6000 Nano assay according to manufacturer's protocol.

The cDNA synthesis for 9, 12, 15, 18, 24, 48, 72 and 96 hpf stages was performed using *Superscript VILO Kit* (ThermoFisher) follow manufacturer's instructions. Alternatively, cDNA synthesis for earlier stages (2.5, 4 and 6hpf) was performed using *QuantiTect Reverse Transcription Kit* (Qiagen) according to manufacturer's protocol. Newly synthetized cDNA samples were stored at -80°C for downstream applications.

3.2.2 Whole embryos RNA extraction and cDNA synthesis from knock-down *tbcd* morphants

Zebrafish *tbcd knock-down* models (morphants), generated by Dr. A. Lauri e Dr. G. Fasano, were collected at 48 hpf and stored at -80°C. The RNA extraction and cDNA synthesis were performed as previously described in paragraph 3.2.1.

For the assessment of precise sizing and quantification of *tbcd* RNA transcripts generated by MO-mediated approach, cDNA of control and morphant samples were assessed by

4200 TapeStation electrophoresis system (Agilent) using *Agilent RNA ScreenTape System* according to manufacturer's manual.

3.2.3 Amplification and Sanger sequencing of *tbcd* PCR fragments from zebrafish morphants

To evaluate the mRNA expression of *tbcd* and *tbce* genes during the development (from embryo early stages to 4 days post fertilization), RT-PCR was performed at different time points of zebrafish embryo development. Specific primers were designed with a melting temperature (TM) from 56 to 57°C and specific size of amplicon of ~ 500 pair of bases (bps) (**Table 5**). The expression of genes of interest were normalized to those of a house-keeping gene, *elongation factor 1 alpha* (*elf-α*). The quality of the primers was assessed *in silico* using online free tools:

- NEB Tm Calculator on-line free tool (https://tmcalculator.neb.com/#!/main)
- NCBI Primer-Blast (https://www.ncbi.nlm.nih.gov/tools/primer-blast/)

Primer	Sequence	Tm	Fragment length
tbce_FW	TGGCGTGTGGTAAATGAGCT	56.3°C	318bps
tbce_RV	CTTAGCTCGCCCTCATCTGG	56.6°C	
tbcd_FW	CATTGGCAGCGTTGTGTTGG	57.4°C	532bps
tbcd_RV	ACCAGCAATGTCACGTCCAT	56.3°C	
elfαFW	CTTCTCAGGCTGACTGTGC	57°C	500bps
elfαRV	CCGCTAGCATTACCCTCC	57°C	

Table 5: List of oligonucleotides used to perform the RT-PCR of zebrafish *tbcd*, *tbce* and *elf-α* genes.

The cDNA obtained from collected stages (see paragraph 3.2.1) was amplified using *GoTaq Green Master Mix DNA Polymerase* (Promega, Cat. N° M7122) following the protocol listed below (**Table 6**):

Component	**25µl reaction**	**Final Concentration**
GoTaq Green Master Mix, 2X	12,5µl	1X
Forward primer, 10µM	2.5µl	1µM
Reverse primer, 10µM	2.5µl	1µM
cDNA template	2µl (*tbcd*) 1µl (*tbce*)	< 250ng
H_2O Nuclease Free	up to 25µl	-

Table 6: GoTaq Green Master Mix DNA polymerase reaction mix.

Under Dr. A. Lauri guidance the specific PCR program (**Table 7**) was used to increase the specificity of amplification reaction as shown below. The correct size of RT-PCR *tbcd* and *tbce* amplicons was verified using 1% agarose electrophoretic gel and images acquired with *Alliance Mini HD9* (Uvitec).

tbcd:

Step	Temperature	Time
Initial denaturation	95°C	2 minutes
30 cycles	95°C 66°C-64°C-62°C 72°C	30 sec-1 minute 35 seconds 1 minute/kb
Final extension	72°C	5 minutes
Hold	4-10°C	∞

tbce:

Step	Temperature	Time
Initial denaturation	95°C	2 minutes
30 cycles	95°C 67°C-65°C-63°C 72°C	30 sec-1 minute 35 seconds 1 minute/kb
Final extension	72°C	5 minutes
Hold	4-10°C	∞

elf-α:

Step	Temperature	Time
Initial denaturation	95°C	2 minutes
30 cycles	95°C 64°C-62°C-60°C 72°C	30 sec-1 minute 35 seconds 10 seconds

Final extension	72°C	3 minutes
Hold	4-10°C	∞

Table 7: Cycling programs of GoTaq Green Master Mix DNA Polymerase used to amplify zebrafish *tbcd*, *tbce* and *elf-α* gene respectively.

3.2.4 Validation of the efficiency of MOss2 morpholino targeting *tbcd* splice site via RT-PCR

To evaluate the effect of splice-site morpholino (ssMO) on injected zebrafish embryos, consisting in *tbcd* exon-skipping or intron retention, we designed specific primers for zebrafish *tbcd* gene upstream exon 1 and downstream exon 5 (**Table 8**). The expected size of amplicon, *in silico* calculated, was 570 bps.

Primer	Sequence	Tm	Fragment length
TBCDFL F1	ATGTCCGTGATGGAGGGTG	65°C	575 bps
TBCDRW	AGAAAGGACTTGGCAACCTCCAG	56.6°C	

Table 8: List of primers used to amplify zebrafish *tbcd* gene from control and morphants cDNA.

PCR reaction was carried out using *Q5 High-Fidelity DNA Polymerase* (NEB), whose PCR reaction protocol and cycling program are descripted as follows (**Table 9 A-B**):

A)

Component	25µl reaction	Final Concentration
5x Q5 Reaction Buffer	5µl	1X
10 mM dNTPs	0.5µl	200µM
10µM Forward primer	1.25µl	0.5µM
10µM Reverse primer	1.25µl	0.5µM
cDNA template	0.8µl (*tbcd*)	< 1.000ng
Q5 High-Fidelity DNA Polymerase	0.25µl	0.02U/µl
H_2O Nuclease Free	up to 25µl	-

B)

Step	Temperature	Time
Initial denaturation	98°C	30 seconds
30 cycles	98°C 64°C-62°C-60°C 72°C	5-10 seconds 10-30 seconds 20-30 seconds/kb
Final extension	72°C	2 minutes
Hold	4-10°C	∞

Table 9: A) *Q5 High-Fidelity DNA Polymerase* reaction and **B)** cycling program.

PCR reactions were run on 1.8% agarose gel and images acquired with *Alliance Mini HD9* (Uvitec) to evaluate the presence of *tbcd* amplicons compatible to an intron retention or exon skipping in *tbcd* ssMO-injected zebrafish embryos. The presence of 570 bps amplicon allowed us to consider the exon 2 skipping as target effect of ssMO on injected zebrafish embryos. Bands were manually excised from the gel and purified with *Monarch DNA Gel Extraction Kit* (NEB) following manufacturer's instruction. PCR's amplicons quantity and quality were analysed using *Tecan Infinite M Plex*. Only samples with optimal absorbance ratio range around 1.8-2.0 at 280/260nm and 1.8-2.2 at 260/230nm were considered acceptable for the next application. To validate the sequence of amplicons, Sanger's sequence reaction was performed with *BigDye™ Terminator v3.1 Cycle Sequencing Kit* (Applied Biosystem) as descripted in **Table 10**:

A)

Component	**20µl reaction**
Big Dye® Terminator 5X Sequencing Buffer	3 µl
Primer 10 µM (forward or reverse)*	1.3 µl
BigDye® Terminator v3.1	1.2 µl
Template	X µl (final concentr. 100 ng/µl)
Nuclease free H_2O	Up to 20 µl

B)

Step	**Temperature**	**Time**
Initial denaturation	96°C	1 minute
25 cycles	96°C 55°C 60°C	15 seconds 5 seconds 4 minutes
Hold	4-10°C	∞

Table 10: **A**) Preparation of Sanger's sequencing PCR reaction mix and **B**) the relative optimized thermal cycler program. *the primers used are listed in the Table 8.

Sequences of *tbcd* amplicons obtained by Sanger's sequencing were then aligned with the entire coding sequence (CDS) of zebrafish *tbcd* reference sequence (https://www.ensembl.org/Danio_rerio/Transcript/Sequence_cDNA?db=core;g=ENSDARG00000098749;r=3:48234445-48327160;t=ENSDART00000161419) using the on-line free tool Benchling (Biology Software, 2023, retrieved from benchling.com) and validate independently by two expert researchers.

3.3 Phenotypic analysis in zebrafish *tbcd* and *tbce* morphants

Control embryos (not injected, not inj), *tbcd* or *tbce* MO-injected embryos and embryos co-injected with *tbcd/tbce* MO and *wild type* form of *tbcd/tbce* were grown until 48 hpf in multi-well plates and checked daily to evaluate embryo survival and gross phenotype. For the detailed analysis, see Results section at Chapter 4. Bright-field images of pooled embryos were acquired at *Leica M205FA* multidimensional fluorescence stereomicroscope.

3.4 Fluorescent immunohistochemistry (IHC) on whole mount zebrafish embryos (morphants and crispants)

Immunohistochemistry (IHC) is a valuable tool to identify the spatial protein expression of specific markers taking advantage of a specific immunological antigen-antibody interaction in tissue fixed at desired stage of development (Corthell, 2014). In our zebrafish models, we used this technique to investigate the expression profile of proteins such as synaptotagmin 2b, Synaptic Vesicle 2A (SV2A), Islet 1/2, β-tubulin and detyrosinated tubulin to label motoneurons primary axon, pre-synaptic vesicles at neuromuscular junction, neuron stem cell, microtubules and their stable conformation (specifically recognizing α-tubulin monomer without a tyrosine group), respectively. The whole procedure, which takes around 3-4 days, was carried out using the following monoclonal/polyclonal primary antibodies:

1. Anti-synaptotagmin 2b isoform (syt2b), produced in mouse (Developmental Studies of Hybridoma Bank, DSHB, znp1);
2. Anti-Synaptic Vesicle 2A (SV2A), produced in mouse (DSHB, SV2);
3. Anti-Islet 1/2 (Genetex), produced in rabbit;

4. Anti-β-tubulin (DSHB), produced in mouse;
5. Anti-detyrosinated tubulin (Merck), produced in rabbit.

To resolve anatomical structure such as muscle fibers and NMJ, conjugate-toxins such as Phalloidin-594 (ThermoFisher) and α-bungarotoxin (α-BTX, ThermoFisher) were combined to the antibodies listed above. Secondary antibodies, conjugated to specific fluorophores, were chosen depending on the species in which the primary antibodies were produced.

Before setting up any immunological reactions, the following steps have been performed:

1. Collection of the embryos at the desired stage, as described in paragraph 3.1.1;
2. dechorionation of the embryos;
3. fixation in paraformaldehyde (PFA) 4%/PBS1X at R.T. for 3h;
4. serial washes with washing buffer (*i.e.* PBS-Triton 0.8%) and storage in fresh PBS1X at 4°C (or in MetOH 100% at -20°C).

All zebrafish samples processed by *whole mount* immunofluorescence were mounted laterally on imaging glass slides and acquired with *Leica Stellaris 5 DM6* microscope with 10X dry or 25X water immersion objectives. Below protocols implemented for our IHC purposes are reported.

3.4.1 Labeling motoneurons innervation and muscles morphology with anti-synaptotagmin Syt2b (znp-1) antibody and phalloidin

1. Bleach samples with bleaching solution (KOH 10%, H_2O_2 30%, H_2O) at R.T. until complete skin depigmentation,
2. perform serial washes in washing buffer (PBS-Triton 0.8%),
3. incubate the samples in PBS-Triton 2% at R.T. for 1 hour and half,
4. incubate the embryos O.N. with phallodin (1:20), at 4°C,
5. wash with washing buffer,
6. incubate samples in Roche Blocking Buffer 1X (BB1X, Roche) with mouse anti-syt2b AbI (znp-1, 1:100) O.N. at 4°C,
7. perform several washes with PBS-Triton 0.8%,
8. incubate samples in BB1X with goat anti-mouse Alexa Fluor 488 (ThermoFisher,1:1000), O.N at 4°C,

9. perform in sequence several washes with PBS-Triton 0.8%,
10. wash samples with glycerol increasing scale up to 80%,
11. store samples in glycerol 80%/PBS1X at 4°C.

3.4.2 Labeling neuromuscular junctions with anti-SV2A antibody and α-BTX

1. Wash embryos with PBS-Triton 0.8%,
2. incubate embryos in cold acetone on ice,
3. wash with H_2O,
4. incubate embryos in collagenase/H_2O (1 mg/ml) for 20 minutes at R.T.,
5. wash embryos and then incubate in blocking solution (5% normal goat serum, 1% BSA, 1% DMSO, 0.1% PBS-Tween20, 0.8% PBS-Triton 0.8%) with mouse anti-SV2A (1:150) and α-BTX Alexa Fluor 488 (1:100), O.N,. at 4°C,
6. wash embryos with PBS-Triton 0.8%,
7. incubate in blocking solution with goat anti-mouse Alexa Fluor 633 (ThermoFisher; 1:1000), O.N. at 4°C,
8. perform washes with PBS-Triton 0.8%,
9. wash samples with glycerol increasing scale up to 80%,
10. store samples in glycerol 80%/PBS1X at 4°C.

3.4.3 Labeling specific MT classes with anti-β tubulin and detyrosinated tubulin antibodies

1. Bleach samples at R.T. as described at 3.5.1,
2. wash embryos with PBS-Triton 0.8%,
3. incubate samples in 10mM Sodium Citrate dihydrate (pH = 6.0), 15’ at 85°C,
4. wash embryos and permeabilize the tissue with Proteinase K (Sigma-Aldrich; 1:1000), at R.T. for 40’,
5. briefly wash embryos and then fix with PFA 4%/PBS1X for 20’ at R.T.,
6. wash the embryos and incubate in blocking solution (5% normal goat serum, 1% BSA, 1% DMSO, 0.1% PBS-Tween20, PBS-Triton 0.8%) with mouse anti-β tubulin (1:100) and rabbit anti-detyrosinated tubulin (1:200), O.N at 4°C,

7. wash embryos and incubate in blocking solution with goat anti-rabbit Star Orange (Abberior; 1:200) and goat anti-mouse Star Red (Abberior; 1:200), O.N at 4°C,
8. perform in sequence several washes with washing buffer,
9. wash samples with glycerol increasing scale up to 80%,
10. store samples in glycerol 80%/PBS1X at 4°C.

Zebrafish *tbcd* G0 crispants were mounted in Abberior Mounting Media and acquired with Abberior 2D STEDYCON microscope (with Dr. Antonella Lauri and Dr. Stefania Petrini from OPBG and Dr. Frédéric Eghiaian, Abberior GmbH; Dr. Alessanddro Rossi, Crisel Instruments) with 100X oil immersion objective.

3.4.4 Labeling cell death and motor neurons soma with anti-islet antibody and TUNEL staining

We followed these steps:

1. Rehydrate samples in decreasing scale of MetOH,
2. briefly wash samples and then perform bleaching at R.T.,
3. wash embryos with PBS-Triton 0.5-0.8%
4. incubate samples in Proteinase K solution (1:1000) for 20' at R.T.,
5. wash samples and then incubate in In Situ Cell Death Detection Kit-TM Red (Roche, Cat. N° 12156792910) reaction solution prepared by following manufacturer's instructions,
6. wash samples in PBS-Triton 0.5-0.8% and then block in blocking solution with mouse anti-islet (1:100), O.N at 4°C,
7. wash embryos and then incubate in blocking solution with goat anti-mouse Alexa Fluor 488, O.N at 4°C,
8. perform in sequence several washes with washing buffer
9. wash samples with glycerol increasing scale up to 80%,
10. Store samples in glycerol 80%/PBS1X at 4°C.

3.5 Data analysis

Raw images of zebrafish motoneurons and muscles were evaluated with free download Fiji ImageJ program (Schindelin, Arganda-Carreras, Frise *et al*, 2012) and 3D reconstruction IMARIS software (v.9.5).

Data were analyzed independently by Dr. A. Lauri and me and statistical assessments were performed using GraphPad software v.9. Normality tests (Shapiro–Wilk and Kolmogorov–Smirnov tests) were run to assess data normal distribution. Parametric data with more experimental groups were analyzed using Two-way ANOVA test, while non-parametric data were analyzed using Kruskal–Wallis test with appropriate *post hoc* test. Survival rate analysis was assessed by Log-Rank (Mantel-Cox) test. Phenotypic penetrance of embryos (crispant G0 and morphants zebrafish models) was analyzed by two-sided Chi-square's test in a 2x2 contingency table. For * p-value $\leq$ 0.05, ** p-value $\leq$ 0.01, *** p-value $\leq$ 0.001. **** p-value $\leq$ 0.0001 (Mishra *et al*., 2019, Ghasemi&Zahediasl, 2012).

4. RESULTS

4.1 Characterization of zebrafish orthologs of TBCD and TBCE and phenotyping in zebrafish transient loss of function models

4.1.1 High TBCD and TBCE a.a. sequence conservation in zebrafish and expression of zebrafish orthologs during different embryonic stages

For their initial characterization of *tbcd* and *tbce* in zebrafish I analysed the conservation of amino acids residues with respect to human TBCD and TBCE orthologues, focusing on the core sequence regions affected by human mutations. From emerging comparative studies in eukaryotes, we know that both TBCE and TBCD are characterized by β- and α-tubulin binding sites, which are necessary for the biogenesis and maintenance of cytoskeletric microtubules (MTs) dynamics. In addition, the cofactors are predicted to have a GTPase activator activity responsible of tubulin hydrolysis and playing a key role in MTs growing and shrinking phases (Serna *et al*., 2015; Grynberg *et al*., 2003; Tian *et al*., 1999). No specific fish paralogs of *tbcd* and *tbce* genes resulted from ZFIN database (The Zebrafish Information Network; *tbcd* ZFIN ID: ZDB-GENE-060823-1; *tbce* ZFIN ID: ZDB-GENE-051030-120) and Ensembl database (Ensembl Genome Browser 109 (Feb 2023); *tbcd* ENSEMBL ID: ENSDARG00000098749, chromosome 3; *tbce* ENSEMBL ID: ENSDARG00000099921, chromosome 11). Thereby, using the free on-line tool *Clustal Omega* (v. 1.2.4) *Multiple Sequence Alignment,* I evaluated the amino acids residues conservation in TBCD and TBCE ortholog proteins. I then used *ExPasy Motif Scan* to predict recognizable protein's structural motifs and domains. The analysis revealed a high degree of amino acids residues conservation between human and zebrafish TBCD and TBCE proteins respectively (**Fig. 23 A-D**). For TBCD mutations causing a neurodevelopmental/neurodegenerative condition in humans are found all along the sequence and many of these mutations, in homozygous or found as compound heterozygous, have been linked to cortical dysgenesis (Caputo *et al*., 2023; Chen *et al*., 2021; Liao *et al*., 2020; Tian *et al*., 2019; Grønborg *et al*., 2018; Zhang *et al*., 2018; Pode-Shakked *et al*., 2017; Edvardson *et al*., 2016; Flex *et al*., 2016; Sferra *et al*., 2016). The figure also shows the amino acids sequence stretch corresponding to exon 9 (green rectangle in **Fig. 23 B**), targeted by gRNAs used to generate stable zebrafish *tbcd* knockout (KO) model (by Dr. A. Lauri, see Results, paragraph 4.2.2).

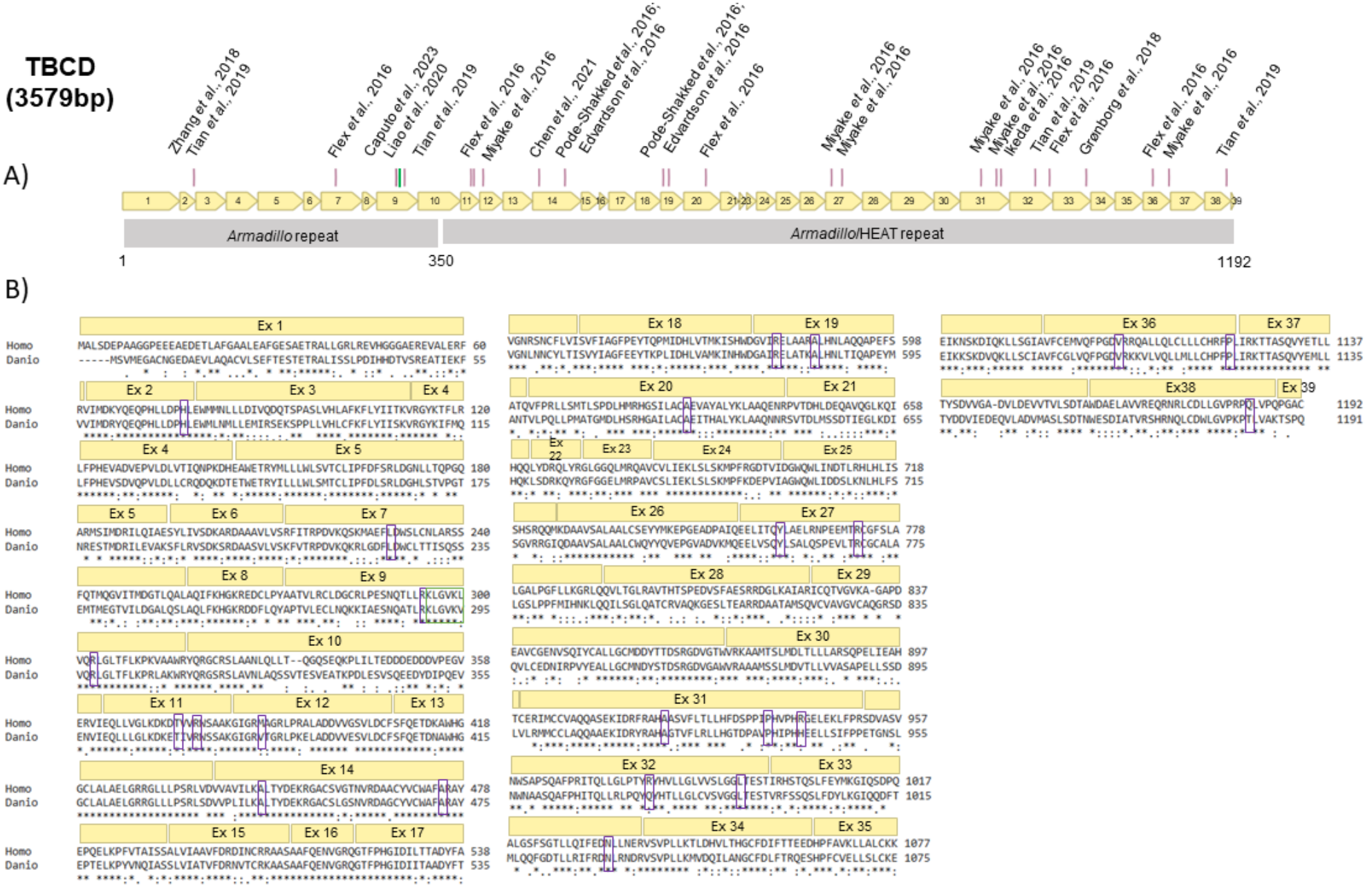
TBCD
(3579bp)
A)
Zhang et al., 2018
Tian et al., 2019
Flex et al., 2016
Caputo et al., 2023
Liao et al., 2020
Tian et al., 2019
Flex et al., 2016
Myake et al., 2016
Chen et al., 2021
Pode-Shakked et al., 2016
Edvardson et al., 2016
Pode-Shakked et al., 2016
Edvardson et al., 2016
Flex et al., 2016
Myake et al., 2016
Myake et al., 2016
Myake et al., 2016
Ikeda et al., 2016
Tian et al., 2019
Flex et al., 2016
Grønborg et al., 2018
Flex et al., 2016
Myake et al., 2016
Tian et al., 2019
1 2 3 4 5 6 7 8 9 10 11 12 13 14 15 16 17 18 19 20 21 23 24 25 26 27 28 29 30 31 32 33 34 35 36 37 38 39
Armadillo repeat
Armadillo/HEAT repeat
1
350
1192
B)
Ex 1
Ex 2
Ex 3
Ex 4
Ex 5
Ex 6
Ex 7
Ex 8
Ex 9
Ex 10
Ex 11
Ex 12
Ex 13
Ex 14
Ex 15
Ex 16
Ex 17
Ex 18
Ex 19
Ex 20
Ex 21
Ex 22
Ex 23
Ex 24
Ex 25
Ex 26
Ex 27
Ex 28
Ex 29
Ex 30
Ex 31
Ex 32
Ex 33
Ex 34
Ex 35
Ex 36
Ex 37
Ex38
Ex 39
Homo MALSDEPAAGGPEEEAEDETLAFGAALEAFGESAETRALLGRLREVHGGGAEREVALERF 60
Danio -----MSVMEGACNGEDAEVLAQACVLSEFTESTETRALISSLPDIHHDTVSREATIEKF 55
Homo RVIMDKYQEQPHLLDPHLEWMMNLLLDIVQDQTSPASLVHLAFKFLYIITKVRGYKTFLR 120
Danio VVIMDRYQEQPHLLDPHLEWMLNMLLEMIRSEKSPPLLVHLCFKFLYIISKVRGYKIFMQ 115
Homo LFPHEVADVEPVLDLVTIQNPKDHEAWETRYMLLLWLSVTCLIPFDFSRLDGNLLTQPGQ 180
Danio LFPHEVSDVQPVLDLLCRQDQKDTETWETRYILLLWLSMTCLIPFDLSRLDGHLSTVPGT 175
Homo ARMSIMDRILQIAESYLIVSDKARDAAAVLVSRFITRPDVKQSKMAEFLDWSLCNLARSS 240
Danio NRESTMDRILEVAKSFLRVSDKSRDAASVLVSKFVTRPDVKQKRLGDFLDWCLTTISQSS 235
Homo FQTMQGVITMDGTLQALAQIFKHGKREDCLPYAATVLRCLDGCRLPESNQTLLRKLGVKL 300
Danio EMTMEGTVILDGALQSLAQLFKHGKRDDFLQYAPTVLECLNQKKIAESNQATLRKLGVKV 295
Homo VQRLGLTFLKPKVAAWRYQRGCRSLAANLQLLT--QGQSEQKPLILTEDDDEDDDVPEGV 358
Danio VQRLGLTFLKPRLAKWRYQRGSRSLAVNLAQSSVTESVEATKPDLESVSQEEDYDIPQEV 355
Homo ERVIEQLLVGLKDKDTVVRNSAAKGIGRMAGRLPRALADDVVGSVLDCFSFQETDKAWHG 418
Danio ENVIEQLLLGLKDKETIVRNSSAKGIGRVTGRLPKELADDVVESVLDCFSFQETDNAWHG 415
Homo GCLALAELGRRGLLLPSRLVDVVAVILKALTYDEKRGACSVGTNVRDAACYVCWAFARAY 478
Danio GCLALAELGRRGLLLPSRLSDVVPLILKALTYDEKRGACSLGSNVRDAGCYVCWAFARAY 475
Homo EPQELKPFVTAISSALVIAAVFDRDINCRRAASAAFQENVGRQGTFPHGIDILTTADYFA 538
Danio EPTELKPYVNQIASSLVIATVFDRNVTCRKAASAAFQENVGRQGTFPHGIDIITAADYFT 535
VGNRSNCFLVISVFIAGFPEYTQPMIDHLVTMKISHWDGVIRELAARALHNLAQQAPEFS 598
VGNLNNCYLTISVYIAGFEEYTKPLIDHLVAMKINHWDGAIRELATKALHNLTIQAPEYM 595
ATQVFPRLLSMTLSPDLHMRHGSILACAEVAYALYKLAAQENRPVTDHLDEQAVQGLKQI 658
ANTVLPQLLPMATGMDLHSRHGAILACAEITHALYKLAAQNNRSVTDLMSSDTIEGLKDI 655
HQQLYDRQLYRGLGGQLMRQAVCVLIEKLSLSKMPFRGDTVIDGWQWLINDTLRHLHLIS 718
HQKLSDRKQYRGFGGELMRPAVCSLIEKLSLSKMPFKDEPVIAGWQWLIDDSLKNLHLFS 715
SHSRQQMKDAAVSALAALCSEYYMKEPGEADPAIQEELITQVLAELRNPEEMTRCGFSLA 778
SGVRRGIQDAAVSALAALCWQYYQVEPGVADVKMQEELVSQVLSALQSPEVLTRCGCALA 775
LGALPGFLLKGRLQQVLTGLRAVTHTSPEDVSFAESRRDGLKAIARICQTVGVKA-GAPD 837
LGSLPPFMIHNKLQQILSGLQATCRVAQKGESLTEARRDAATAMSQVCVAVGVCAQGRSD 835
EAVCGENVSQIYCALLGCMDDYTTDSRGDVGTWVRKAAMTSLMDLTLLLARSQPELIEAH 897
QVLCEDNIRPVYEALLGCMNDYSTDSRGDVGAWVRAAAMSSLMDVTLLVVASAPELLSSD 895
TCERIMCCVAQQASEKIDRFRAHAASVFLTLLHFDSPPIPHVPHRGELEKLFPRSDVASV 957
LVLRMMCCLAQQAAEKIDRYRAHAGTVFLRLLHGTDPAVPHIPHHEELLSIFPPETGNSL 955
NWSAPSQAFPRITQLLGLPTYRVHVLLGLVVSLGGLTESTIRHSTQSLFEYMKGIQSDPQ 1017
NWNAASQAFPHITQLLRLPQYQVHTLLGLCVSVGGLTESTVRFSSQSLFDYLKGIQQDFT 1015
ALGSFSGTLLQIFEDNLLNERVSVPLLKTLDHVLTHGCFDIFTTEEDHPFAVKLLALCKK 1077
MLQQFGDTLLRIFRDNLRNDRVSVPLLKMVDQILANGCFDLFTRQESHPFCVELLSLCKE 1075
EIKNSKDIQKLLSGIAVFCEMVQFPGDVRRQALLQLCLLLCHRFPLIRKTTASQVYETLL 1137
EIKKSKDVQKLLSCIAVFCGLVQFPGDVRKKVLVQLLMLLCHPFPLIRKTTASQVYEMLL 1135
TYSDVVGA-DVLDEVVTVLSDTAWDAELAVVREQRNRLCDLLGVPRPQLVPQPGAC 1192
TYDDVIEDEQVLADVMASLSDTNWESDIATVRSHRNQLCDWLGVPKPTLVAKTSPQ 1191

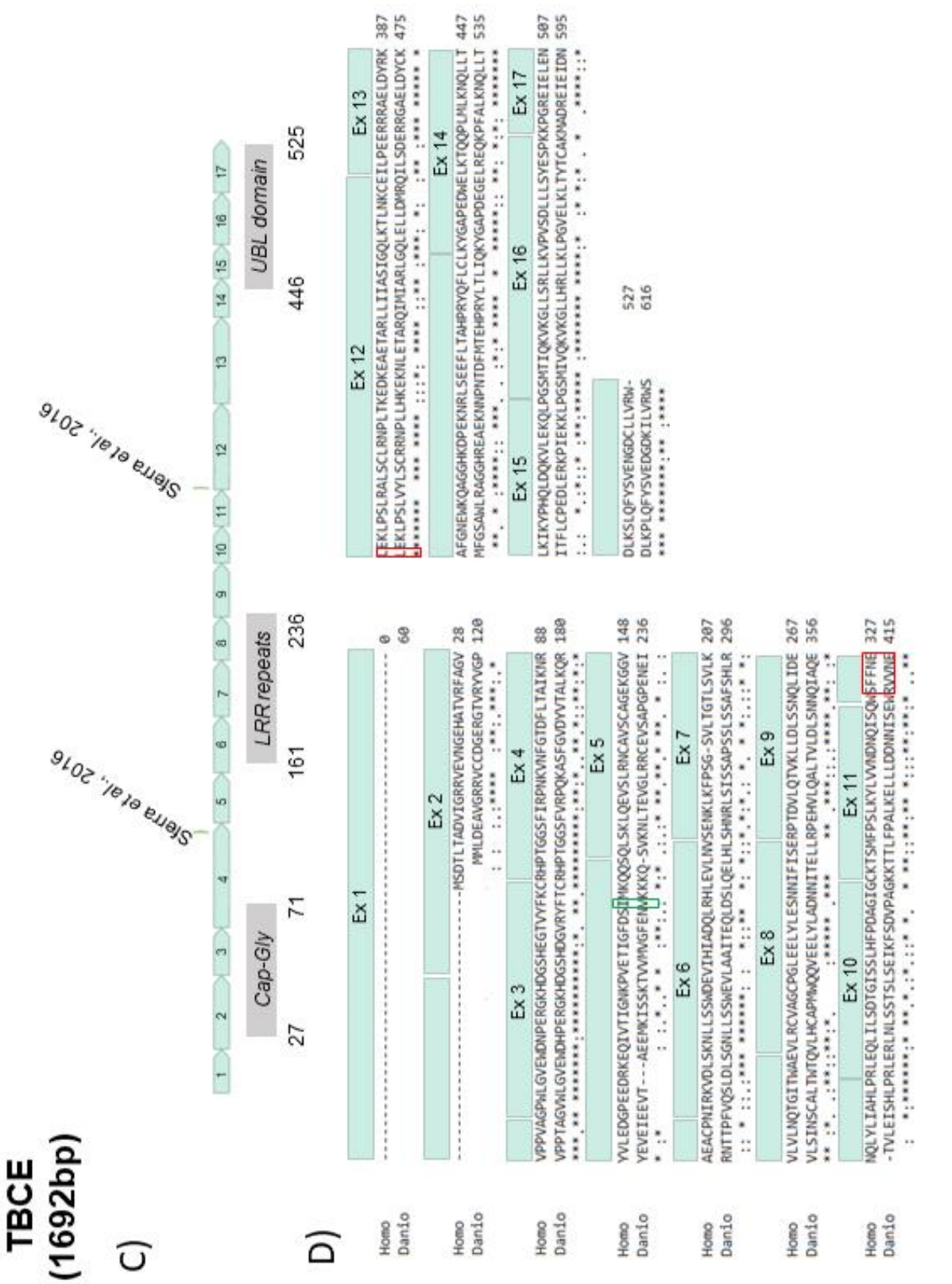

Fig. 23: **Multiple alignment of TBCD and TBCE in human and zebrafish. A**) Exon sequence of TBCD gene and relative protein's domains. Purple lines indicate a subset of *TBCD* mutations reported in literature. **B**) Purple rectangles showed the amino acids residues conserved and altered in TBCD pediatric subjects.

Green rectangle showed a partial amino acids sequence relative to exon 9 targeted by gRNAs to establish zebrafish *tbcd* KO stable line. **C**) Exon sequence of *TBCE* gene and relative protein's domains. Purple pipes indicated *TBCE* gene mutations reported in literature. **D**) Green and red rectangles showed the amino acids residues conserved and altered in TBCE pediatric subjects. Alignment was performed with *Clustal Omega* (v. 1.2.4) *Multiple Sequence Alignment*. Protein motifs prediction was performed with *ExPasy Motif Scan.* Abbreviation: Ex, exon.

Starting from this evidence, in order to define the time window of *tbcd* and *tbce* expressions, necessary to interpret the phenotype caused by *tbcd* and *tbce* transient LoF, I carried out semi-quantitative RT-PCR (*Reverse Transcription Coupled to the Polymerase Chain Reaction*) analysis starting from the cDNA retrotranscribed from RNA collected at different stages of zebrafish embryonic development. As shown in **Fig. 24**, zebrafish orthologs *tbcd* and *tbce* are already expressed from earliest embryogenesis phases (2.5-6 hpf), included the period in which primary motoneurons are being developed (9-18 hpf).

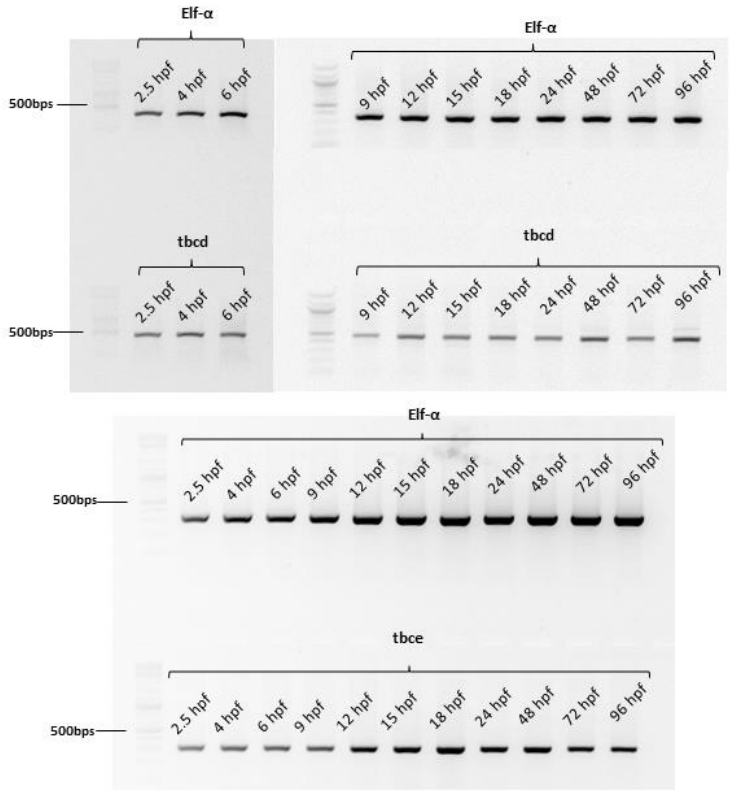

Fig. 24: ***tbcd* and *tbce* temporal expression profiles during zebrafish development**. Semiquantitative RT-PCR of *tbcd* and *tbce* in comparison with gene *elf-α* used as internal house-keeping control. hpf, hours post-fertilization; bps, base pairs.

4.1.2 Phenotype characterization of *tbcd* and *tbce* zebrafish morphants

In the context of a general laboratory effort, the generation of *tbcd* and *tbce* transient LoF models in zebrafish was conceived and carried through a double approach consisting in the microinjection of synthetic antisense oligonucleotides (morpholino, MO) in biological replicates in 1-cell stage embryos (**Fig. 25**).

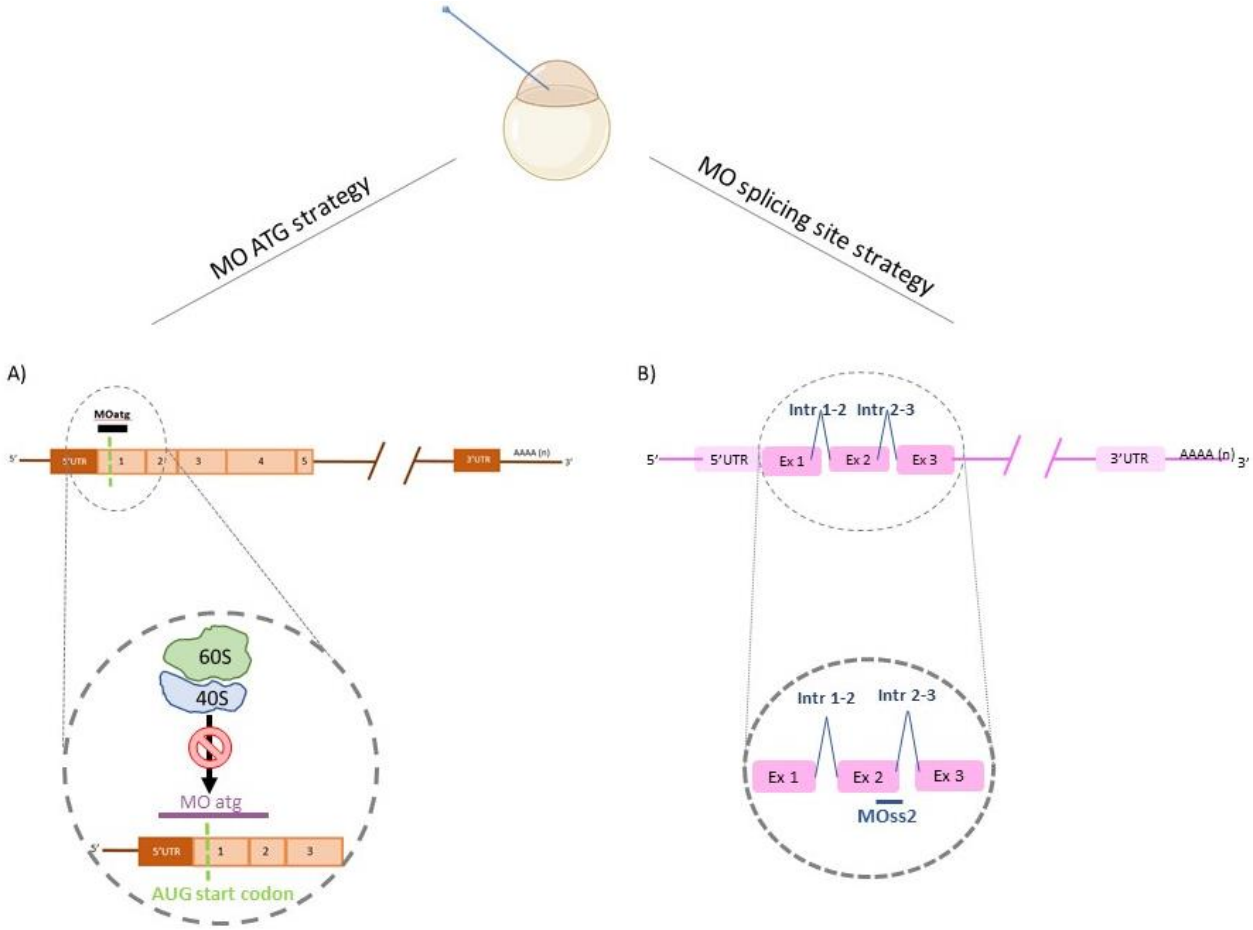

Fig. 25: **General scheme of microinjection of different morpholinos (MO) against *tbcd* in zebrafish 1-cell stage embryos**. **A**) Target sequence of ATG-morpholino (MO atg) used designed at the ATG start codon. **B**) Target sequence of splice site morpholino 2 (MOss2) used designed at the splice junction upstream and downstream exon 2 respectively. Icon source: Biorender.

After the microinjection of *tbcd* and *tbce* morpholino (MO) into 1-cell stage zebrafish embryos (Dr. A. Lauri), I actively participated in the experiments carried out to investigate of the impact of downregulation of these tubulin chaperone cofactors during development (stage of 24 and 48 hpf) using the not injected siblings as internal controls. The first parameter analyzed was the embryos survival rate that was checked at both embryonic stage for each injection experiment. From this analysis, it was revealed that *tbcd* MOss2

morphants showed a milder dose-dependent survival compared to not injected controls (**Figure 26 A**). On contrary, the downregulation of zebrafish endogenous *tbce* mRNA with MO 5'UTR ATG determined a significant lower survival rate in dose-dependent manner (**Figure 26 B**).

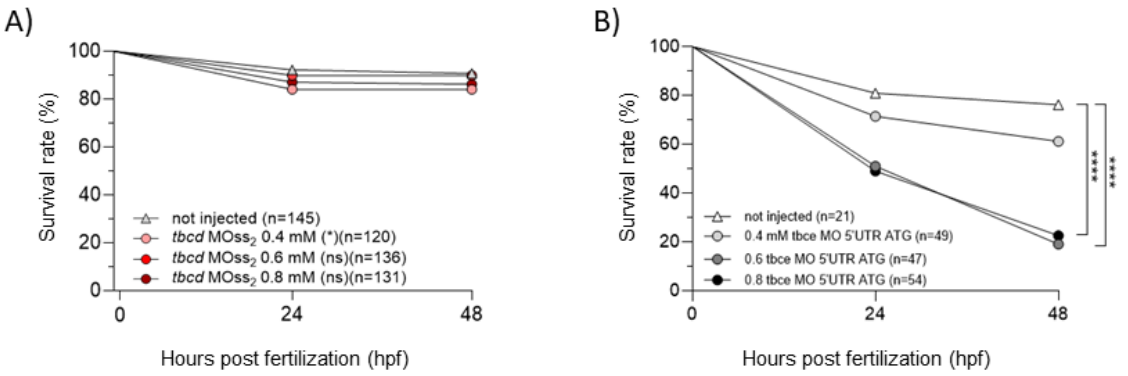

Fig. 26: **Survival rate expressed in percentage in *tbcd* MOss2 and *tbce* 5'UTR ATG transient LoF models**. **A**) The survival rate in *tbcd* MOss2 morphants indicates a milder dose-dependent effect on survival rate (* p-value <0.05) while **B**) in *tbce* 5'UTR ATG model the survival rate decreased in relation to the concentration of morpholino 5'UTR ATG microinjected (**** p-value <0.0001). Log-rank (Mantel-Cox) test. Data analyzed with Dr. Giulia Fasano.

From this analysis, it was revealed that *tbcd* MOss2 morphants showed a milder dose-dependent survival compared to not injected controls (**Figure 26 A**). On contrary, the downregulation of zebrafish endogenous *tbce* mRNA with MO 5'UTR ATG determined a significant lower survival rate in dose-dependent manner (**Figure 26 B**). The differences in survival observed (**Fig. 26**) between both transient models could be linked to the milder effects induced by altering the mRNA splicing event (which do not alter the reading frame in our *tbcd* model) instead preventing the protein translation. Therefore, to exclude the hypothesis that the reported effects are due to the different protocol used, independently from this PhD work, expert personnel in the lab have generated a *tbcd* 5' UTR ATG morphant model in which it was not observed an increase in mortality rate compared to *tbcd* MOss2 morphant. In this model the phenotypes classes also appeared fairly similar (these data are now shown here as they do not belong to this PhD work). Further evidence of *tbcd* LoF-dependent effects are enforced and supported by crispant G0 whose survival

rate does not differ significally from MOss2 (see paragraph 4.2.2, **Fig. 34 A**). On the basis of these preliminary evidence, it seems that during embryogenesis TBCD LoF is more tolerated than TBCE LoF. This hypothesis could be further tested in the future, using complementary genetic approaches.

Next, based on the observed alterations of the trunk and tail morphology (**Figure 27 A and D**), we classified the gross phenotype of embryos in three classes for tbcd morphants and four classes for tbce morphants respectively, resumed in **Table 11** below:

A) *tbcd* MOss2:

CLASS NAME	PHENOTYPE OBSERVED
Normal	Normal body length and no visible curvatures, as in not injected controls
Mild	Delayed and/or curved tail
Severe	Severely curved and malformed tail

B) *tbce* MO-5' UTR ATG:

CLASS NAME	PHENOTYPE OBSERVED
Normal	Normal body length and no visible curvatures, as in not injected controls
Mild	Mildly tail curvature
Moderate 1	Curly (tail with single/multiple curvature points) and malformed tail
Moderate 2	Curly and short tail
Severe	Extremely short tail (no tail)

Table 11: **List of distinct phenotypes of zebrafish *tbcd* and *tbce* morphants observed at 48hpf induced to the downregulation of endogenous tbcd and tbce mRNAs *knock-down***.

The morphological analysis showed a statistically alteration of trunk morphology at 48 hpf in both *tbcd* and *tbce* transient models. In detail, *tbcd* MOss2 morphants show a higher incidence of mild phenotype than control siblings and partially rescued with the microinjection of $TBCD^{WT}$ mRNA (**Fig. 27 B-C**). On the other hand, a strong dose-

dependent effect was observed in *tbce* LoF morphants with higher percentages of severe phenotypes. Also, in this case, the rescue of worsen phenotypes was observed when human $TBCE^{WT}$ mRNA was injected (**Fig. 27 E-F**).

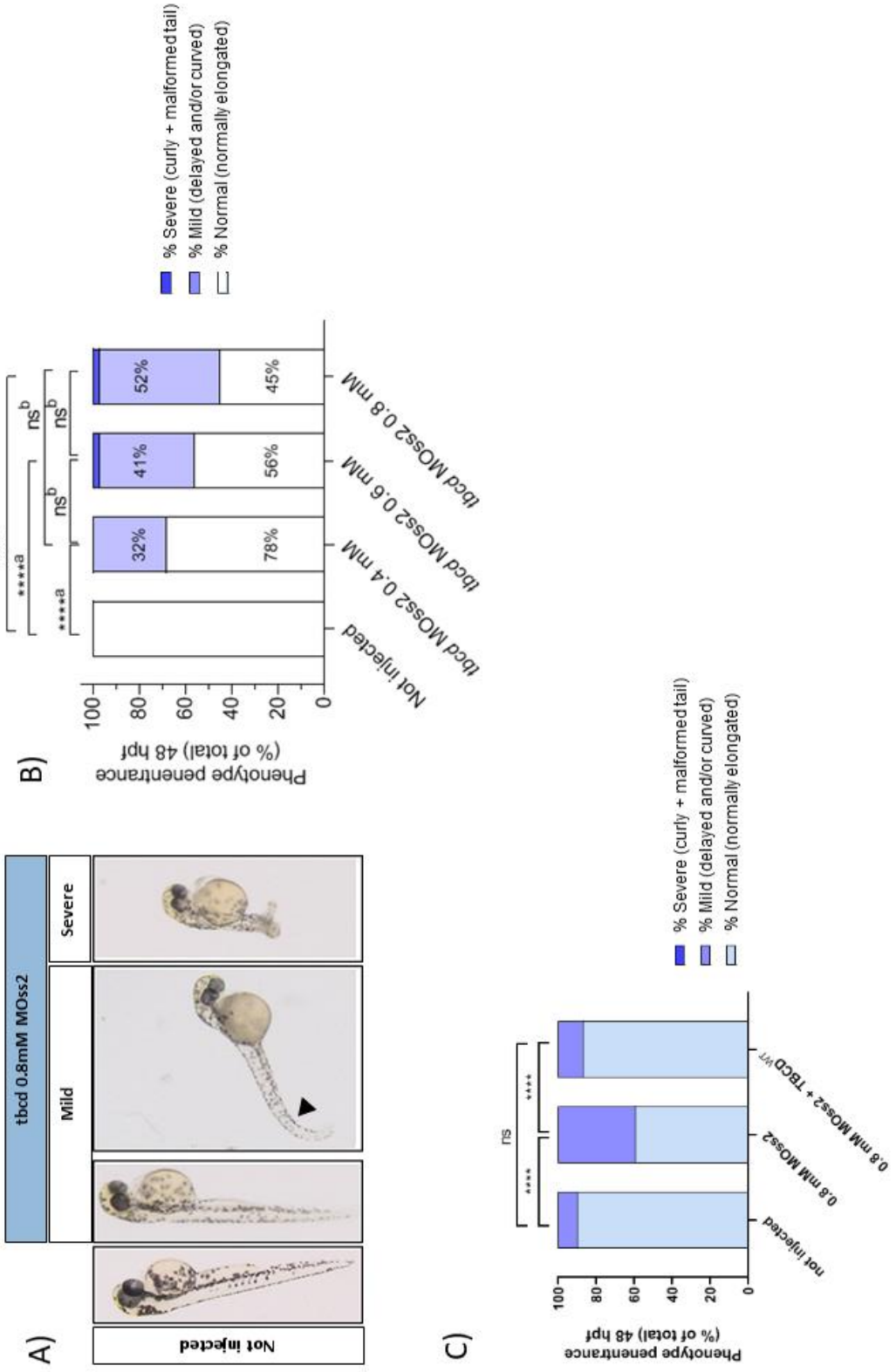

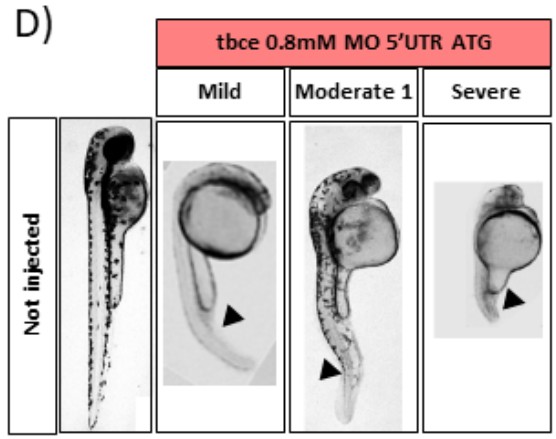
D)
tbce 0.8mM MO 5'UTR ATG
Mild
Moderate 1
Severe
Not injected

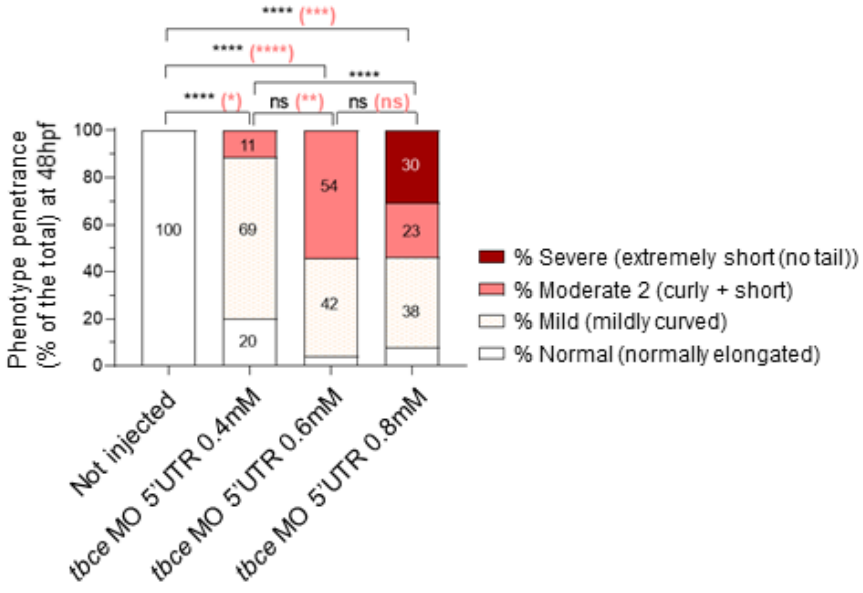
E)
Phenotype penetrance (% of the total) at 48hpf
100
80
60
40
20
0
**** (***)
**** (****)
**** (*)
ns (**)
ns (ns)
****
100
11
69
20
54
42
30
23
38
Not injected
tbce MO 5'UTR 0.4mM
tbce MO 5'UTR 0.6mM
tbce MO 5'UTR 0.8mM
% Severe (extremely short (no tail))
% Moderate 2 (curly + short)
% Mild (mildly curved)
% Normal (normally elongated)

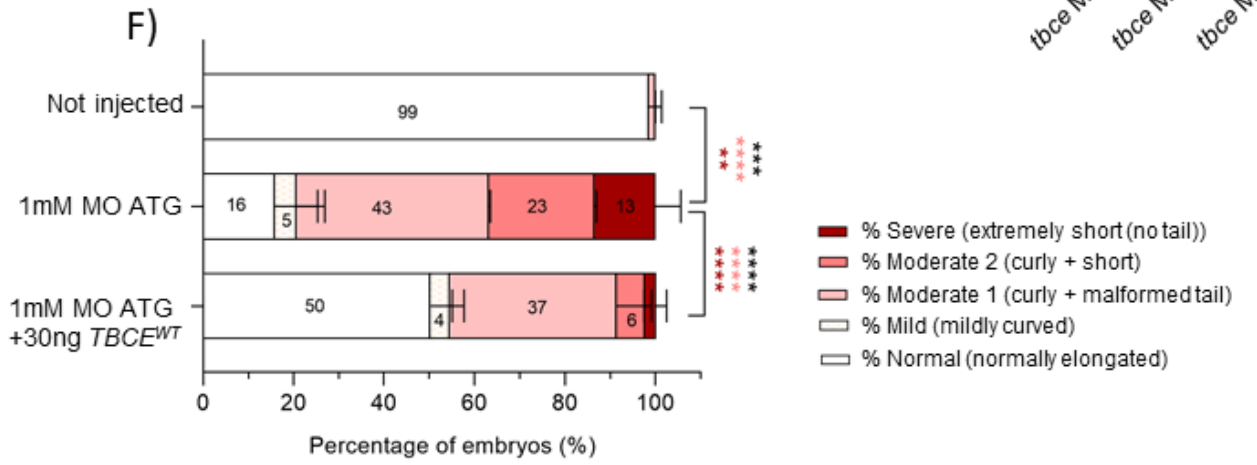
F)
Not injected
1mM MO ATG
1mM MO ATG
+30ng TBCE^WT
99
16
5
43
23
13
50
4
37
6
0
20
40
60
80
100
Percentage of embryos (%)
% Severe (extremely short (no tail))
% Moderate 2 (curly + short)
% Moderate 1 (curly + malformed tail)
% Mild (mildly curved)
% Normal (normally elongated)

Fig. 27: **Bright-fields images of representative *tbcd* and *tbce* LoF transient model embryos (morphants)**. **A**) *tbcd* morphants embryos showed three different classes of phenotypes (normal, mild and severe) as explained in the main text. **B**) Phenotypic penetrance analysis of zebrafish *tbcd* MOss2 embryos at 48 hpf at different concentration of morpholino splicing site 2 showed a specific *tbcd* dose-dependent response. **C**) Rescue of milder phenotype in zebrafish *tbcd* MOss2 embryos at 48 hpf with 50ng of $TBCD^{WT}$. **D**) *tbce* morphants embryos showed five different classes of phenotypes (normal, mild, moderate (1 and 2) and severe) as explained in the main text. **E**) Phenotypic penetrance analysis of zebrafish *tbce* MO 5'UTR ATG embryos at 48 hpf at different concentration of morpholino showed a specific and strong dose-dependent effect. **F**) Rescue of severe phenotype in zebrafish *tbce* 5'UTR ATG embryos at 48 hpf with 30ng of $TBCE^{WT}$. Asterisks indicate statistically significant differences compared to control embryos (not injected) based on Chi's-squared test in a 2x2 contingency table (ns, not significant; ** p-value <0.01; *** p-value <0.001; **** p-value <0.0001). Black arrows: trunk and tail abnormalities. Data obtained and analysed with Dr. A. Lauri and Dr. G. Fasano.

4.1.2 Molecular validation of MOss2 approach on zebrafish *tbcd* morphants

For *tbcd* LoF, I contributed to validate the downregulation approach using MOss (splice site in *tbcd*) as base to investigate in more detailed the genotype-phenotype correlation in terms of morpho-anatomical alterations underlying the gross phenotype observed in *tbcd* MOss2 transient model. To this aim, I performed a semiquantitative RT-PCR on cDNA retrotranscribed from RNA extracted from 48 hpf not injected control and morphants embryos and separated on electrophoretic gel (**Figure 28 A**). As expected, PCR successfully amplified only one fragment from control embryos cDNA about 570 bps (base pairs), corresponding to the expected $tbcd^{WT}$ specimen, and two fragments for *tbcd* MOss2 conditions, clearly discriminated by the agarose gel: an upper band and lower band of approximately of 570 bps and 510 bps respectively. To confirm that the latter corresponds to the predicted exon 2 skipping from the mature $tbcd^{WT}$ transcript, I purified and sequenced the PCR fragments via Sanger's sequencing method (SeqStudioGenetic Analyzer, Applied Biosystems). Once obtained the sequenced outputs, I aligned them against the CDS of zebrafish *tbcd* reference sequence provided by Ensembl Genome Browser database (ENSEMBL ID: ENSDART00000161419). The alignment was also performed independently by two expert researchers using different analytic tools (data not showed). The analysis confirmed our hypothesis and the absence of the exon 2 in *tbcd* cDNA was obtained in all morphants embryos and likely produced an aberrant protein (**Figure 28 B**).

A)

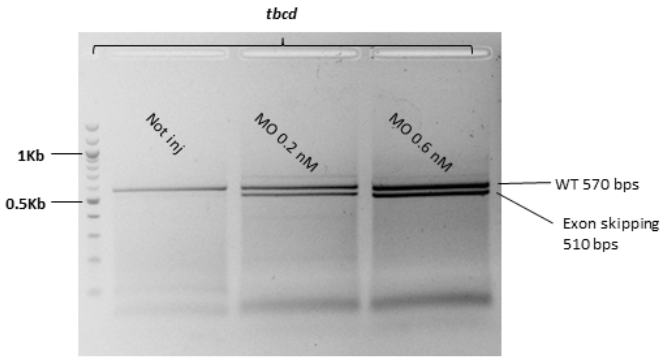

B)

Fig. 28: **A) Electrophoresis profile of the targeted exon amplified from cDNA of 48 hpf zebrafish *tbcd* morphants and not injected controls**. **B) Sanger sequencing confirmation of exon 2 skipping obtained in zebrafish morphant via MOss2** (red rectangle, dashed lines indicate missing nucleotide in exon 2 sequence of zebrafish tbcd cDNA obtained from morphant's RNA retrotranscription). The alignment was performed with the free on-line tool *Benchling*.

It is worth mentioning that parallelly to the molecular validation of MOss2 I contributed to, other researchers of the zebrafish lab carried out also Western Blot assay for tbcd protein expression evaluation using V5-tagged zebrafish construct transfected in cells from a standard cell culture line. As reported in **Fig. 29 A**, the immunoblotting analysis confirmed that, in transiently transfected human cells with zebrafish synthetic *tbcd* DNA harboring a deletion of exon 2 (*Dr tbcd*$^{\Delta exon2}$-V5) mimicking the aberrant version observed in fish upon MOss2 injection, expression of tbcd is reduced about ~50% compared to cells expressing the *wild type* construct (*Dr tbcd*^{WT}-V5). Immunoblot protocol to detect endogenous level of tbcd in zebrafish control and mutant protein's extract is currently being improving and initial results are obtained confirming *in vitro* data (**Fig. 29 B**).

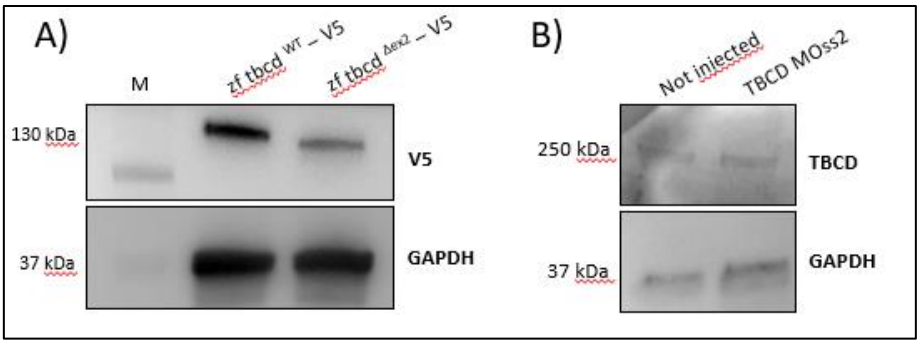

Fig. 29: **Immunoblotting analysis and tbcd protein level quantification. A-A'**) tbcd protein level is reduced in transiently transfected human cells with zebrafish *tbcd* synthetic mRNA exon 2 skipping. **B**) initial analysis of endogenous tbcd protein in control (not injected) and morphants is currently improving by Dr. Valeria Bonavolontà. GADPH was chosen as internal housekeeping control gene. M, marker.

4.2 Assessment of spinal motoneurons in zebrafish *tbcd* and *tbce* transient loss of function models

4.2.1 Quantitative analysis of motoneurons development in *tbcd* morphants

Altered axon outgrowth and errors pathfinding are common defective developmental features in zebrafish models of neurodegenerative disorders (Lissouba *et* al., 2018; McWhorter *et al*, 2003). From data collected, to assess how the LoF of *tbcd* impairs the correct morphogenesis of spinal cord motoneurons since the earliest stages of synaptogenesis, we decided to look into defects of motoneuron's primary axon extension by analysing the spatial expression patterning of *synaptotagmin-2b isoform* (znp1) (Fox&Sanes, 2007, Eisen *et al*., 1989) by immunohistochemistry assay (IHC). In labelled embryos, under Dr. A. Lauri guidance, I quantified primary axon length and topological descriptors of morphology in not injected controls versus *tbcd* morphants at 48 hpf. This developmental stage was chosen because by 48 hpf synaptogenesis is well underway and remains relatively simpler to analyse. Moreover, primary motor axons have quantifiable extended branches and form synapses with the lateral myosepta and muscle fibers (Liu and Westerfield, 1992; Myers *et* al., 1986). We focused on *synaptotagmin-2b* given that as calcium sensor transmembrane protein localized in the neurotransmitter's vesicles, it represents an appropriate pre-synaptic neurites marker. In **Fig. 30 A-C** I reported the results of the immunofluorescence against syt-2b protein imaged using confocal

microscopy in not injected and tbcd morphants embryos at 48 hpf resulting optimal to emphasize primary caudal (CaP MNs) and middle (MiP MNs) motoneurons (refer to chapter 1.3.3 for spinal motoneuron's classification in zebrafish). I scored CaP MNs aberrant phenotypes by analysing the 3D (*x,y,z*) full stack imaging dataset with Fiji software (Schindelin *et al*., 2012). A "*Score 0*" was assigned to all motoneurons showing an extended primary axon over the branching point (BP) as observed in not injected controls, "*Score 1*" was assigned to all motoneurons with normal primary axon and shorter distal portion, "*Score 2*" was instead destined to all motoneurons with severe primary axon truncation (**Fig. 30 C**). The results of the analysis confirm the presence of short primary neurites in *tbcd* morphant compared to control (**** p-value <0.0001) and rescued $TBCD^{WT}$ siblings (*** p-value <0.001) confirming the specificity of *tbcd* MOss effect on the phetypes observed in zebrafish larvae as expected. We occasionally observed also error pathfinding (**Fig. 30 B and D**).

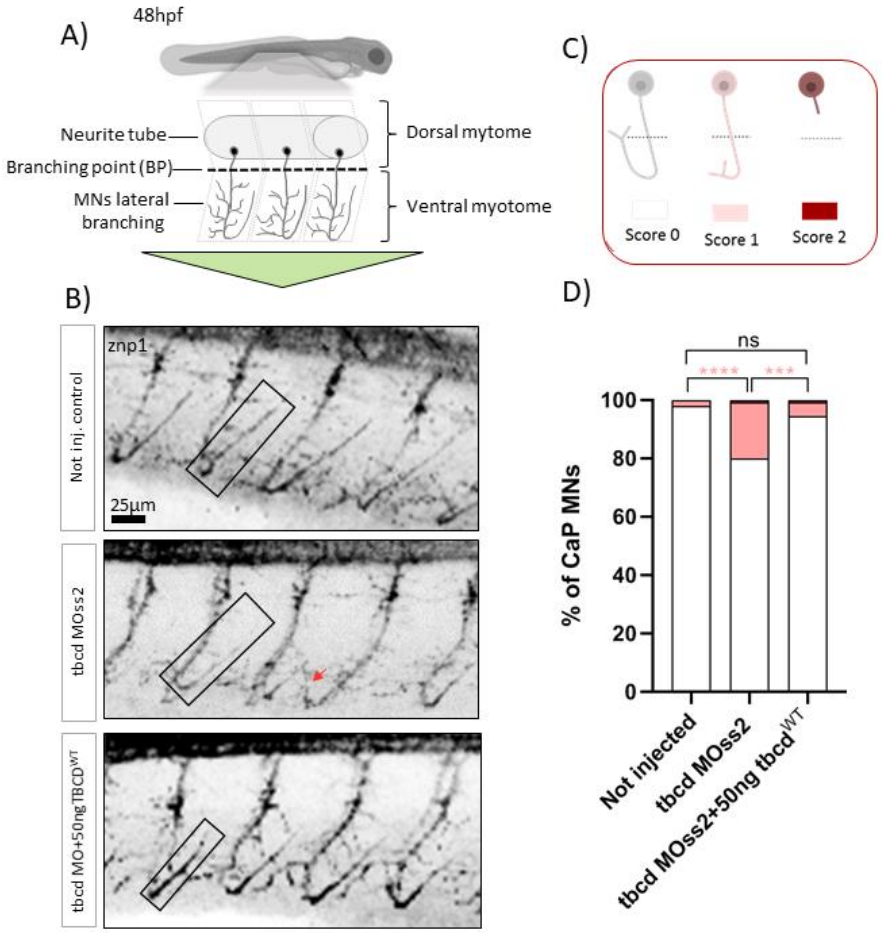

Fig. 30: **Whole-mount immunofluorescence against synaptotagmin 2b isoform (znp1) performed on MNs in not injected, *tbcd* morphants (+ or - *$TBCD^{WT}$*) embryos at 48 hpf**. Confocal Z-projections are

shown. **A**) Schematic representation of zebrafish CaP MNs at 48 hpf emerging from the neural tube and innervating the ventral myotome hemisegment (light grey dashed rectangle). **B**) *tbcd* morphants spinal CaP MNs exhibit shorter neurites (black rectangle) and pathfinding errors (red arrow) in comparison with not injected and rescued morphant embryos expressing $TBCD^{WT}$. Images obtained using Leica Stellaris 5 DM6 confocal microscope with 10X dry objective. **C**) Graphical drawing and classification of aberrant CaP MNs morphological phenotypes observed in zebrafish *tbcd* morphants at 48 hpf. **D**) Penetrance analysis of CaP MNs primary axon extension defects in embryos stained with znp1. N = 6 CaP MNs for each embryo of each experimental group (N = 5 embryos) in two biological replicates. Asterisks indicate statistically significant differences compared to control embryos (not injected) based on Chi's-squared test in a 2x2 contingency table (ns, not significant; *** p-value <0.001; **** p-value <0.0001). hpf, *hours post-fertilization*. Icon source: Biorender.

We further stratified the morpho-anatomical characterization of aberrant CaP MNs in our transient zebrafish *tbcd* LoF models by measuring different parameters. I quantified CaP MNs primary axon length with on-line free *Fiji* software *Simple Neurite Tracer* tool, then I performed analysis of morphological changes in volume, sphericity and polarization of zebrafish control and morphants CaP MNs using *IMARIS* software. For each embryo (N = 5 for each experimental group) I reconstructed 10 CaP MNs considering 2 geometrical shape descriptors for the analysis. I measured:

1. Ventral CaP MNs total axon length;
2. Ventral CaP MNs volume;
3. The straightness, describing the topological changes of the polarization in the biological structure considered. Values closer to 1 indicate a lack of polarity;
4. The convex hull, the smallest convex polygon containing the whole cell shape, describes the sphericity of an object.

1. Measure of ventral CaP MNs length

Starting from the CaP MNs gross phenotype penetrance analysis, I quantified zebrafish motor neurons primary axon length using the tool analysis *Simple Neurite Tracer* of *Fiji* software. Filament ROI (Region of Interest) measures were traced choosing as "starting point" the point from which the MN arise from the neurite tube and as "ending point" the maximum distal portion of the axon. In accordance with data collected so far, our analysis confirmed a significantly reduction (**** p-value <0.0001) of CaP MNs axon outgrowth in tbcd morphant embryos compared to not injected control siblings. In addition, CaP

MNs aberrant neurite extension is slightly rescued when *TBCD*^{WT} mRNA is co-injected with *tbcd* morpholino (**Fig. 31 E**).

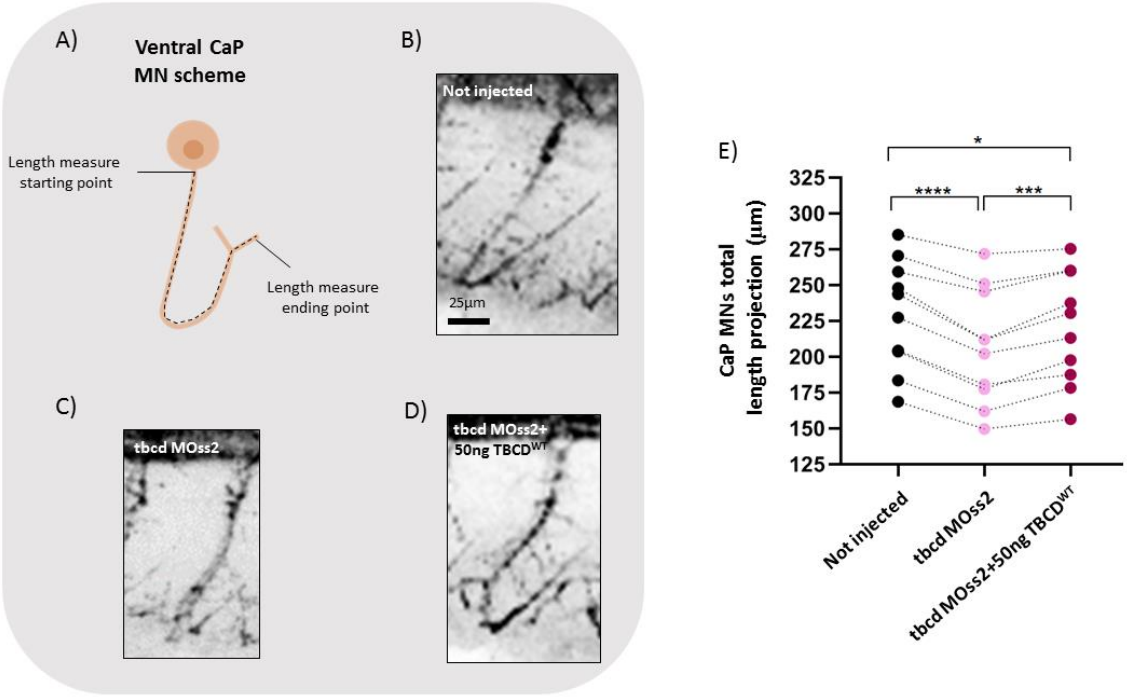

Fig. 31: ***tbcd* downregulation in zebrafish morphants embryos lead to reduced extension of CaP MNs primary axon**. Confocal Z-projections are shown. **A**) Schematic drawing of a ventral CaP MN at 48 hpf. Dashed black line indicates the ROI length measured for MN extension analysis. **B**) Insets of z-projections from confocal 3D images acquired with Leica Stellaris 5 showing a representative CaP MN in not injected control, **C**) *tbcd* morphant and **D**) *tbcd* rescued embryos. **E**) Scatter plot of all data points for MNs axon extension. Each value obtained represents the mean of the measurements of paired MNs evaluated for each embryo analysed from 2 biological replicates. Asterisks indicate statistically significant differences compared to control embryos (not injected) based on Two-way ANOVA test with Dunn's *post hoc* corrections (* p-value <0.05; *** p-value <0.001; **** p-value <0.0001). hpf, hours *post-fertilization*. Icon source: Biorender. Data obtained and analysed with Dr. A. Lauri.

2-4. Measurement of volume, polarity and sphericity of CaP MN primary axons

MTs are highly dynamic and strongly polarized structures whose function is closely related to their shape (OpenStax Collage Biology, 2015). We observed that aberrant CaP MNs exhibited not only incomplete extension of primary axon through the ventral muscle parenchyma but seemed to have other altered characteristics. Indeed, they appeared more "thick" (likely due to larger axon diameter) and straighter (less orientated) and occupying

less volume. To clear these aspects, I carried out a detailed morphogenic analysis with 3D *IMARIS* imaging software which allows to reconstruct semi-manually biological structures acquired at confocal microscope (**Fig. 32 A-B'**). Then, assuming MN axon as a cylinder, I used *IMARIS* algorithms to evaluate volume, straightness, and convex hull parameters.

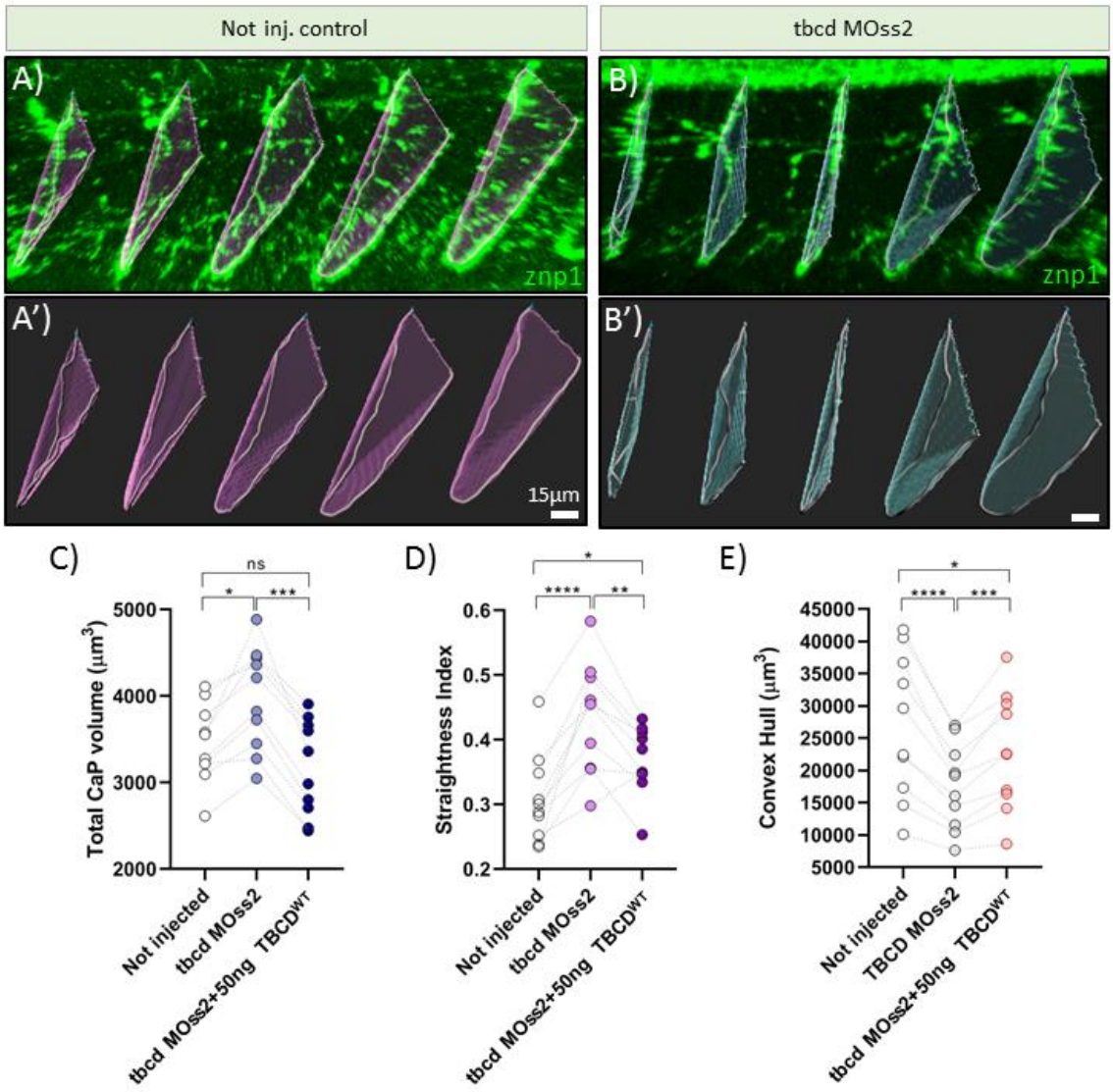

Fig. 32: Examples of 3D reconstruction and analysis of convex hull of zebrafish CaP MNs stained with znp1 in A) not injected and B) *tbcd* morphants at 48 hpf. Confocal Z-projections are shown. **A'-B'**) The minimal convex polyhedron (purple and light blue area respectively) enveloping all distal points of each reconstructed CaP MN. **C-E**) Graphs showing all the data points for volume, straightness and convex hull analysis respectively. Asterisks indicate statistically significant differences compared to control

embryos (not injected) based on One-way ANOVA test with Dunnet's *post hoc* test (ns, not significant; * p-value <0.05; ** p-value <0.01; *** p-value <0.001; **** p-value <0.0001).

The analyses confirmed a significant increase in volume of *tbcd* morphants CaP MN primary axon (* p-value <0.05) compared to control siblings. Interestingly, they also resulted not correctly orientated in the surroundings appearing indeed straighter (*** p-value <0.001) and occupying less space in the myotome (**** p-value <0.0001) (**Fig. 32 C-E**).

4.2.2 Confirmation of motoneurons development in *tbcd* loss of function crispants (G0 generation)

Despite being a rapid approach to study gene LoF, approaches using morpholinos are transient approaches and result in a *knock down* of the gene. Therefore, phenotypes requiring long-term and/or sustained suppression, such as neurodegenerative events, may not be observed using those molecular strategies (Tran *et al*., 2020) and the establishment of a stable model as tool for long-term analysis is required instead. Therefore, to cross-validate results obtained by morpholino and to exclude the hypothesis that the phenotypes observed in zebafish *tbcd* transient model were induced by morpholino toxicity injection, during this project Dr. A. Lauri conceived the generation and the assessment of *tbcd knock-out* (KO) crispant (generation 0, G0) using a dedicated CRISPR-Cas9 approach optimized in zebrafish and I focused on its phenotypic characterization (**Fig. 33**). Of note, as mentioned in paragraph 4.1.2, stable *tbcd* G0 crispant show a survival rate comparable with *tbcd* morphants microinjected with morpholino splicing site (**Fig. 34 A**) supporting the hypothesis that LoF of *tbcd* might be compensated during early zebrafish embryogenesis.

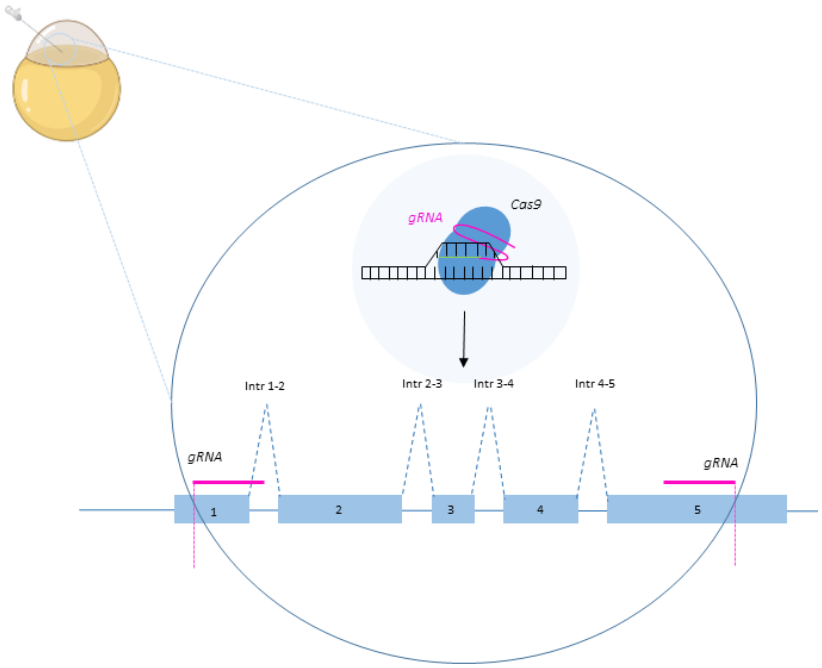

Fig. 33: **Schematic representation of zebrafish genomic sequence targeted by sgRNAs (single guide RNA) and Cas9 to generate KO animals**. Icon source: Biorender. Strategy designed by Dr. A. Lauri in collaboration with Dr. F. Del Bene (Istitute de la vision, Paris, France).

After the establishment and the genotyping of *tbcd* crispants carried out in the lab by Dr. A. Lauri and Dr. M.Venditti, to validate early spinal MNs development in the resulting crispants and compare to the effect observed with transient downregulation models, I performed the immunohistochemistry assay (IHC) against specific pre-synaptic neurites and muscles markers and carried out a gross phenotyping of aberrant CaP MNs at 48 hpf to map their axonal projections in terms of extension and morphology, as already done for *tbcd* morphants in chapter 4.2.1. Interestingly, in addition to reduce axon length, we particularly noticed alterations of CaP MNs axon pathfinding, *i.e.* lateral branching patterning (**Fig. 34 B-E**) and we decide to investigate this deeper. To this aim, I scored CaP MNs aberrant phenotypes by analysing the 3D (*x,y,z*) full stack imaging dataset with *Fiji* software. Now, I assigned "*Score 0*" to all motoneurons showing normal branching morphology as observed in not injected controls, "*Score 1*" to all motoneurons with ectopic innervation and/or axon guidance defects (*i.e.* errors pathfinding), "*Score 2*" to all motoneurons (often also short) with excessive branching **(Fig. 35 A, A')**.

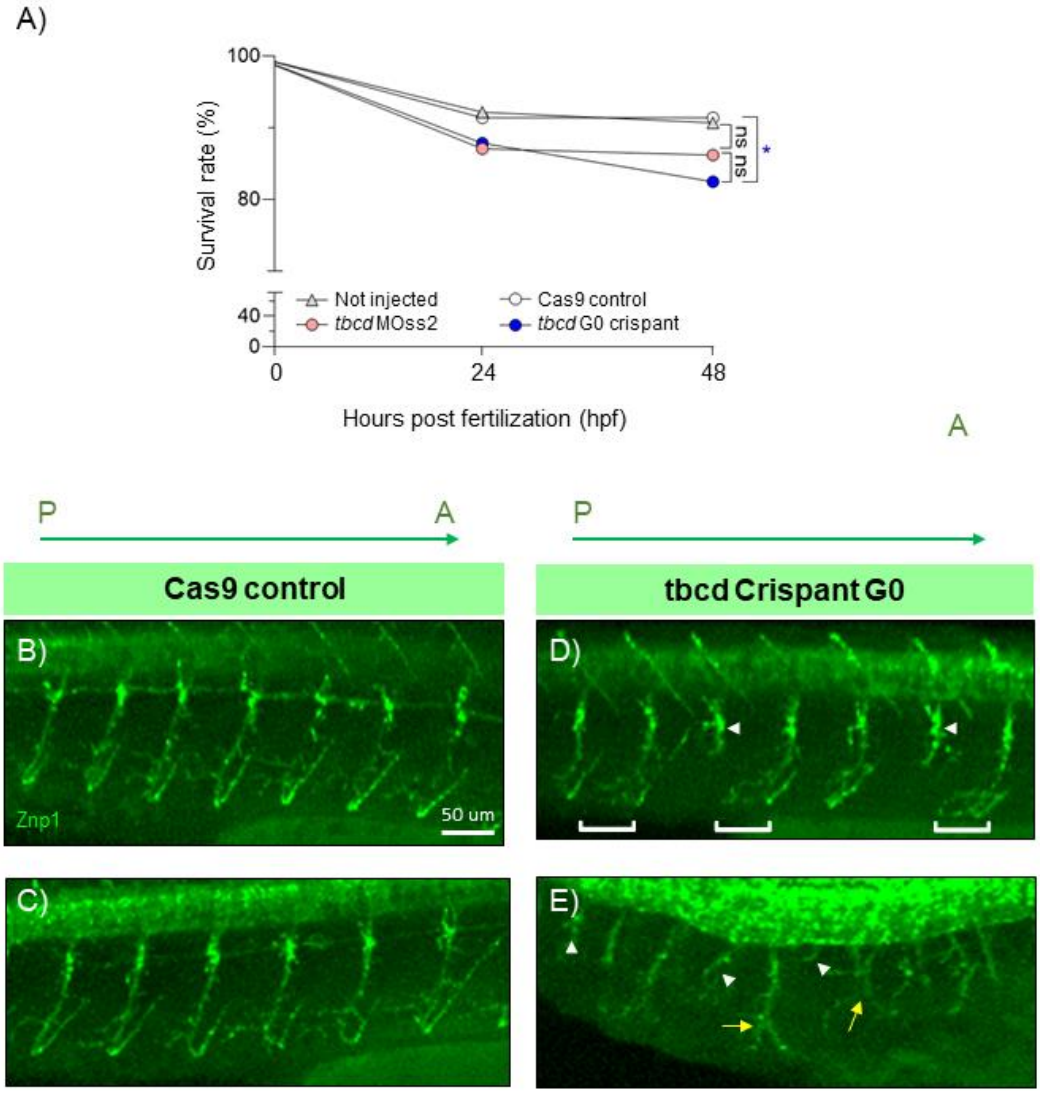

Fig. 34: **A**) Survival rate expressed in percentage in stable *tbcd* G0 crispant LoF model (*p-value <0.05) compared to *tbcd* MOss2. Log-rank (Mantel-Cox) test. N. of embryos = 139 (Cas9 control), 208 (*tbcd* G0 crispant), 145 (not injected), 131 (*tbcd* MOss2). Data analyzed with Dr. Giulia Fasano. **B-E**) Confocal Z-projections from 3D confocal images showing a representative zebrafish controls (B, C) and G0 (D, E) *tbcd* crispants at 48hpf labelled with znp1 antibody. 10X magnification. The green arrow indicates samples orientation along antero- (A) posterior (P) axis. White arrowhead: severe axon truncation; white brackets: defective lateral branching; yellow arrow: error pathfinding.

As expected and confirming the results obtained with MO, analysis in crispants confirmed the presence of short primary neurites conversely to normal controls (injected only with Cas9) (**Fig. 35 B, B'**). The dataset on G0 *tbcd* crispants supports the evidence that reduced levels of tbcd impact negatively spinal CaP MNs development during vertebrate embryogenesis.

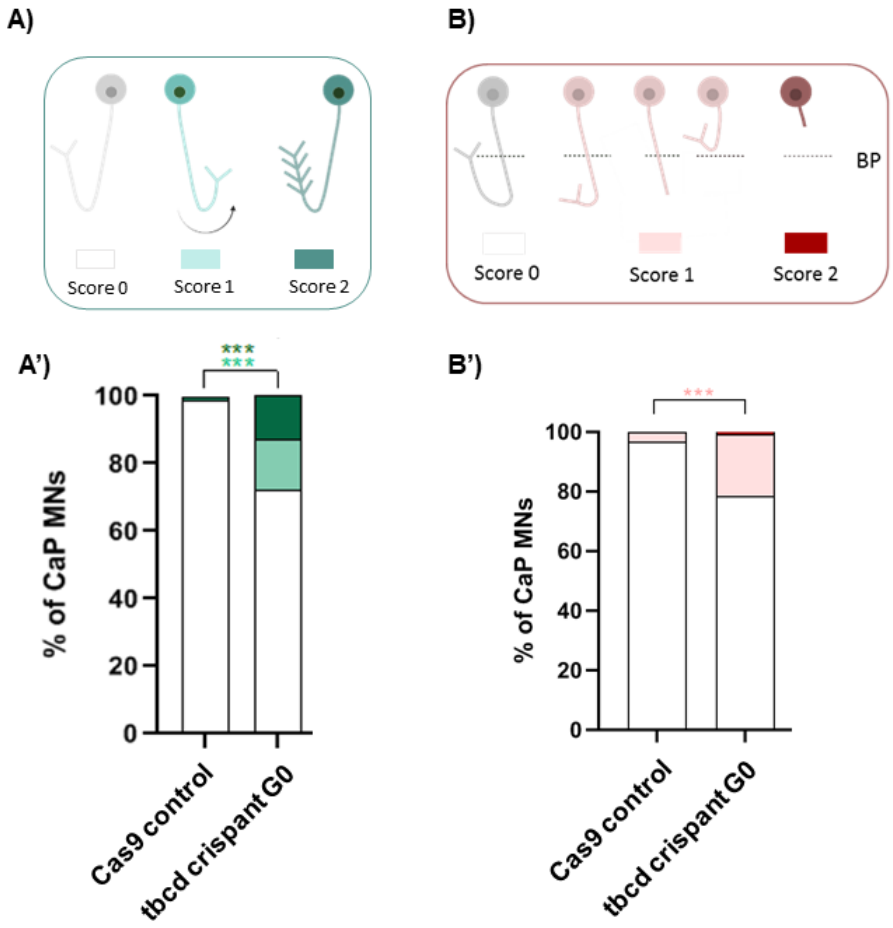

Fig. 35: CaP MNs branching phenotyping and axonal length analyses in *tbcd* crispants G0 at 48 hpf compared to control siblings (Cas9). A) Schematic drawing illustrating branching morphology score assignment. **A'**) Penetrance analysis of CaPs innervation defects in embryos stained with znp1. N = 10 MNs for each embryo of each experimental group. Asterisks indicate statistically significant differences compared to control embryos (Cas9) based on Chi's-squared test in a 2x2 contingency table (*** p-value <0.001). **B**) Schematic drawing and classification of CaP MN neurite extension defects observed in zebrafish *tbcd* crispants G0 at 48 hpf. **B'**)) Penetrance analysis of CaPs extension defects in embryos stained with znp1. N = 10 MNs for each embryo of each experimental group. Asterisks indicate statistically significant differences compared to control embryos (Cas9) based on Chi's-squared test in a 2x2 contingency table (*** p-value <0.001). N = 10 MNs. Icon source: Biorender.

Next, we asked if defects in axonal extension and branching abnormalities could be detected already at the earliest stage of MNs synaptogenesis (between 18-30 hpf). We took advantage of the *synaptic vesicle 2* (SV2) marker, a transmembrane protein involved in the neurotransmitters release, which allows labelling of neurite axon and its immature branching spines (**Fig. 36**). Our analysis showed that concomitantly to a reduction of

neurite extension (**Fig. 37 A**), the number of spines protruding from the main axonal shaft of *tbcd* crispant embryos is significantly lower compared to normal controls (injected only with Cas9) (**** p-value <0.0001) (**Fig. 37 B**), indicating an overall reduced development of spinal MNs.

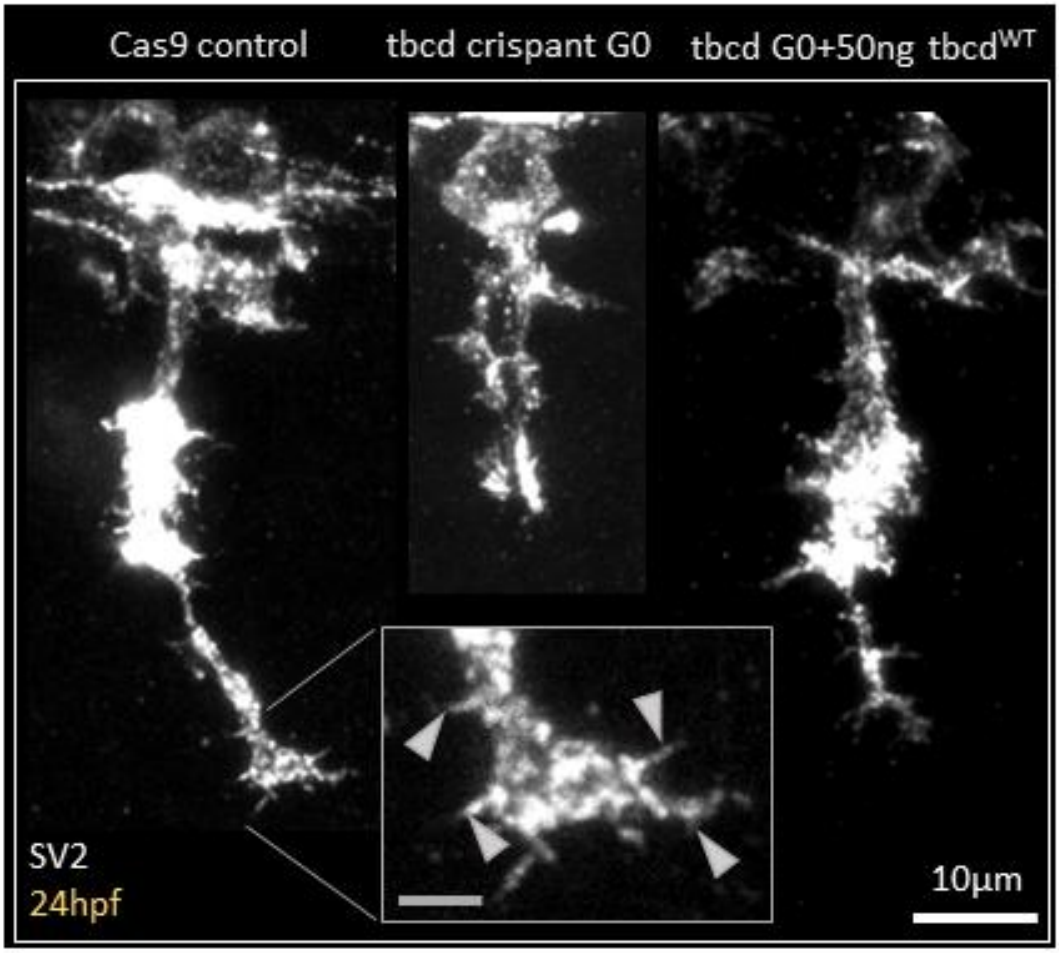

Fig. 36: **Confocal Z-projection from 3D confocal images showing representative zebrafish controls (Cas9), *tbcd* G0 crispants and rescued embryos at 24 hpf labelled with SV2 antibody** (63X magnification). Grey arrowheads in the inset indicate protruding spines from the main axon shaft in the distal portion. Inset scale bar: 5 µm.

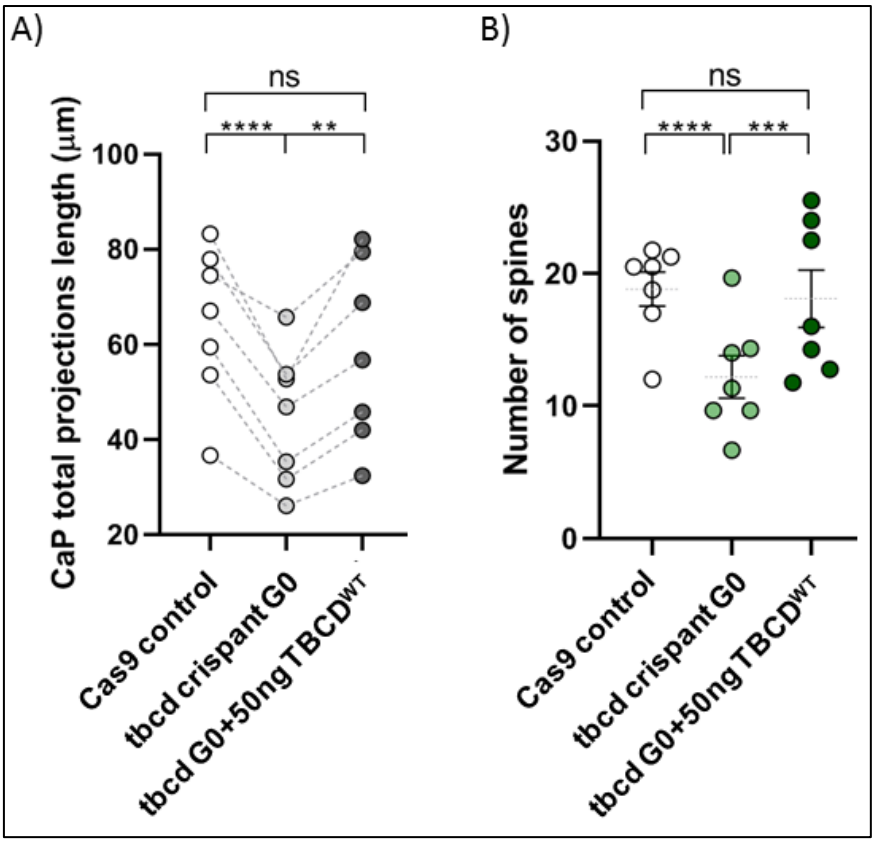

Fig. 37: **Graphs showing the quantification and all the data points for spine and neurite extension analyses**. **A**) Each point represents the mean value of spines number for each CaP MNs analysed. Asterisks indicate statistically significant differences compared to control (Cas9) based on One-way ANOVA test with Dunnet's *post hoc* corrections (ns, not significant; *** p-value <0.001; ****p<0.0001). N = 7 CaP MNs. **B**) Each value obtained represent the mean of the axon length of paired CaP MNs evaluated for each embryo analysed. Asterisks indicate statistically significant differences compared to control (Cas9) based on Two-way ANOVA test with Dunn's *post hoc* corrections (ns, not significant; ** p-value <0.001; ****p<0.0001) N = 10 MNs.

4.2.3 Analysis of motoneurons development in *tbce* morphants

Next, I contributed to initiate the gross phenotype analysis of transient zebrafish CaP MNs mutants obtained by downregulating *tbce* expression using specific ATG-morpholino approach (see Chapter 1.3.4). This time, we took direct advantage of using the transgenic line *Tg:*(mnxGal4:HSP70/10UAS:lynRFP) in which zebrafish CaP MNs appeared red-positive fluorescent (**Fig. 38 A**, for details see chapter 1.3.4) and clearly visible in live imaging using confocal microscopy and allowing to bypass long immunofluorescence assays. Axonal outgrowth was assessed as previously described for *tbcd* transient mutants, using *Fiji Simple Neurite Tracer* tool. "*Score 0*" was assigned to all

motoneurons showing a normally extended primary axon over the branching point (BP) as observed in not injected controls, "*Score 1*" to all motoneurons with normal primary axon but appearing shorter and/or not able to extend over the BP, "*Score 2*" to all motoneurons with severe primary axon truncation.

As shown in **Fig. 38 B-D**, *tbce* knockdown embryos at 48 hpf exhibit extremely short and truncated neurites compared to controls and rescued siblings (not injected and *tbce* MO 5'UTR ATG+30ng $TBCE^{WT}$). Error pathfinding were also visible in morphant fish.

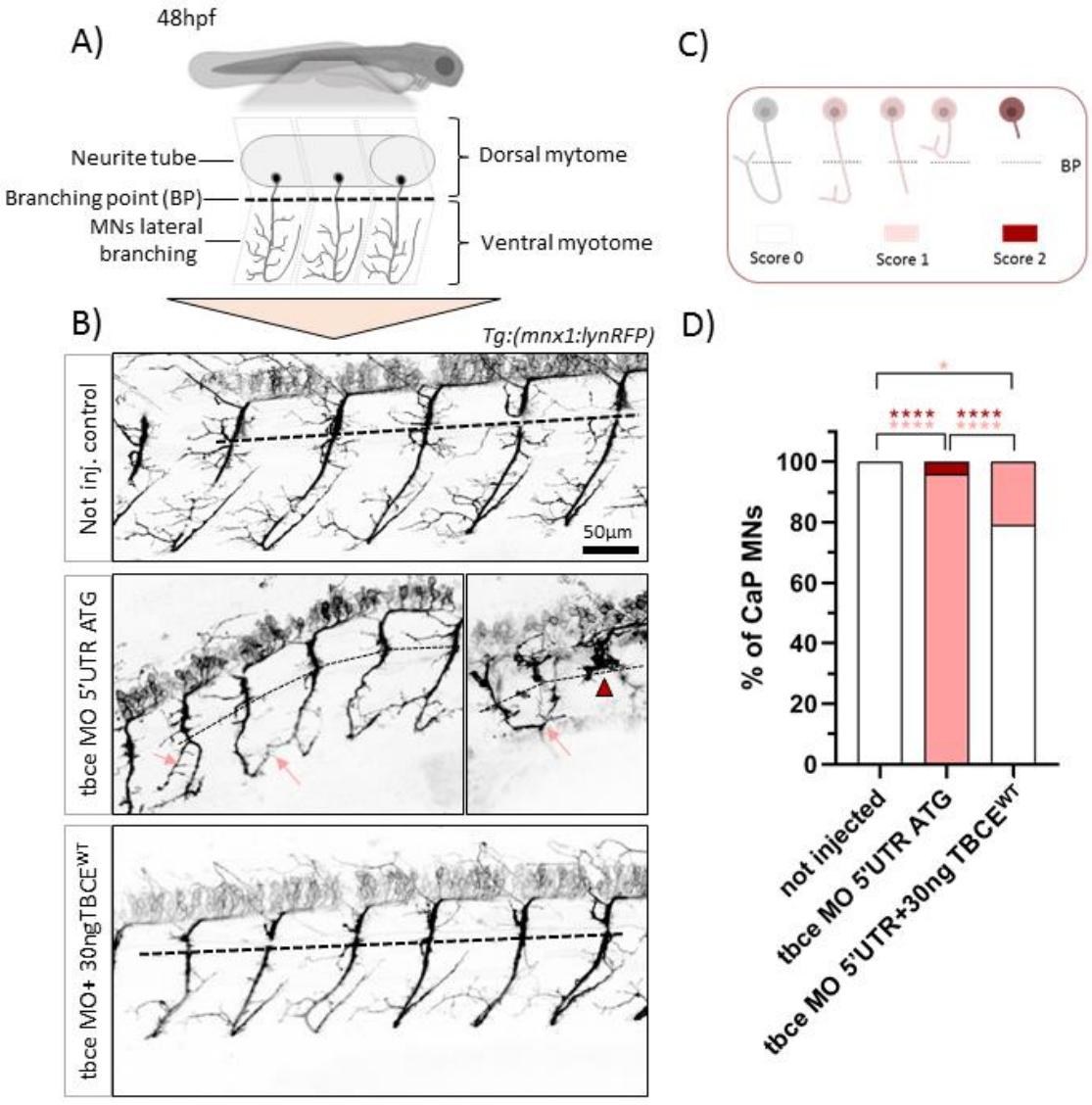

Fig. 38: **Zebrafish *tbce* morphants at 48 hpf exhibit aberrant motor axon extension and error pathfinding**. **A**) Schematic representation of zebrafish CaP MNs at 48 hpf emerging from the neurite tube and innervating the ventral myotome hemisegment (light grey rectangle). **B**) *tbce* morphants showed short and aberrant spinal neurites (pink arrows) and truncated ones (dark red triangle) not observed in not injected

and in those rescued with *TBCE*^{WT}. Images obtained using Leica Stellaris 5 DM6 confocal microscope with 25X water immersion objective. **C**) Graphical drawing and classification of aberrant CaP MNs morphological phenotypes observed in zebrafish *tbce* morphants at 48 hpf. **D**) Penetrance analysis of CaP MNs primary axon extension. N = 5 for not injected, N = 6 for *tbce* morphants and rescued embryos. Asterisks indicate statistically significant differences compared to control embryos (not injected) based on Chi's-squared test in a 2x2 contingency table (ns, not significant; *** p-value <0.001; **** p-value <0.0001). hpf, *hours post-fertilization*. Icon source: Biorender.

4.3 Analysis of spinal motoneurons innervation defects and muscles morphologies in zebrafish *tbcd* crispants (G0)

Since many pediatric patients harboring *TBCD* LoF mutations exhibit clear signs of neurodegeneration, leading to para/tetraplegia (Flex *et* al., 2016), to expand the analysis and assess possible underlying impairment of innervation and synaptogenesis, we analysed *tbcd* crispants at later developmental stages, when these morphological traits are recognizable (Varshney *et al*., 2015). Therefore, we decided to investigate deeper on the morphological alterations of MNs innervation and muscle fibers organization in a population of highly penetrant stable *tbcd* crispant G0 mutants at 72 hpf, which carried out different mutations in the genomic *tbcd* sequence (mapped by Dr. A. Lauri and Dr. M. Venditti, data not shown). In this context, I contribute by performing an immunohistochemistry assay (IHC) with specific markers on 72 hpf control and mutant larvae by analysing the *synaptotagmin-2b isoform* (znp1) expression patterning which labels specifically pre-synaptic neurites. Further, to visualize the delicate architecture of contractile muscle fibers, I used the conjugated *Phalloidin-594* which binds F-actin microfilaments responsible for muscle contraction (Pinto *et al*., 2020).

In details, for the innervation analysis I focused on the ventral region of 3 anterior myotomes cropped from each 3D (*x,y,z*) superficial stack z-planes images (**Fig. 39 A**). Then, I equally thresholded the images and calculated the mean fluorescence intensity signals of pre-synaptic structures labelled with znp1 antibody with Fiji software (**Fig. 39 B**).

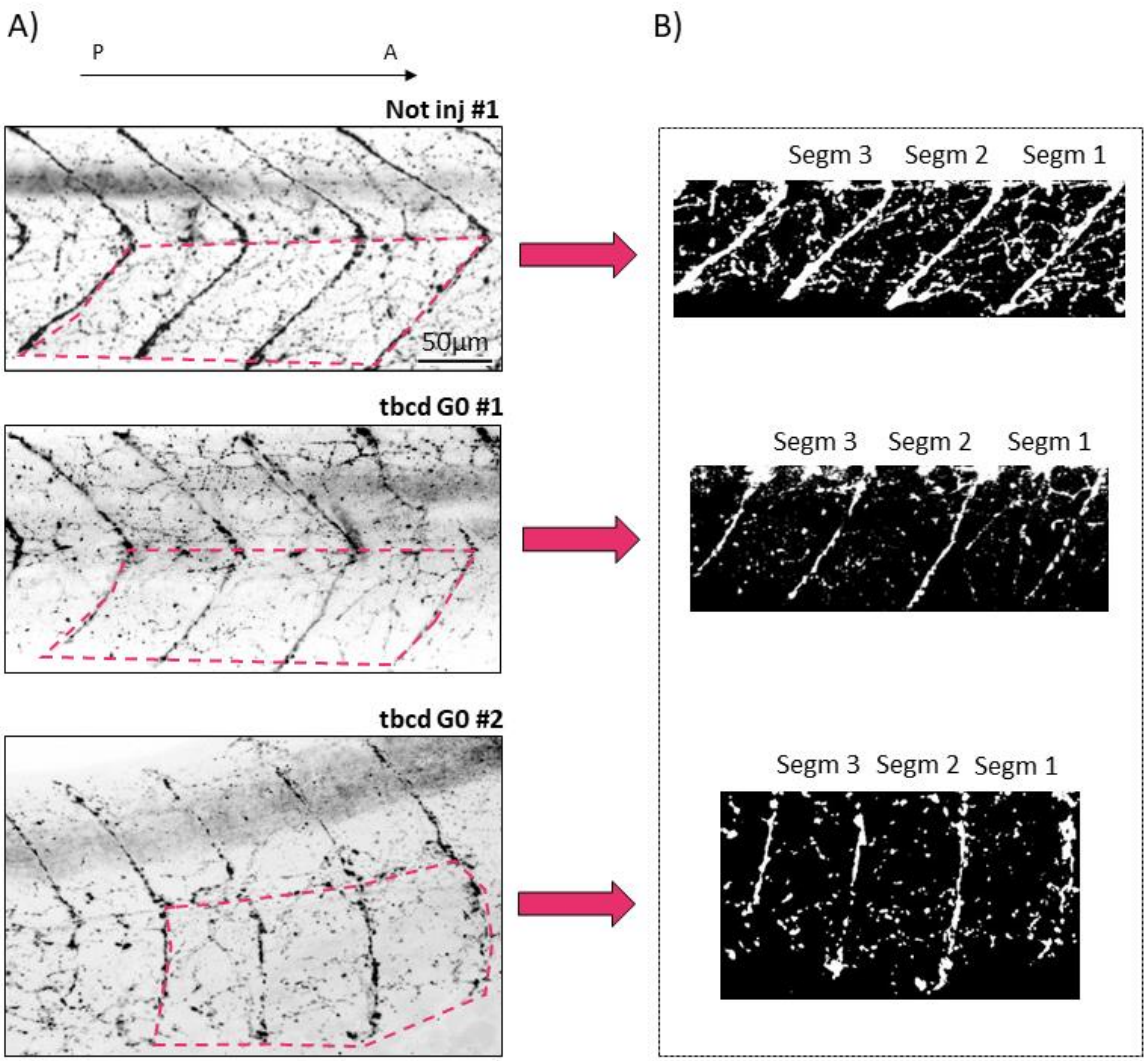

Fig. 39: **Confocal Z-projections of *tbcd* crispants G0 showing a consistent reduction of superficial muscle innervation at 72 hpf compared to not injected siblings**. 25X magnification. Representative images of not injected and *tbcd* mutants before (**A**) and after (**B**) applying the thresholding in *Fiji*. Magenta dashed ROIs around selected myotomes were traced to crop each ventral region of interest for the analysis. A, anterior; P, posterior.

Interestingly, our analysis confirmed that 72 hpf *tbcd* crispants G0 had a loss of superficial myotome innervation (* p-value <0.05) which could be possibly linked to a failure in neuromuscular junctions (NMJ) formation (Tay *et al*., 2021) (**Fig. 40**), that should be assessed in the future.

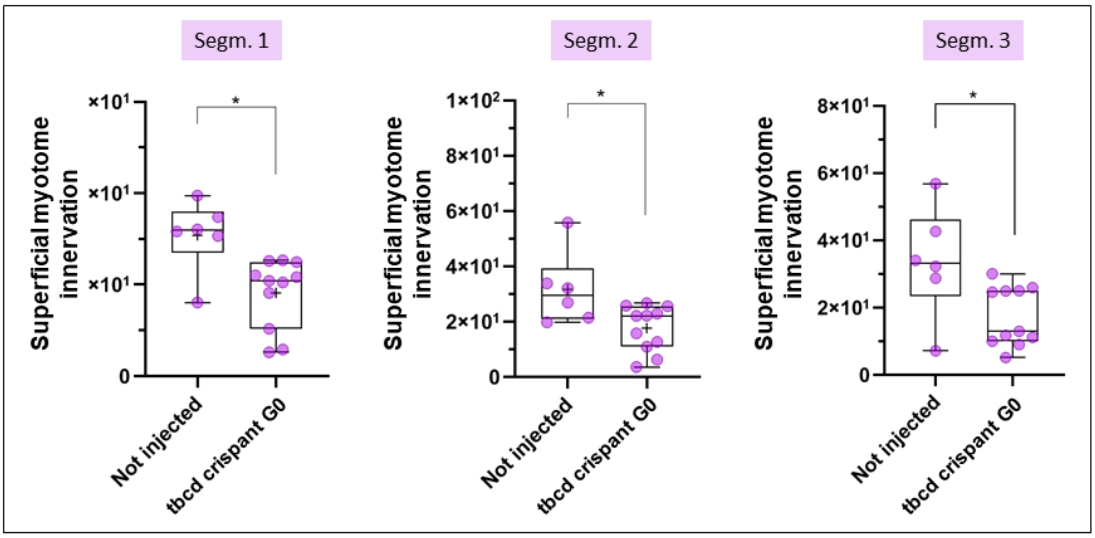

Fig. 40: Graphs showing quantification and data points relative to the loss of superficial muscle innervation in *tbcd* crispant fish compared to not injected controls at 72 hpf. Each point represents the mean value of fluorescence intensity of myotome segment analysed for each embryo. Asterisks indicate statistically significant differences compared to control (not injected) based on paired parametric T-Student test (* p-value < 0.05). N = 6 not injected; N = 11 crispant embryos.

Muscles gross-phenotyping was instead evaluated by scoring the presence/absence at least of 3 morphological structures (**Fig. 41 A-B**) such as:

1) presence of the *chevron* myosepta (which separate each myotome from the another),
2) the integrity of the fibers (locally opened like a "bubble"),
3) disruption of the myotomes.

I assigned "+" to all the embryos with at least one of the aberrant muscles phenotypes observed, "++" with at least two aberrant phenotypes and "+++" with all 3 aberrant phenotypes. I assessed that *tbcd* G0 mutants showed a higher incident of abnormal muscle morphologies not assessable in control siblings (* p-value <0.05) (**Fig. 41 C**).

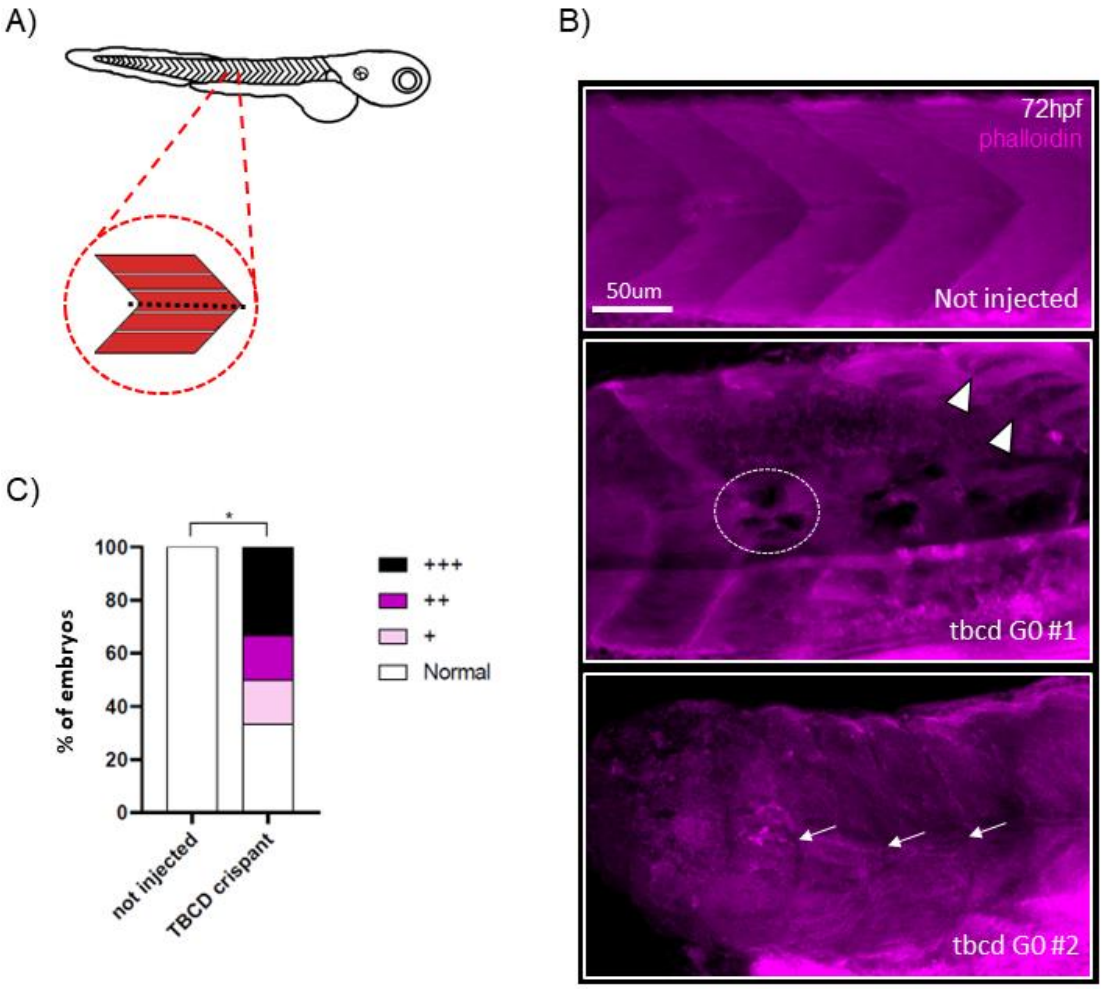

Fig. 41: confocal Z-projections showing *tbcd* crispants G0 at 72 hpf with disrupted muscle organization and a loss of shape of the main fibers. 25Xmagnification. **A**) Schematic representation of the trunk musculature in a 72 hpf zebrafish embryo (sagittal section). The dorsal and ventral hemi-segments (separated by black dashed line) of a zebrafish myotome are shown in red circle. **B**) Z-projections from confocal 3D images showing a myotome close-up in a not injected control and *tbcd* crispant G0 larvae at 72 hpf stained with phalloidin marking F-actin filaments. The latter two show aberrant muscles phenotypes quantified in C). White arrows: loss of typical chevron boundary shape; white triangles: fibers locally opened; white dashed circle: impaired myotome. **C**) Two tails Chi's-square test (* $p < 0.05$; (+) presence at least of one phenotype, (++) presence at least of two phenotypes, (+++) presence at least of all three phenotypes). Data are expressed as percentage of embryos, N = 6.

4.4 Preliminary investigation of microtubules defects in *tbcd* loss of function zebrafish models

4.4.1 2D super-resolution imaging of stable microtubules in growing neurites of *tbcd* Crispr G0 at early embryonic stage

Experiements on patients-derived fibroblast cells suggested that the LoF of this tubulin chaperon protein determined an unbalanced shift towards an excessive MTs polymerization (Flex *et al*., 2016). Once we confirmed the developmental defects of CaP MNs neurites in both transient and stable zebrafish tubulinopathy models, we started investigating further underlying microtubules (MTs) alterations. To assess this hypothesis, I performed an immunofluorescence on 24 hpf control and *tbcd* crispant embryos using antibodies directed against *β-tubulin* (one of the MTs building blocks) and *detyrosinated α-tubulin*, a modified tubulin missing of a tyrosine residue which represent a modification providing stability to the tubulin polymer. This developmental stage was chosen because by 24 hpf MNs have started growing through the ventral musculature and showed a clearly identifiably shape, but embryonic tissue is still simple such that imaging at high resolution could be performed. The status of MT could be best visualized using improved imaging resolution such STED technology. During a STED demonstration stand (event hosted by Pediatric Hospital Bambino Gesù), with Dr. A. Lauri, Dr. F. Eghiaian (Abberior GmbH), Dr. A. Rossi (Crisel Instruments) and Dr. S. Petrini, I acquired representative images of CaP MNs in control and mutant embryos at 24 hpf using 2D *Super-Resolution* STED microscopy (STimulated Emission Depletion; Vicidomini *et al*., 2013) (**Fig. 42 A-B**). For each CaP MNs acquired (N = 3) from each embryo analyzed, I measured the length of the second half distal portion (growing cone) of MTs primary shaft labeled with β- and detyrosinated α-tubulin. Then, I preliminarly attempted to assess the detyrosinated α-tubulin coverage along β-tubulin main scaffold as follow:

$$\text{Coverage} = \frac{\text{detyrosinated α tubulin length}}{\text{β−tubulin length}}$$

From this pilot experiment and quantification, I observed that *tbcd* crispants G0 showed a high level of detyrosinated tubulin (coverage) already at earlier embryonic stage (* p-value <0.05).

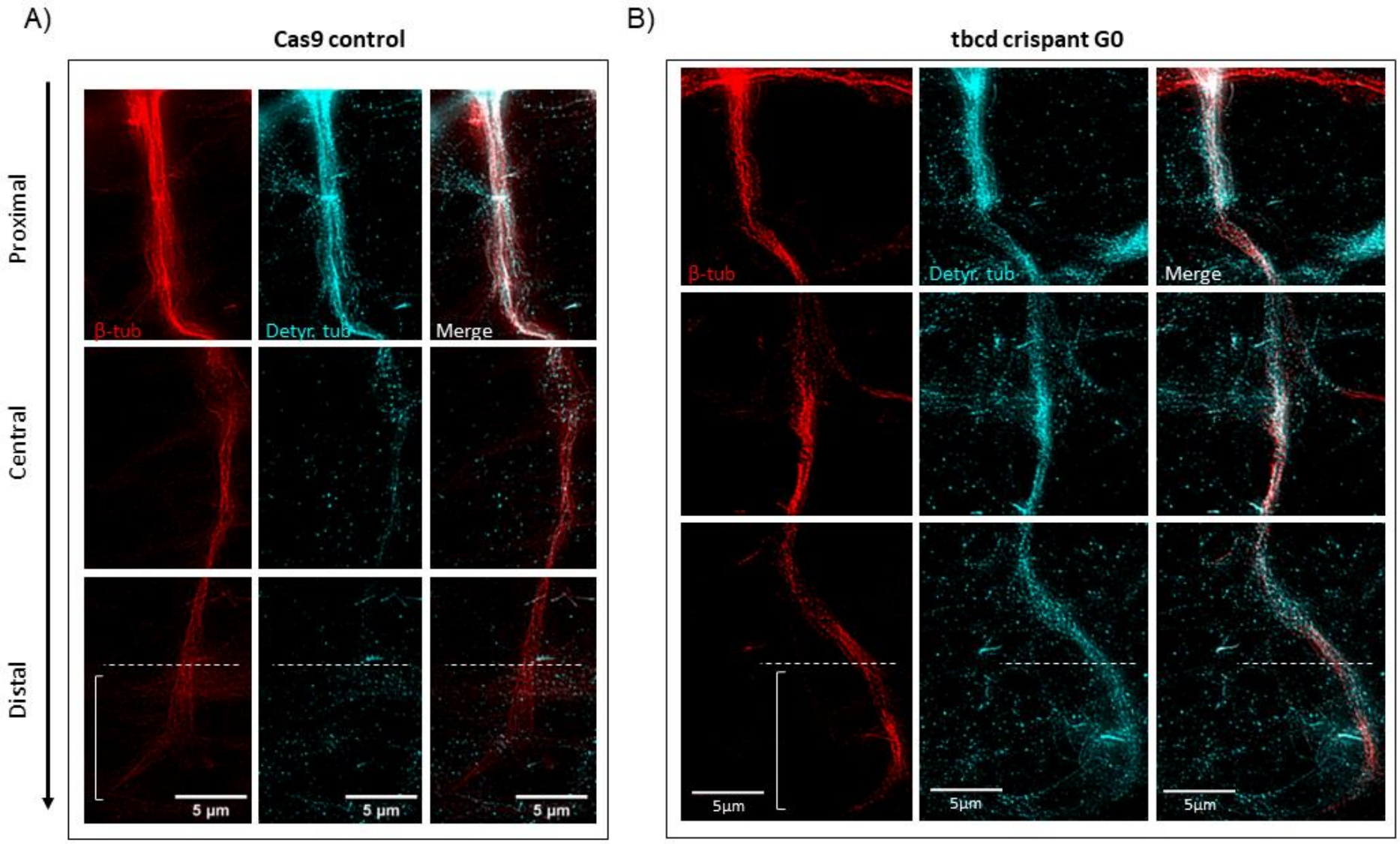
A)
Cas9 control
Proximal
Central
Distal
β-tub
Detyr. tub
Merge
5 µm
5 µm
5 µm
B)
tbcd crispant G0
β-tub
Detyr. tub
Merge
5µm
5µm
5µm

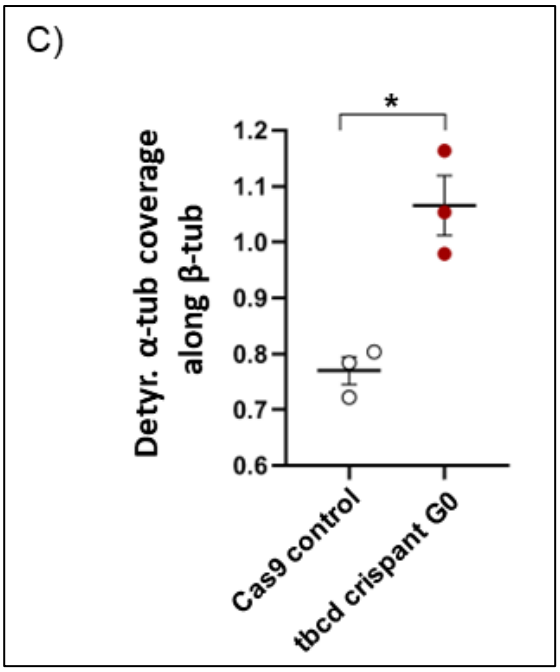

Fig. 42: STED Z-projections showing tubulin in zebrafish *tbcd* crispant spinal neurons and quantification. 100X magnification**.** Z-projections from 2D STED microscopy (*x,y,z*) images showing CaP MNs in **A**) control and **B**) *tbcd* crispant G0 larvae at 24 hpf stained with β-tubulin (in red) and detyrosinated α-tubulin (in cyan). Dashed white line ideally divides the growing cone in two portions which the analysed one is indicated by white brackets. **C**) Each point represents the ratio between MTs distal portion lengths evaluated in both channels for each CaP MNs of each embryo analysed. Asterisks indicate statistically significant differences compared to control (Cas9) based paired on T-Student test (* p-value <0.05). N = 3 MNs.

5. DISCUSSION

The overall purpose of this PhD thesis was to examine the functional impact LoF of *TBCD* and *TBCE* caused by a series of rare genetic variants recently discovered by examining the basic development of motor neurons in *Danio rerio* (zebrafish) *in vivo* disease model. In particular, my PhD work was focused on:

1. the initial characterization of the orthologous genes in zebrafish confirming the usefulness of this vertebrate organism for the study of neurodevelopmental disorder with early signs of neurodegenerative traits (**part I**);
2. the contribution to understanding the impact of LoF variants on the motor neuron's morphology, using transient and stable zebrafish models of disease (**part II**);
3. initial investigation on the possible molecular mechanisms affecting the microtubules (MTs) dynamic instability and leading to neurodegeneration (**part III**).

1. PART I

Rare diseases, for which 80% of the cases are linked to genetic alterations, are extremely debilitating conditions often causative of a dramatic decrease in quality and life expectancy of affected patients many of whom are still orphans of a diagnosis (Nguengang Wakap *et al*., 2020). Therefore, from 2015 the "Molecular Genetics and Functional Genomics" laboratory led by Dr. M. Tartaglia is actively involved in an ambitious research project aiming to provide a molecular diagnosis for these orphan patients, relying on the *whole exome sequencing* (WES) as an initial approach. As discussed in paragraph 1.1.3, for the understanding of pathogenetic mechanisms underlying genetic disorders is necessary to develop experimental models, such as *in vitro* and *in vivo*, in which new candidate disease-causing variants identified through WES can be validated and functionally characterized to allow the development of innovative patient-specific therapeutic strategies. *In vitro* approaches are insufficient for the investigation of the genotype-phenotype correlation at physio-pathological level since they are an extremely simplified representation of an entire organism, especially for those disorders involving the nervous system, where relevant tissue and structures are often inaccessible, and whose functionality rely on an intricate network of cell-cell and cell-

environment interactions and conditions which are not reproducible in the lab (Slanzi *et al*., 2020). Therefore, *in vivo* models are indispensable for an accurate characterization of pediatric diseases, to confirm the genotype causality and molecular mechanisms underlying the pathological event.

Zebrafish combines many genetic and physiological advantages of studying different cellular processes with a wide range of high-throughput approaches as advanced molecular biology techniques, biochemistry, high resolution microscopy and genetic manipulation system (see paragraph 1.3.4). Moreover, zebrafish brain physiology is well described and addressable with not invasive techniques thanks to the transparency of the embryos. By exploiting the genetic and technological characteristics of this vertebrate model, our team (Dr. A. Lauri, Dr. G. Fasano, Dr. M. Venditti, and I) used this model organism to examine the consequences of *tbcd* and *tbce* LoF on motor neuron development and homeostasis *in vivo*, since they are sensitive to cytoskeleton alterations.

Before the establishment of a stable KO model of disease (G2 onwards) currently on going and carried out different researchers in the zebrafish lab, in the first part of my PhD work I contributed to the characterization of *TBCD* and *TBCE* orthologous genes via comparative analysis of amino acids sequences and predicted protein motif and domains. Noteworthy, many of noted genetic variants validated in tubulin-chaperon genes and reported in literature are missense mutations found in different but highly hotspot conserved amino acid residues leading to partial protein stability and half-life (Edvardson *et al*., 2016; Sferra *et al*., 2016), protein structure and folding (Pode-Shakked *et al*., 2017; Flex *et al*., 2016), impairment of protein-protein interactions (Chen *et al*., 2021; Miyake *et al*., 2016; Sferra *et al*., 2016). In addition, mutations in genes encoding for tubulin chaperon proteins which led to a partial reduction protein's stability also showed a reduced ability to participate to αβ-tubulin dimers assembly/disassembly from cytoskeletal MTs (Edvardson *et al*., 2016; Flex *et al*., 2016; Miyake *et al*., 2016; Sferra *et al*., 2016).

Despite the effects of impaired microtubules have already been found in neurodegenerative diseases (Clark *et al*., 2016; Dubey *et al*., 2015; Tarrade *et al*., 2006), is not clear how altered MTs stability affects the nervous system development and its physiological activities in *in vivo* context. As showed by amino acid sequences alignment, zebrafish *tbcd* and *tbce* protein sequences show 65% and 52% of amino acid residues

conservation with human *TBCD* and *TBCE* orthologues respectively making it a convenient vertebrate organism to model tubulinopathies diseases.

2. PART II

Following these results and starting from the idea that tubulinopathies can be modeled reliably in zebrafish embryos, we used transient morpholino strategies as preliminarily approach to investigate tubulin chaperone proteins LoF effects on motor neurons morphogenesis. We demonstrated that decreasing dosages of TBCD and TBCE proteins lead to defective motor neurons development with altered neurite extension, branching and pathfinding errors. Similar phenotypes at the level of motoneurons were observed in fish models of Amyotrophic Lateral Sclerosis (ALS), Spinal muscular atrophy (SMA) and Hereditary spastic paraplegia (HSP) (Van Schoor *et al*., 2024; Miller *et* al., 2015; Babin *et al*., 2014; Fassier *et al*., 2010; Wood *et al*., 2006) where involvement of microtubules was also demonstrated (Bora et al., 2021; Clark et al., 2016; Mackay-Sim et al., 2010; Wen et al., 2010; Fanara et al., 2007). Morphological neurites aberrations induced by the altered genetic dosage of tubulin chaperon cofactor proteins have been already observed in the invertebrate fly fruit model (*Drosophila melanogaster*) in which TBCD depletion seems to promote ectopic dendrite arborization, neurite shortening and altered morphology of olfactory projection neurons (PNs) suggesting the involvement of the tubulin chaperon protein in the neuronal morphogenesis, dendrite development and axon maintenance (Okumura *et al*., 2015). With respect to TBCD, Pode-Shakked (2016) documented that zebrafish *tbcd* morphant, generated with 5' UTR ATG approach, shown microcephaly, altered muscles fibers organization and mild trunk/tail curvatures/shortening. The latter phenotypes were observed also in the zebrafish *tbcd* MO splicing site model proposed and confirm the specificity of these effects of TBCD knockdown on development. Besides that, the contribute of tubulin chaperon cofactor in neurite development and homeostasis in highly specialized cells population such as spinal motor neurons were not already evaluated in any *in vivo* model. My analysis on pre-synaptic neurite by immunofluorescence assay (IF) of *znp1* together with a stratified 3D morphogenic characterization reveal a shortening of primary MNs neurites with altered branching, a diminishing of polarity and less myotome occupancy in *tbcd* morphants. We observed a similar morphological outcome (*i.e.* neurite extension) also in *tbce* morphants. A mouse model of TBCE LoF is already available (*pmn* mutant) that shows

neurodegeneration in the motoneurons and further support our findings (Bellouze *et al*., 2014; Bommel *et al*., 2002). In the light of these results and considered the limitation of the transient approach for long-term suppression studies and the milder effects induced by gene expression down-regulation, we asked about the possibility 1) to confirm the observed cellular phenotype in stable *TBCD* mutant embryos with 2) expectation of a worsening of the phenotype itself and 3) what happened to MNs development and survival. Of note, to this aim, stable mutant embryos were generated by Dr. A. Lauri by injecting specific gRNA using CRISPR-Cas9 *genome editing* technology (Albadri *et al*., 2017) to target initial *tbcd* exons such to generate KO model. The establishment up to F2-F3 generation is still being carrying out by different colleagues in the zebrafish lab, however in the second part of my PhD. we focused our analysis on the G0 generation, which is widely used for phenotypic analysis as an approximation of homozygous LoF model (Espino-Saldaña *et al*., 2020). Zebrafish *tbcd* crispants model confirmed specific evidence that corroborated our initial hypothesis: indeed, using immunofluorescence combined to confocal imaging microscopy, we demonstrated that an altered dosage of TBCD induced aberrant MNs morphologies and, moreover, we showed aberrant innervation and muscle organization at later stages of embryogenesis (not observed in the transient models) probably linked to a failure in synapses formation, and then loss, which is clearly associated to neurodegeneration (Buettner *et al*., 2021; Tay *et al*., 2021; Simon *et al*., 2019; Spring *et al*., 2019; Wishart *et al*., 2006). In fact, from comparative studies present in literature, it is known that synapses and spMNs losses occur prior to cell body loss (see Appendix 6.3) that is a hallmark coinciding with the onset of the neurodegenerative symptoms (Carlini, Triplett, Pellizzoni, 2022; Courtney *et al*., 2019; Martineau *et al*., 2018; Gould *et al*., 2006) such as motor milestones loss observed in *TBCD* pediatric patients.

PART III

Flex (2016) documented that defective TBCD functions has remarkable effects on MTs dynamics by perturbing the polymerization rate and stability of microtubule (Flex *et al*., 2016). Starting from this evidence, we hypothesized that the dose-dependent effects on MN's development and correct muscle innervation is linked to the crucial role of the TBCD protein in the fine tuning of MTs network poly- and depolymerization which seem to be extremely sensitive to the precise TBCD levels (Edvardson *et al*., 2016). Different

works in literature suggest that local cytoskeletal protein synthesis and modifications at the growth cone remarkably contribute to the axonal guidance (Biswas&Kalil, 2018; Stoeckli, 2018; Baas *et al*., 2016; Dubey et al., 2015). Given the opportunity to use 2D STED *super resolution* microscopy and by analyzing the coverage length of detyrosinated α-tubulin (post-translational modification of MTs stability) among the MT's β-tubulin main shaft, we found an unbalance shift toward an increasing polymerization rate in zebrafish *tbcd* crispants as observed in patient-derived *in vitro* cellular model (Flex *et al*., 2016).

In summary, all the data collected during my PhD thesis indicate that tubulin chaperons tbcd and tbce proteins LoF in zebrafish embryos has a strong and specific effect on the formation and maturation of early spinal MNs: zebrafish *tbcd* transient model presents a milder alteration in MNs morphogenesis while in stable crispant mutants the process is strongly affected and seems to be paired with the synapse's impairment. S*uper resolution* technology now allowing to visualize biological structures bigger less the 100 nm, preliminary data assessed on MTs assembly carried out on early stable *tbcd* G0 crispant suggests that excessive MTs polymerization could explain MNs extension defects observed so far. Moreover, *tbcd* crispant G0 showed an aberrant muscle organization, not observable in the transient model, probably linked to a failure in synapses formation. These results brought us to support the hypothesis that the correct tubulin chaperone protein dosage is mandatory to ensure the correct MNs development and pathfinding during embryogenesis.

Therefore, taken together all the findings provided by my work resumed in **Fig. 43**, and considered the heterogeneity of crispants penetrance phenotypes, we would like to test next on stable KO mutants whether *tbcd* complete LoF could generate these types of cellular defects depending on altered microtubules assembly and to clarify the molecular pathogenetic mechanism which could explain the MNs "dying-back" phenomenon observed in a number of motor neurons diseases (Yaron&Schuldiner, 2016; Dubey *et al*., 2015; Wood *et al*., 2006), included tubulinopathies disorders. Further studies will be required to test whether a neurodegenerative aspect is observed in addition to the neurodevelopmental defects and what is the impact of TBCD and TBCE on neuronal function. In the future, the presence of cellular markers that could help to define the asymptomatic time window during which it is may possible to rescue or delay the onset

of neurodegeneration symptoms could be performed by testing battery of drugs commonly used to prevent MTs polymerization.

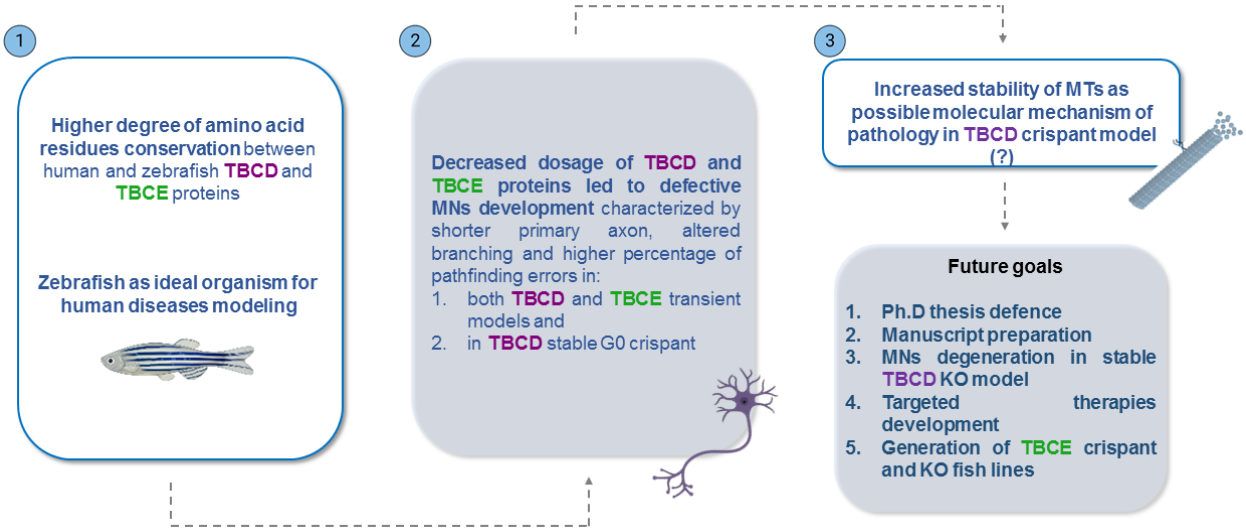

Fig. 43: Schematic diagram summarizing my PhD results and discussion.

6. APPENDIX

Preliminary investigation on primary motoneurons (CaP spMNs) apoptosis profile in *tbcd* KO fish spinal cord

The pathogenic processes underlying MND are likely to be multifactorial and current understanding of the neurodegenerative process suggests that the mechanisms leading to motor neuron death can be attributed to oxidative stress, protein aggregation, damage to critical cellular processes (*e.g.* axonal transport) and organelles such as mitochondria and cytoskeleton (Ragagnin *et al*, 2019; Shaw, 2005). These mechanisms should be investigated in the near future in the *tbcd/tbce* KO fish models generated.

Besides the data collected so far during my PhD, both in *tbcd* morphants and early G0 crispant embryos, in the last part of my work I attempted to evaluate occurrence of spMNs death in late *tbcd knock-out* (KO) G3 fish established by colleagues in the lab. Besides the necessity to use stable CRISPR-Cas9 for longitudinal studies (Varshney et al., 2015), crispant have limitations as they are heterogeneous mosaics for the mutation. Therefore, the aim of the analysis and of future work of this project is to test further and deepen the evidence of the detrimental impact of *tbcd* LoF on spMNs development and homeostasis in stable *tbcd* KO animals characterized by homogenous genetic background. In this context, I began to perform immunofluorescences on late *tbcd* KO G3 mutants by combining Islet 1-2 antibody (ISL LIM Homeobox 1-2), labelling developing motor neurons, with the In-Situ Cell Death Detection Kit, TMR red (Roche), labelling apoptotic cells, by following manufacturer's instructions. Interestingly, the preliminary analysis seems to confirm that, at later stages of development, $tbcd^{-/-}$ showed a higher occurrence of apoptotic events in the ventral spinal cord (* p-value <0.05) if compared to $tbcd^{+/+}$ and $tbcd^{+/-}$ (**Fig. 1 Appendix**). In the future, it will be necessary to investigate also the MNs death profile in the early spinal cord of stable *tbcd* KO G3 to assess neurodegeneration and understand the underlying mechanism.

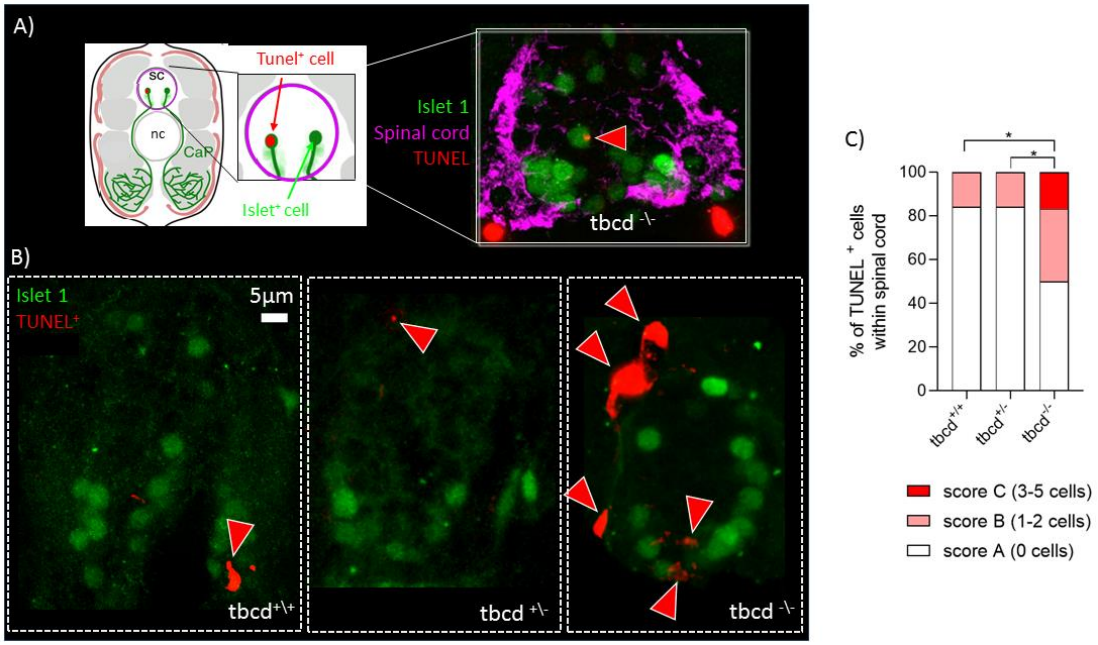

Fig. 1 Appendix: Stable *tbcd*$^{-/-}$ mutant fish showed a higher percentage of apoptotic events at later stage of development. A) Schematic representation of transversal section of zebrafish spinal cord showing CaP MNs rising from the spinal cord and innervating the ventral fast musculature. **B**) Z-projections from 3D microscopy (*x,y,z*) images showing MNs body cells in *tbcd*$^{+/+}$, *tbcd*$^{+/-}$ and *tbcd*$^{-/-}$ respectively at late stages stained with Islet 1-2 (in green) and In Situ Cell Death Detection Kit, TMR red (TUNEL^{+}, in red). Red arrowheads indicate apoptotic cells in the spinal cord. **C**) Analysis of the occurrence of apoptotic events in spMNs. N = 3 samples for *tbcd*$^{+/+}$, *tbcd*$^{+/-}$ and *tbcd*$^{-/-}$. Asterisks indicate statistically significant differences between all the genetic conditions based on Chi's-squared test in a 2x2 contingency table (* p-value <0.05).

7. BIBLIOGRAFY

Ain N. U., Muhammad N., Dianatpour M., Baroncelli M., Iqbal M., Fard M. A. F., Bukhari I., Ahmed S., Hajipour M., Tabatabaie Z., Foroutan H., Nilsson O., Faghihi M. A., Makitie O., Naz S. Biallelic TMEM251 variants in patients with severe skeletal dysplasia and extreme short stature. *Human Mutation*, 2021;42(1):89-101. doi: 10.1002/humu.24139.

Albadri S., De Santis F., Di Donato V., Del Bene F. CRISPR/Cas9-Mediated Knockin and Knockout in Zebrafish. In: Jaenisch R, Zhang F, Gage F, editors. *Genome Editing in Neurosciences*. Research and Perspectives in Neurosciences. Springer, Cham., 2017; pages 41-49. https://doi.org/10.1007/978-3-319-60192-2_4

Ali S., Champagne D. L., Spainkand H. P., Richardson M. K. Zebrafish Embryos and Larvae: A NewGeneration of Disease Models and Drug Screens. *Birth Defects Research* (Part C), 2011; 93:115–133. DOI: 10.1002/bdrc.20206.

Alhindi A., Boehm I., Chaytow H. Small junction, big problems: Neuromuscular junction pathology in mouse models of amyotrophic lateral sclerosis (ALS). *Journal of Anatomy*, 2022;241(5):1089-1107. doi: 10.1111/joa.13463.

Anzalone A.V., Koblan L. W., Liu, D. R. Genome editing with CRISPR–Cas nucleases, base editors, transposases and prime editors. *Nature Biotechnology*, 2020; 38, 824–844. https://doi.org/10.1038/s41587-020-0561-9

Arber S., Han B., Mendelsohn M., Smith M., Jessell T. M., Sockanathan S. Requirement for the Homobox Gene Hb9 in the Consolidation of Motor Neuron Identity. *Neuron*, 1999; Volume 23, Issue 4, pages 659-674. DOI: 10.1016/s0896-6273(01)80026-x.

Arora R. A. and Khan Y. S. Motor Neuron Disease. [Updated 2023 May 20]. In: StatPearls [Internet]. Treasure Island (FL): *StatPearls Publishing*; 2023 Jan. Available from: https://www.ncbi.nlm.nih.gov/books/NBK560774/.

Assoni A.F., Foijer F., Zatz M. Amyotrophic Lateral Sclerosis, FUS and Protein Synthesis Defects. *Stem Cell Reviews and Reports*, 2023, 19, 625–638. DOI: 10.1007/s12015-022-10489-8.

Avilés E. C., Wilson N. H., Stoeckli E. T. Sonic hedgehog and Wnt: antagonists in morphogenesis but collaborators in axon guidance. *Frontiers in Cellular Neuroscience*, 2013, 10;7:86. https://doi.org/10.3389/fncel.2013.00086.

Baas P. W., Rao A. N., Matamoros A. J., Leo L. Stability properties of neuronal microtubules. *Cytoskeleton* (Hoboken), 2016; 73(9):442-60. doi: 10.1002/cm.21286.

Babin P. J., Goizet C., Raldúa D. Zebrafish models of human motor neuron diseases: Advantages and limitations. *Progress in Neurobiology*, 2014; Volume 118, pages 36-58. DOI: 10.1016/j.pneurobio.2014.03.001.

Bahi-Buisson N and Maillard C. Tubulinopathies Overview, 2016 Mar 24 [Updated 2021 Sep 16]. In: Adam M. P., Mirzaa G. M., Pagon R. A. *et al*., editors. *GeneReviews*® [Internet]. Seattle (WA): University of Washington, Seattle; 1993-2023. https://www.ncbi.nlm.nih.gov/books/NBK350554/.

Bakkar N., Starr A., Rabichow B. E., Lorenzini I., McEachin Z. T., Kraft R., Chaung M., Macklin-Isquierdo S., Wingfield T., Carhart B., Zahler N., Chang W. H., Bassell G. J., Betourne A., Boulis N., Alworth S. V., Ichida J. K., August P. R., Zarnescu D. C., Sattler R., Bowser R. The M1311V variant of ATP7A is associated with impaired trafficking and copper homeostasis in models of motor neuron disease. *Neurobiology of Disease,* 2021; 149:105228. 10.1016/j.nbd.2020.105228.

Bamshad M. J., Ng S. B., Bigham A. W., Tabor H. K., Emond M. J., Nickerson D. A., Shendure J. Exome sequencing as a tool for Mendelian disease gene discovery. *Nature Reviews Genetics*, 2011 Sep 27;12(11):745-55. DOI: 10.1038/nrg3031.

Bandmann O., Burton E. A. Genetic zebrafish models of neurodegenerative diseases. *Neurobiology of Disease,* 2010; 40, 58–65. DOI: 10.1016/j.nbd.2010.05.017.

Bartolini E. Inherited Developmental and Epileptic Encephalopathies. *Neurology International*, 2021, 13(4), 555-568. doi: 10.3390/neurolint13040055.

Bashaw G. J., Klein R. Signaling from axon guidance receptors. *Cold Spring Harbor Perspectives in Biology*, 2010;2(5):a001941. DOI: 10.1101/cshperspect.a001941.

Bashirzade A. A, Zabegalov K. N., Volgin A. D., Belova A. S., Demin K. A., de Abreu M. S., Babchenko V. Y., Bashirzade K. A., Yenkoyan K. B., Tikhonova M. A., Amstislavskaya T. G., Kalueff A. V. Modeling neurodegenerative disorders in zebrafish. *Neuroscience & Biobehavioral Reviews*, 2022;138:104679. DOI: 10.1016/j.neubiorev.2022.104679.

Bauer C. K., Calligari P., Radio F. C., Caputo V., Dentici M. L., Falah N., High F., Pantaleoni F., Barresi S., Ciolfi A., Pizzi S., Bruselles A., Person R., Richards S., Cho M. T., Claps Sepulveda D. J., Pro S., Battini R., Zampino G., Digilio M. G., Bocchinfuso G., Dallapiccola B., Stella L., Tartaglia M. (2018). Mutations in KCNK4 that Affect Gating Cause a Recognizable Neurodevelopmental Syndrome. *American Journal of Human Genetics*, Volume 103, Issue 4, pp 621-630, Oct 04, 2018. doi: 10.1016/j.ajhg.2018.09.001.

Bello-Rojas S., Istrate A. E., Kjshore S., McLean D. L. Central and peripheral innervation patterns od defined axial motor units in larval zebrafish. *Journal of Comparative Neurobiology*., 2019; bioRxiv 559062. DOI: 10.1002/cne.24689.

Bellouze S., Schäfer M. K., Buttigieg D., Baillat G., Rabouille C., Haase G. Golgi fragmentation in pmn mice is due to a defective ARF1/TBCE cross-talk that coordinates COPI vesicle formation and tubulin polymerization. *Human Molecular Genetics*, 2014; 23(22):5961-75. doi: 10.1093/hmg/ddu320.

Berg E. M., Björnfors E. R., Pallucchi I., Picton L. D., El Manira A. Principles Governing Locomotion in Vertebrates: Lessons From Zebrafish. *Frontiers in Neural Circuits*, 2018;12:73. https://doi.org/10.3389/fncir.2018.00073.

Bhati M., Llamosas E., Jacques D.A., Jeffries C.M., Dastmalchi S., Ripin, N., Nicholas H.R., Matthews J.M., Interactions between LHX3- and ISL1-family LIM-homeodomain transcription factors are conserved in *Caenorhabditis elegans*. *Scientific Reports*, 2017; 7, 4579. DOI:10.1038/s41598-017-04587-8.

Bhattacharjee A., Sokolsky T., Wyman S. K., Reese M. G., Puffenberger E., Strauss K., Morton H., Parad R. B., Naylor E. W. Development of DNA confirmatory and high-risk diagnostic testing for newborns using targeted next-generation DNA sequencing. *Genetics in Medicine*, 2015;17(5):337-47. doi: 10.1038/gim.2014.117.

Bill B. R., Petzold A. M., Clark K. J., Schimmenti L. A., Ekker S. C. A primer for morpholino use in zebrafish. *Zebrafish,* 2009; 6(1):69-77. doi: 10.1089/zeb.2008.0555.

Biswas S., Kalil K. The Microtubule-Associated Protein Tau Mediates the Organization of Microtubules and Their Dynamic Exploration of Actin-Rich Lamellipodia and Filopodia of Cortical Growth Cones. *The Journal of Neuroscience*, 2018; 38(2):291-307. doi: 10.1523/JNEUROSCI.2281-17.2017.

Bobone S., Pannone L., Biondi B., Solman M, Flex E., Canale V. C., Calligari P., De Faveri C., Gandini T., Quercioli A., Torini G., Venditti M., Lauri A., Fasano G., Hoeksma J., Santucci V., Cattani G., Bocedi A., Carpentieri G., Tirelli V., Sanchez M., Peggion C., Formaggio F., den Hertog J., Martinelli S., Bocchinfuso G., Tartaglia M., Stella L. Targeting Oncogenic Src Homology 2 Domain-Containing Phosphatase 2 (SHP2) by Inhibiting Its Protein–Protein Interactions. *Journal of Medicinal Chemistry*, 2021 64 (21), 15973-15990. doi: 10.1021/acs.jmedchem.1c01371.

Bommel H., Xie G., Rossoll W., Wiese S., Jablonka S., Boehm T., Sendtner M. Missense mutation in the tubulin-specific chaperone E (Tbce) gene in the mouse mutant progressive motor neuronopathy, a model of human motoneuron disease. *Journal of Cell Biology*, 2002;159(4):563-9. doi: 10.1083/jcb.200208001.

Bonsignorio D., Perego L., Del Giacco L., Cotelli F. Structure and macromolecular composition of the zebrafish egg chorion. *Zygote*, 1996; 4(2):101-8. DOI: 10.1017/s0967199400002975.

Bora G., Hensel N., Rademacher S., Koyunoğlu D., Sunguroğlu M., Aksu-Mengeş E., Balcı-Hayta B., Claus P., Erdem-Yurter H. Microtubule-associated protein 1B dysregulates microtubule dynamics and neuronal mitochondrial transport in spinal muscular atrophy. *Human Molecular Genetics*, 2021; 29(24):3935-3944. doi: 10.1093/hmg/ddaa275.

Bose P., Armstrong G. A. B., Drapeau P. Neuromuscular junction abnormalities in a zebrafish loss-of-function model of TDP-43. *Journal of Neurophysiology*, 2019;121(1):285-297. doi: 10.1152/jn.00265.2018.

Braasch I., Gehrke A. R., Smith J. J., Kawasaki K., Manousaki T., Pasquier J., Amores A., Desvignes T., Batzel P., Catchen J., Berlin A. M., Campbell M. S., Barrel D., Martin K. J., Mulley J. F., Ravi V., Lee A. P., Nakamura T., Chalopin D., Fan S., Wcisel D., Cañestro C., Sydes J., Beaudry F. E. G., Sun Y., Hertel J., Beam M. J., Fasold M., Ishiyama M., Johnson J., Kehr S., Lara M., Letaw J. H., Litman G. W., Litman R. T., Mikami M., Ota T., Ratan Saha N., Williams L., Stadler P. F., Wang H., Taylor J. S., Fontenot Q., Ferrara A., Searle S. M. J., Aken B., Yandell M., Schneider I., Yoder J. A., Volff J-N., Meyer A., Amemiya C. T., Venkatesh B., Holland P. W. H., Guiguen Y., Bobe J., Shubin N. H., Di Palma F., Alföldi J., Lindblad-Toh K., Postlethwait J. H. The spotted gar genome illuminates vertebrate evolution and facilitates human-teleost comparisons. *Nature Genetics*., 2016; 48, pages427–437. Doi: https://doi.org/10.1038/ng.3526.

Brinkley W. Microtubules: a brief historical perspective. *Journal of Structural Biology*. 1997; 118(2):84-6. DOI: 10.1006/jsbi.1997.3854.

Brinkman E. K., Chen T., de Haas M., Holland H. A., Akhtar W., van Steensel B. Kinetics and Fidelity of the Repair of Cas9-Induced Double-Strand DNA Breaks. *Molecular Cell*, 2018;70(5):801-813.e6. doi: 10.1016/j.molcel.2018.04.016.

Buettner J. M., Sime Longang J. K., Gerstner F., Apel K. S., Blanco-Redondo B., Sowoidnich L., Janzen E., Langenhan T., Wirth B., Simon C. M. Central synaptopathy is the most conserved feature of motor circuit pathology across spinal muscular atrophy mouse models. *iScience*, 2021;24(11):103376. doi: 10.1016/j.isci.2021.103376.

Bunnik E. M. and K. Le Roche. An Introduction to Functional Genomics and Systems Biology. *Advance in Wound Care*, 2013, 2(9):490-498. doi: 10.1089/wound.2012.0379.

Butler R., Wood J. D., Landers J. A., Cunliffe V. T. Genetic and chemical modulation of spastin-dependent axon outgrowth in zebrafish embryos indicates a role for impaired microtubule dynamics in hereditary spastic paraplegia. *Disease Models & Mechanisms*, 2010; 3(11-12):743-51. doi: 10.1242/dmm.004002.

Butti Z., Pan Y. E., Giacomotto J., Patten S. A. Reduced C9orf72 function leads to defective synaptic vesicle release and neuromuscular dysfunction in

zebrafish. *Communication Biology*. 2021; 4:792. https://doi.org/10.1038/s42003-021-02302-y.

Caputo M., Martinelli I., Fini N., Gianferrari G., Simonini C., Trovato R., Santorelli F. M., Tessa A., Mandrioli J., Zucchi E. A Variant in TBCD Associated with Motoneuronopathy and Corpus Callosum Hypoplasia: A Case Report. *International Journal of Molecular Sciences,* 2023; 24(15):12386. doi: 10.3390/ijms241512386.

Carlini M. J., Triplett M. K., Pellizzoni L. Neuromuscular denervation and deafferentation but not motor neuron death are disease features in the Smn2B/- mouse model of SMA. *PLoS One*, 2022;17(8):e0267990. doi: 10.1371/journal.pone.0267990.

Catela C., Kratsios P. Transcriptional mechanisms of motor neuron development in vertebrates and invertebrates. *Developmental Biology*, 2021, Volume 457, pages 193-204. DOI: 10.1016/j.ydbio.2019.08.022.

Caudron F., Denarier E., Thibout-Quintana J. C., Brocard J., Andrieux A., Fourest-Lieuvin A. Mutation of Ser172 in yeast β tubulin induces defects in microtubule dynamics and cell division. *PLoS One*, 2010; 5(10):e13553. doi: 10.1371/journal.pone.0013553.

Chen, C-L., Lee C-N., Chien Y-H., Hwu W-L., Chang T-M., Lee N-C. Novel Compound Heterozygous Variants in TBCD Gene Associated with Infantile Neurodegenerative Encephalopathy. *Children,* 2021; 8, 1140. DOI: 10.3390/children8121140.

Chilton J. K. Molecular mechanisms of axon guidance. *Developmental Biology*, 2006; Volume 292, Issue 1, pages 13-24. DOI: 10.1016/j.ydbio.2005.12.048.

Chitnis A. B., Dawid I. B. Chapter 20: Neurogenesis in Zebrafish Embryos. *Methods in Cell Biology*, 1998; pp. 367–386. https://doi.org/10.1016/S0091-679X(08)61835-X.

Ciura S., Lattante S., Le Ber I., Latouche M., Tostivint H., Brice A., Kabashi E. Loss of function of C9orf72 causes motor deficits in a zebrafish model of

amyotrophic lateral sclerosis. *Annals of Neurology*, 2013;74(2):180-7. doi: 10.1002/ana.23946.

Clark J. A., Yeaman E. J., Blizzard C. A., Chuckowree J. A., Dickson T. C. A Case for Microtubule Vulnerability in Amyotrophic Lateral Sclerosis: Altered Dynamics During Disease. *Frontiers in Cellular Neuroscience*, 2016; 10:204. doi: 10.3389/fncel.2016.00204.

Coppola A., Lombari P., Mazzella E., Capolongo G., Simeoni M., Perna A. F., Ingrosso D., Borriello M. Zebrafish as a Model of Cardiac Pathology and Toxicity: Spotlight on Uremic Toxins. *International Journal of Molecular Sciences*, 2023; 24(6):5656. DOI: 10.3390/ijms24065656.

Corthell J. T. (2014), Chapter 10 - Immunohistochemistry, Editor(s): John T. Corthell, Basic Molecular Protocols in Neuroscience: Tips, Tricks, and Pitfalls, *Academic Press*, 2014, Pages 91-103, ISBN 9780128014615, https://doi.org/10.1016/B978-0-12-801461-5.00010-1.

Courtney N. L., Mole A. J., Thomson A. K., Murray L. M. Reduced P53 levels ameliorate neuromuscular junction loss without affecting motor neuron pathology in a mouse model of spinal muscular atrophy. *Cell Death Disease*, 2019; 10(7):515. https://doi.org/10.1038/s41419-019-1727-6.

D'Elia K. P., Dasen J. S. Development, functional organization, and evolution of vertebrate axial motor circuits. *Neural Development*, 2018; 13:10. https://doi.org/10.1186/s13064-018-0108-7.

Da Costa M. M., Allen C. E., Higginbottom A., Ramesh T., Shaw P. J., McDermott C. J. A new zebrafish model produced by TILLING of SOD1-related amyotrophic lateral sclerosis replicates key features of the disease and represents a tool for in vivo therapeutic screening. *Disease Models & Mechanisms*, 2014;7(1):73-81. DOI: 10.1242/dmm.012013.

Damianidou E., Mouratidou L., Kyrousi C. Research models of neurodevelopmental disorders: The right model in the right place. *Frontiers in Neuroscience*, 2022; 16:1031075. doi: 10.3389/fnins.2022.1031075.

Dent E. W., Gupton S. L., Gertler, F. B. The growth cone cytoskeleton in axon outgrowth and guidance. *Cold Spring Harbor Perspectives in Biology*; 2011; 3:a001800. doi: 10.1101/cshperspect.a001800.

Dolan J., Walshe K., Alsbury S., Hokamp K., O'Keeffe S., Okafuji T., Miller S. F. C., Tear G., Mithcell K. J. The extracellular Leucine-Rich Repeat superfamily; a comparative survey and analysis of evolutionary relationships and expression patterns. *BMC Genomics*, 2007; 8, 320. DOI: 10.1186/1471-2164-8-320.

Domínguez-Oliva A., Hernández-Ávalos I., Martínez-Burnes J., Olmos-Hernández A., Verduzco-Mendoza A., Mota-Rojas D. The Importance of Animal Models in Biomedical Research: Current Insights and Applications. *Animals*, 2023; 13(7):1223. https://doi.org/10.3390/ani13071223.

Dubey J., Ratnakaran N., Koushika S. P. Neurodegeneration and microtubules dynamics: death by thousand cuts. *Frontiers in Cellular Neuroscience*, 2015; 9:343. https://doi.org/10.3389/fncel.2015.00343.

Edvardson S., Tian G., Cullen H., Vanyai H., Ngo L., Bhat S., Aran A., Daana M., Da'amseh N., Abu-Libdeh B., Cowan N. J., Heng J. I., Elpeleg O. Infantile neurodegenerative disorder associated with mutations in TBCD, an essential gene in the tubulin heterodimer assembly pathway. *Human Molecular Genetics,* 2016; 1;25(21):4635-4648. doi: 10.1093/hmg/ddw292.

Eisen J.S., Pike S.H., Debu B. The growth cones of identified motoneurons in embryonic zebrafish select appropriate pathways in the absence of specific cellular interactions. *Neuron*, Volume 2, Issue 1, January 1989, Pages 1097-1104. DOI: 10.1016/0896-6273(89)90234-1.

El Ghouzzi V., Boncompain G. Golgipathies reveal the critical role of the sorting machinery in brain and skeletal development. *Nature Communication*, 2022; 13, 7397. https://doi.org/10.1038/s41467-022-35101-y.

Engeszer R. E., Patterson L. B., Rao A. A., Parichy D. M. Zebrafish in the Wild: A Review of Natural History and New Notes from the Field. *Zebrafish*, 2017; 4(1): 21-U126. DOI: 10.1089/zeb.2006.9997.

Espino-Saldaña A. E., Rodríguez-Ortiz R., Pereida-Jaramillo E., Martínez-Torres A. Modeling Neuronal Diseases in Zebrafish in the Era of CRISPR. *Current*

Neuropharmacology, 2020, 18(2):136-152. doi: 10.2174/1570159X17666191001145550.

Fanara P., Banerjee J., Hueck R. V., Harper M. R., Awada M., Turner H., Husted K. H., Brandt R., Hellerstein M. K. Stabilization of hyperdynamic microtubules is neuroprotective in amyotrophic lateral sclerosis. *Journal of Biological Chemistry*, 2007; 282(32):23465-72. doi: 10.1074/jbc.M703434200.

Fasano G., Muto V., Radio F.C., Venditti M., Mosaddeghzadeh N., Coppola S., Paradisi G., Zara E., Bazgir F., Ziegler A., Chillemi G., Bertuccini L., Tinari A., Vetro A., Pantaleoni F., Pizzi S., Conti L.A., Petrini S., Bruselles A., Prandi I.G., Mancini C., Chandramouli B., Barth M., Bris C., Milani D., Selicorni A., Macchiaiolo M., Gonfiantini M.V., Bartuli A., Mariani R., Curry C.J., Guerrini R., Slavotinek A., Iascone M., Dallapiccola B., Ahmadian M.R., Lauri A., Tartaglia M. (2022). Dominant *ARF3* variants disrupt Golgi integrity and cause a neurodevelopmental disorder recapitulated in zebrafish. *Nature Communication* 13, 6841 (2022). DOI: 10.1038/s41467-022-34354-x.

Fassier C., Hutt J. A., Scholpp S., Lumsden A., Giros B., Nothias F., Schneider-Maunoury S., Houart C., Hazan J. Zebrafish atlastin controls motility and spinal motor axon architecture via inhibition of the BMP pathway. *Nature Neuroscience*, 2010; 13(11):1380-7. doi: 10.1038/nn.2662.

Federazione Italiana Malattie Rare. MonitoRARE: VIII Report on the situation of people living with a rare disease in Italy, 2022. https://download2.eurordis.org/rdpolicy/National%20Plans/Italy/6.Executive%20summary_MONITORare%20VIII_2022_English.pdf.

Ferguson J. L., Shive H. R. Sequential Immunofluorescence and Immunohistochemistry on Cryosectioned Zebrafish Embryos. *Journal of Visualized Experiments*, 2019; (147), e59344. DOI: 10.3791/59344.

Flex E., Albadri S., Radio F. C., Cecchetti S., Lauri A., Priolo M., Kissopoulos M., Carpentieri G., Fasano G., Venditti M., Magliocca V., Bellacchio E., Welch C. L., Colombo P. C., Kochav S. M., Chang R., Barrick R., Trivisano M., Micalizzi A., Borghi R., Messina E., Mancini C., Pizzi S., De Santis F., Rosello M., Specchio N., Compagnucci C., McWalter K., Chung W. K., Del Bene F., Tartaglia M. Dominantly acting KIF5B variants with pleiotropic cellular consequences cause

variable clinical phenotypes. *Human Molecular Genetics*. 2023, 32(3):473-488. doi: 10.1093/hmg/ddac213.

Flex E., Niceta M., Cecchetti S., Thiffault I., Au M. G., Capuano A., Piermarini E., Ivanova A. A., Francis J. W., Chillemi G., Chandramouli B., Carpentieri G., Haaxma C. A., Ciolfi A., Pizzi S., Douglas G. V., Levine K., Sferra A., Dentici M. L., Pfundt R. R., Le Pichon J-B., Farrow E., Baas F., Piemonte F., Dallapiccola B., Graham Jr. J. M., Sounders C. J., Bertini E., Kahn R. A., Koolen D. A., Tartaglia M. (2016). Biallelic Mutations in TBCD, Encoding the Tubulin Folding Cofactor D, Perturb Microtubule Dynamics and Cause Early-Onset Enchephalopathy. *American Journal of Human Genetics*, 2016; Volume 99, Issue 4, p 962-973. Doi: 10.1016/j.ajhg.2016.08.003.

Foster L. A., Salajegheh M. K. Motor Neuron Disease: Pathophysiology, Diagnosis, and Management. *The American Journal of Medicine*, Volume 132, Issue 1, Jan 2019, pages 32-37. DOI: 10.1016/j.amjmed.2018.07.012.

Fourest-Lieuvin A., Peris L., Gache V., Garcia-Saez I., Juillan-Binard C., Lantez V., Job D. Microtubule regulation in mitosis: tubulin phosphorylation by the cyclin-dependent kinase Cdk1. *Molecular Biology of the Cell*, 2006; 17(3):1041-50. doi: 10.1091/mbc.e05-07-0621.

Fox M.A., Sanes J.R. Synaptotagmin I and II are present in distinct subsets of central synapses. *Journal of Comparative Neurology*. 2007 Jul 10;503(2):280-96. doi: 10.1002/cne.21381. PMID: 17492637. DOI: 10.1002/cne.21381.

Franker M. A. M., Hoogenraad C. C. Microtubule-based transport – basic mechanisms, traffic rules and role in neurological pathogenesis. *Journal of Cell Science*, 2013; 126: 2319-2329. DOI: 10.1242/jcs.115030.

Garnham C. P., Roll-Mecak A. The chemical complexity of cellular microtubules: Tubulin post-translational modification enzymes and their roles in tuning microtubule functions. *Cytoskeleton*, 2012; 69: 442-463. DOI: 10.1002/cm.21027.

Ghasemi A., Zahediasl S. Normality Tests for Statistical Analysis: A Guide for Non-Statisticians. *International Journal of Endocrinology and Metabolism*. 2012. 10(2). doi: 10.5812/ijem.3505.

Giacomotto J., Rinkwitz S., Becker T. Effective heritable gene knockdown in zebrafish using synthetic microRNAs. *Nature Communication*, 2015;6, 7378. https://doi.org/10.1038/ncomms8378.

Gould T. W., Buss R. R., Vinsant S., Prevette D., Sun W., Knudson C. M., Milligan C. E., Oppenheim R. W. Complete dissociation of motor neuron death from motor dysfunction by Bax deletion in a mouse model of ALS. The *Journal of Neuroscience*. 2006;26(34):8774-86. doi: 10.1523/JNEUROSCI.2315-06.2006.

Gouti M., Metzis V., Briscoe J. The route to spinal cord cell types: a tale of signals and switches. *Trends in Genetics*, 2015; Volume 31, Issue 6, pages 282-289. DOI: 10.1016/j.tig.2015.03.001.

Grillner S., El Manira A. Current Principles of Motor Control, with Special Reference to Vertebrate Locomotion. *Physiological Reviews*, 2020;100(1):271-320. DOI: 10.1152/physrev.00015.2019.

Grønborg S., Risom L., Ek J., Larsen K. B., Scheie D., Petkov Y., Larsen V. A., Dunø M., Joensen F., Østergaard E. A Faroese founder variant in TBCD causes early onset, progressive encephalopathy with a homogenous clinical course. *European Journal of Human Genetics*, 2018; 26, 1512–1520. doi: 10.1038/s41431-018-0204-5.

Groves M. R., Barford D. Topological characteristics of helical repeat proteins. *Current Opinion in Structural Biology*; 1999, 9:383-389. doi: 10.1016/s0959-440x(99)80052-9.

Grynberg M., Jaroszewski L., Godzik A. Domain analysis of the tubulin cofactor system: a model for tubulin folding and dimerization. *BMC Bioinformatics*. 2003, 4, Article number: 46 (2003). DOI: 10.1186/1471-2105-4-46.

Gudimchuk N. B., McIntosh J. R. Regulation of microtubule dynamics, mechanics and function through the growing tip. *Nature Reviews Molecular Cell Biology*, 2021; 22, 777–795. DOI: 10.1038/s41580-021-00399-x.

Hamilton F. An account of the fishes found in the river Ganges and its branches. *Constable*, 1822; Vol. 1. DOI: https://doi.org/10.5962/bhl.title.6897.

Hirokawa N., Niwa S., Tanaka Y. Molecular motors in neurons: transport mechanisms and roles in brain function, development, and disease. *Neuron*, 2010; 68, 610–638. DOI: 10.1016/j.neuron.2010.09.039.

Halpern M. E., Rhee J., Goll M. G., Akitake C. M., Parsons M., Leach S. D. Gal4/UAS transgenic tools and their application to zebrafish. *Zebrafish*, 2008; 5(2):97-110. doi: 10.1089/zeb.2008.0530.

Holland L. Z. chapter 4 - Invertebrate Origins of Vertebrate Nervous Systems. *Evolutionary Neuroscience (Second Edition)*. 2020; pages 51-73. https://doi.org/10.1016/B978-0-12-820584-6.00004-0.

Holland L. Z. Chordate roots of the vertebrate nervous system: expanding the molecular toolkit. *Nature Review Neuroscience*, 2009, 10, 736–746. DOI: 10.1038/nrn2703.

Holmes A. D., White K. A., Pratt M. A, Johnson T. B., Likhite S., Meyer K., Weimer J. M. Sex-split analysis of pathology and motor-behavioral outcomes in a mouse model of CLN8-Batten disease reveals an increased disease burden and trajectory in female Cln8mnd mice. *Orphanet Journal of Rare Diseases*, 2022;17(1):411. DOI: 10.1186/s13023-022-02564-7.

Ikeda T., Nakahara A., Nagano R., Utoyama M., Obara M., Moritake H., Uechi T., Mitsui J., Ishiura H., Yoshimura J., Doi K., Kenmochi N., Morishita S., Nishino I., Tsuji S., Nunoi H. TBCD may be a causal gene in progressive neurodegenerative encephalopathy with atypical infantile spinal muscular atrophy. *Journal of Human Genetics,* 2017;62(4):473-480. doi: 10.1038/jhg.2016.149.

Ikenaka, K., Tsukada, Y., Giles, A. C., Arai T., Nakadera Y., Nakano S., Kawai K., Mochizuki H., Katsuno M., Sobue G., Mori I. A behavior-based drug screening system using a *Caenorhabditis elegans* model of motor neuron disease. *Scientific Reports*, 2019; 9, 10104. https://doi.org/10.1038/s41598-019-46642-6.

Jaworski J., Kapitein L. C., Gouveia S. M., Dortland B. R., Wulf P. S., Grigoriev, I., Camera P., Spangler S. A., Di Stefano P., Demmers J., Krugers H., Defilippi P., Akhmanova A., Hoogenraad C. C. Dynamic microtubules regulate

dendritic spine morphology and synaptic plasticity. *Neuron*, 2009; 61, 85–100. DOI: 10.1016/j.neuron.2008.11.013.

Jin S., Pan L., Liu Z., Wang Q., Xu Z., Zhang Y. Q. *Drosophila* Tubulin-specific chaperone E functions at neuromuscular synapses and is required for microtubule network formation. *Development*, 2009; 136(9): 1571-1581. DOI: 10.1242/dev.029983.

Joshi S., Yu D. Chapter 8 – Immunofluorescence. Editor(s): Morteza Jalali, Francesca Y. L. Saldanha, Mehdi Jalali. *Basic Science Methods for Clinical Researchers*, Academic Press, 2017, Pages 135-150, https://doi.org/10.1016/B978-0-12-803077-6.00008-4.

Kabashi E., Bercier V., Lissouba A., Liao M., Brustein E., Rouleau G. A., Drapeau P. FUS and TARDBP but not SOD1 interact in genetic models of amyotrophic lateral sclerosis. *PLoS Genetics,* 2011;7(8):e1002214. doi: 10.1371/journal.pgen.1002214.

Kahn O. I., Sharma V., Gonzalez-Billault C., Baas P. W. Effects of kinesin-5 inhibition on dendritic architecture and microtubule organization. *Molecular Biology of the Cell*, 2015;26(1):66-77. doi: 10.1091/mbc.E14-08-1313.

Kapitein L. C., Hoogenraad C. C. Building the Neuronal Microtubule Cytoskeleton. *Neuron*, 2015; Volume 87, Issue 3, pages 492-506. DOI: 10.1016/j.neuron.2015.05.046.

Kawakami K., Asakawa K., Muto A., Wada H. Tol2-mediated transgenesis, gene trapping, enhancer trapping, and Gal4-UAS system. *Methods in Cell Biology*, 2016;135:19-37. doi: 10.1016/bs.mcb.2016.01.011.

Keil J. M., Seo J., Hsu W. H., Howell M. D., Singh R. A short antisense oligonucleotide ameliorates symptoms of severe mouse models of spinal muscular atrophy. *Molecular Therapy*, 2014; 3(7):e174. doi: 10.1038/mtna.2014.23.

Kemmler C. L., Moran H. R., Murray B. F., Scoresby A., Klem J. R., Eckert R. L., Lepovsky E., Bertho S., Nieuwenhuize S., Burger S., D'Agati G., Betz C., Puller A. C., Felker A., Ditrychova K., Bötschi S., Affolter M., Rohner N., Lovely C. B., Kwan K. M., Burger A., Mosimann C. Next-generation plasmids for

transgenesis in zebrafish and beyond. *Development*, 2023;150(8):dev201531. doi: 10.1242/dev.201531.

Kerk S. Y., Kratsios P., Hart M., Mourao R., Hobert O. Diversification of C. elegans Motor Neuron Identity via Selective Effector Gene Repression. *Neuron*, 2017; 93, pages 80-98. DOI: 10.1016/j.neuron.2016.11.036.

Kimmel C. B., Ballard W. W., Kimmel S. R., Ullman B., Schilling T. F. Stages of Embryonic Development of the Zebrafish. *Developmental Dynamics.* 1995, 203:255-310. DOI: 10.1002/aja.1002030302.

Ko S. K., Chen X., Yoon J., Shin I. Zebrafish as a good vertebrate model for molecular imaging using fluorescent probes. *Chemistry Sociecty Reviews,* 2011;40(5):2120-30. doi: 10.1039/c0cs00118j.

Kuijpers, M., and Hoogenraad, C. C. Centrosomes, microtubules and neuronal development. *Molecular and Cellular Neuroscience*, 2011; 48, 349–358. DOI: 10.1016/j.mcn.2011.05.004.

Jinek M., Chylinski K., Fonfara I., Hauer M., Doudna J. A., Charpentier, E. A programmable dual-RNA-guided DNA endonuclease in adaptive bacterial immunity. *Science*, 2012; 337, 816–821. doi: 10.1126/science.1225829

Landgraf M., Thor S. Development of Drosophila motoneurons: specification and morphology. *Seminars in Cell and Developmental Biology*, 2006; 17, 3–11. DOI: 10.1016/j.semcdb.2005.11.007.

Lauri A., Fasano G., Venditti M., Dallapiccola B., Tartaglia M. In vivo Functional Genomics for Undiagnosed Patients: The Impact of Small GTPases Signaling Dysregulation at Pan-Embryo Developmental Scale. *Frontiers in Cell and Developmental Biology*, 2021; 9:642235. doi: 10.3389/fcell.2021.642235.

Lauterbach, M. A. Finding, defining and breaking the diffraction barrier in microscopy – a historical perspective. *Optical Nanoscopy*, 2012; 1,8. https://doi.org/10.1186/2192-2853-1-8.

Leroy F., Lamotte d'Incamps B., Imhoff-Manuel R.D., Zytnicki D. Early intrinsic hyperexcitability does not contribute to motoneuron degeneration in amyotrophic lateral sclerosis. *eLife*, 2014; 3:e04046. DOI: 10.7554/eLife.04046.

Létard P., Drunat S., Vial Y., Duerinckx S., Ernault A., Amram D., Arpin S., Bertoli M., Busa T., Ceulemans B., Desir J., Doco-Fenzy M., Elalaoui S. C., Devriendt K., Faivre L., Francannet C., Geneviève D., Gérard M., Gitiaux C., Julia S., Lebon S., Lubala T., Mathieu-Dramard M., Maurey H., Metreau J., Nassererreddine S., Nizon M., Pierquin G., Pouvreau N., Rivier-Ringenbach C., Rossi M., Schaefer E., Sefiani A., Sigaudy S., Sznajer Y., Tunca Y., Guilmin Crepon S., Alberti C., Elmaleh-Bergès M., Benzacken B., Wollnick B., Woods C. G., Rauch A., Abramowicz M., El Ghouzzi V., Gressens P., Verloes A., Passemard S. Autosomal recessive primary microcephaly due to ASPM mutations: An update. Erratum in: *Human Mutation* 2019;40(1):127. DOI: 10.1002/humu.23617.

Liao J., Huang T., Srour M., Xiao Y., Chen Y., Lin S., Chen L., Hu Y., Men L., Wen J., Li B., Wen F., Xiong L. Status Epilepticus Manifested as Continuous Epileptic Spasms. *Frontiers in Neurology*, 2020; 11:65. doi: 10.3389/fneur.2020.00065.

Lin Y.C., Niceta M., Muto V., Vona B., Pagnamenta A.T., Maroofian R., Beetz C., van Duyvenvoorde H., Dentici M.L., Lauffer P., Vallian S., Ciolfi A., Pizzi S., Bauer P., Grüning N.M., Bellacchio E., Del Fattore A., Petrini S., Shaheen R., Tiosano D., Halloun R., Pode-Shakked B., Albayrak H.M., Işık E., Wit J.M., Dittrich M., Freire B.L., Bertola D.R., Jorge A.A.L., Barel O., Sabir A.H., Al Tenaiji A.M.J., Taji S.M., Al-Sannaa N., Al-Abdulwahed H., Digilio M.C., Irving M., Anikster Y., Bhavani G.S.L., Girisha K.M.; Genomics England Research Consortium; Haaf T., Taylor J.C., Dallapiccola B., Alkuraya F.S., Yang R.B., Tartaglia M. SCUBE3 loss-of-function causes a recognizable recessive developmental disorder due to defective bone morphogenetic protein signaling. *American Journal of Human Genetics*. 2021 Jan 7;108(1):115-133. doi: 10.1016/j.ajhg.2020.11.015.

Link M., Chung H., Jolly A., Withers M., Tepe B., Arenkiel B. R., Shah P. S., Krogan N. J., Aydin H., Geckinli B. B., Tos T., Isikay S., Tuysuz B., Mochida G. H., Thomas A. X., Clark R. D., Mirzaa G. M., Lupski J. R., Bellen H. J. Mutations in ANKLE2, a ZIKA Virus Target, Disrupt an Asymmetric Cell Division Pathway in Drosophila Neuroblasts to Cause Microcephaly. *Developmental Cell*. 2019; Volume 51, Issue 6, pages 713-729. doi: 10.1016/j.devcel.2019.10.009.

Lissouba A., Liao M., Kabashi E., Drapeau P. Transcriptomic analysis of zebrafish TDP-43 transgenic lines. *Frontiers in Molecular Neuroscience*, 2018; 11:463. doi: 10.3389/fnmol.2018.00463.

Liu C., Chen Y., Xie Y., Xiang M. Tubulin Post-translational Modifications: Potential Therapeutic Approaches to Heart Failure. *Frontiers in Cell and Developmental Biology*, 2022; 10:872058. doi: 10.3389/fcell.2022.872058.

Liu D.W., M Westerfield M. Clustering of muscle acetylcholine receptors requires motoneurons in live embryos, but not in cell culture. *Journal of Neuroscience*, 1 May 1992, 12 (5) 1859-1866. doi: 10.1523/JNEUROSCI.12-05-01859.1992.

Mackay-Sim A. Hereditary Spastic Paraplegia: From Genes, Cells and Networks to Novel Pathways for Drug Discovery. *Brain Science*, 2021; 11(3):403. doi: 10.3390/brainsci11030403.

Maillard C., Roux C. J., Charbit-Henrion F., Steffann J., Laquerriere A., Quazza F., Bahi Buisson N. Tubulin mutations in human neurodevelopmental disorders. *Seminars in Cell Developmental Biology*, 2023; Volume 127, pages 87-95. doi: 10.1016/j.semcdb.2022.07.009.

Martin N., Jaubert J., Gounon P., Salido E., Haase G., Szatanik M., Guenet J. L. A missense mutation in Tbce causes progressive motor neuronopathy in mice. *Nature Genetics*, 2002; 32,443-447. doi: 10.1038/ng1016.

Martineau É., Di Polo A., Vande Velde C., Robitaille R. Dynamic neuromuscular remodeling precedes motor-unit loss in a mouse model of ALS. *Elife*, 2018; 7:e41973. doi: 10.7554/eLife.41973.

Martinelli S., Krumbach O. K. F., Pantaleoni F., Coppola S., Amin E., Pannone L., Nouri K., Farina L., Dvorsky R., Lepri F., Buchholzer M., Konopatzki R., Walsh L., Payne K., Pierpont M. E., Vergano S. S., Langley K. G., Larsen D., Farwell K. D., Tang S., Mroske C., Gallotta I., Di Schiavi E., della Monica M., Lugli L., Rossi C., Seri M., Cocchi G., Henderson L., Baskin B., Alders M., Mendoza-Londono R., Dupuis L., Nickerson D. A., Chong J. X., The University of Washington Center for Mendelian Genomics, Meeks N., Brown K., Causey T., Cho M. T., Demuth S., Digilio M. C., Gelb B. D., Bamshad M. J., Zenker M., Reza

Ahmadian M., Hennekam R. C, Tartaglia M., Mirzaa G. M. Functional Dysregulation of CDC42 Causes Diverse Developmental Phenotypes. *American Journal of Human Genetics*, 2018, Volume 102, Issue 2, pp 309-320. doi: 10.1016/j.ajhg.2017.12.015.

Marwaha S., Knowles J. W., Ashley E.A. A guide for the diagnosis of rare and undiagnosed disease: beyond the exome. *Genome Medicine*, 2022, 14, 23. doi: 10.1186/s13073-022-01026-w.

Mastrangelo M. Clinical approach to neurodegenerative disorders in childhood: an update overview. *Acta Neurologica Belgica*, 2019, 119:511-521. doi: 10.1007/s13760-019-01160-0.

Matamoros A. J., Baas P. W. Microtubules in health and degenerative disease of the nervous system. *Brain Research Bulletin*, 2016; Volume 126, Part 3, pages 217-225. doi: 10.1016/j.brainresbull.2016.06.016.

Matsubara S., Kawada T., Sakai T., Aoyama M., Osugi T., Shiraishi A., Satake H. The significance of *Ciona intestinalis* as a stem organism in integrative studies of functional evolution of the chordate endocrine, neuroendocrine, and nervous systems. *General and Comparative Endocrinology*. 2016; Volume 227, pages 101-108. doi: 10.1016/j.ygcen.2015.05.010.

McLean D. L., Fetcho, J. R. Spinal Interneurons Differentiate Sequentially from Those Driving the Fastest Swimming Movements in Larval Zebrafish to Those Driving the Slowest Ones. *Journal of Neuroscience*, 2009; 29 (43) 13566-13577. DOI: https://doi.org/10.1523/JNEUROSCI.3277-09.2009.

McWhorter M.L., Monani U.R., Burghes A.H., Beattie C.E. Knockdown of the survival motor neuron (Smn) protein in zebrafish causes defects in motor axon outgrowth and pathfinding. *Journal of Cell Biology*. 2003 Sep 1; 162(5): 919–932. doi: 10.1083/jcb.200303168.

Menelaou E., McLean D. L. A Gradient in Endogenous Rhythmicity and Oscillatory Drive Matches Recruitment Order in an Axial Motor Pool. *Journal of Neuroscience*, 2012; 32 (32) 10925-10939. doi: 10.1523/JNEUROSCI.1809-12.2012.

Menelaou E., Svoboda K. R. Secondary motoneurons in juvenile and adult zebrafish: Axonal pathfinding errors caused by embryonic nicotine exposure. *The* Journal of Comparative Neurology, 2008; Volume 512, Issue 3, pages 305-322. doi: 10.1002/cne.21903.

Miceli M., Exertier C., Cavaglià M., Gugole E., Boccardo M., Casaluci R. R., Ceccarelli N., De Maio A., Vallone B., Deriu M. A. ALS2-Related Motor Neuron Diseases: From Symptoms to Molecules. *Biology*. 2022; 11(1):77. doi: 10.3390/biology11010077.

Michaels T. C. T., Feng S., Liang H., Mahadevan L. Mechanics and kinetics of dynamic instability. *eLife*, 2020; 9:e54077. doi: 10.7554/eLife.54077.

Miller N., Feng Z., Edens B. M., Yang B., Shi H., Sze C. C., Hong B. T., Su S. C., Cantu J. A., Topczewski J., Crawford T. O., Ko C. P., Sumner C. J., Ma L., Ma Y. C. Non-aggregating tau phosphorylation by cyclin-dependent kinase 5 contributes to motor neuron degeneration in spinal muscular atrophy. *The Journal of Neuroscience*, 2015; 35(15):6038-50. doi: 10.1523/JNEUROSCI.3716-14.2015.

Mishra P., Pandey C.M., Singh U., Gupta A., Sahu C., Keshri A. Descriptive statistics and normality tests for statistical data. *Annals of Cardiac Anaesthesia*. 2019 Jan-Mar;22(1):67-72. doi: 10.4103/aca.ACA_157_18.

Mitchison T and Kirschner M. Dynamic instability of microtubule growth. *Nature*, 1984; 312, 237-242. doi: 10.1038/312237a0.

Miyake N., Fukai R., Ohba C., Chihara T., Miura M., Shimizu H., Kakita A., Imagawa E., Shiina M., Ogata K., Okuno-Yuguchi J., Fueki N., Ogiso Y., Suzumura H., Watabe Y., Imataka G., Leong H. Y., Fattal-Valevski A., Kramer U., Miyatake S., Kato M., Okamoto N., Sato Y., Mitsuhashi S., Nishino I., Kaneko N., Nishiyama A., Tamura T., Mizuguchi T., Nakashima M., Tanaka F., Saitsu H., Matsumoto N. Biallelic TBCD mutations cause early-onset neurodegenerative encephalopathy. *American Journal of Human Genetics*. 2016; 99(4):950-961. doi: 10.1016/j.ajhg.2016.08.005.

Morrice J. R., Gregory-Evans C. Y., Shaw C. A. Animal models of amyotrophic lateral sclerosis: A comparison of model validity. *Neural Regeneration Research*, 2018;13(12):2050-2054. doi: 10.4103/1673-5374.241445.

Morton D. J., Jalloh B., Kim L., Kremsky I., Nair R. J., Nguyen K. B., Rounds C., Sterrett M. C., Brown B., Le T., Karkare M.C., McGaughey K. D., Sheng S., Leung S. W., Fasken M. B., Moberg K. H., Corbett A. H. A Drosophila model of Pontocerebellar Hypoplasia reveals a critical role for the RNA exosome in neurons. *PLoS Genetetic*, 2020, 16(7): e1008901. doi: 10.1371/journal.pgen.1008901.

Motta M., Solman M., Bonnard A. A., Kuechler A., Pantaleoni F., Priolo M., Chandramouli B., Coppola S., Pizzi S., Zara E., Ferilli M., Kayserili H., Onesimo R., Leoni C., Brinkmann J., Vial Y., Kamphausen S. B., Thomas-Teinturier C., Guimier A., Cordeddu V., Mazzanti L., Zampino G., Chillemi G., Zenker M., Cavé H., den Hertog J., Tartaglia M. Expanding the molecular spectrum of pathogenic SHOC2 variants underlying Mazzanti syndrome. *Human Molecular Genetics*, Volume 31, Issue 16, 15 August 2022, Pages 2766–2778. doi: 10.1093/hmg/ddac071.

Motta M., Fasano G., Gredy S., Brinkmann J., Bonnard A. A., Simsek-Kiper P. O., Gulec E. Y., Essaddam L., Utine G. E., Guarnetti Prandi I., Venditti M., Pantaleoni F., Radio F. C., Ciolfi A., Petrini S., Consoli F., Vignal C., Hepbasli D., Ullrich M., de Boer E., Vissers L. E. L. M., Gritli S., Rossi C., De Luca A., Ben Becher S., Gelb B. D., Dallapiccola B., Lauri A., Chillemi G., Schuh K., Cavé H., Zenker M., Tartaglia M. SPRED2 loss-of-function causes a recessive Noonan syndrome-like phenotype. *American Journal of Human Genetics*. 2021 Nov 4;108(11):2112-2129. doi: 10.1016/j.ajhg.2021.09.007.

Myers P.Z., Eisen J.S., Westerfield M. Development and Axonal Outgrowth of Identified Motoneurons in the Zebrafish. *Journal of Neuroscience*, August 1986, 6(E): 2278-2269. doi: 10.1523/JNEUROSCI.06-08-02278.1986.

Nashabat M., Al Qahtani X. S., Almakdob S., Altwaijri W., Ba-Armah D. M., Hundallah K., Al Hashem A., Al Tala S., Maddirevula S., Alkuraya F. S., Tabarki B., Alfadhel M. The landscape of early infantile epileptic encephalopathy in a consanguineous population. *Seizure*, 2019, 69, 154–172. doi: 10.1016/j.seizure.2019.04.018.

Nguengang Wakap S., Lambert D. M., Olry A., Rodweel C., Gueydan C., Lanneau V., Murphy D., Le Cam Y., Rath A. Estimating cumulative point

prevalence of rare diseases: analysis of the Orphanet database. *European Journal of Human Genetics*, 2020, 28, 165–173. doi: 10.1038/s41431-019-0508-0.

Nieto-Garai J. A., Olazar-Intxausti J., Anso I., Lorizate M., Terrones O., Contreras F. X. Super-Resolution Microscopy to Study Interorganelle Contact Sites. *International Journal of Molecular Sciences*, 2022;23(23):15354. doi: 10.3390/ijms232315354.

Nithianantham S., Le S., Seto E., Jia W., Leary J., Corbett K. D., Moore J. K., Al-Bassam J. Tubulin cofactors and Arl2 are cage-like chaperones that regulate the soluble αβ-tubulin pool for microtubule dynamics eLife 4:e08811, 2015. doi: 10.7554/eLife.08811.

Nogales E., Wolf S. G., Downing K. H. Structure of the alpha beta tubulin dimer by electron crystallography. *Nature*, 1998; 391:199–203. doi: 10.1038/34465.

Nogales E., Whittaker M., Milligan R. A., Downing K. H. High-Resolution Model of Microtubules. *Cell*, 1999; Volume 96, pages 79-88. doi: 10.1016/s0092-8674(00)80961-7.

Okumura M., Sakuma C., Miura M., Chihara T. Linking cell surface receptors to microtubules: tubulin folding cofactor D mediates Dscam functions during neuronal morphogenesis. *Journal of Neuroscience*, 2015; 4;35(5):1979-90. doi: 10.1523/JNEUROSCI.0973-14.2015.

Omar A., Marwaha K., Bollu P. C. Physiology, Neuromuscular Junction. [Updated 2023 May 1]. In: *StatPearls* [Internet]. Treasure Island (FL): *StatPearls Publishing;* 2023. Available from: https://www.ncbi.nlm.nih.gov/books/NBK470413/.

Ori-McKenney K. M., McKenney R. J., Huang H. H., Li T., Meltzer S., Jan L. Y., Vale R. D., Wiita A. P., Jan Y. N. Phosphorylation of β-Tubulin by the Down Syndrome Kinase, Minibrain/DYRK1a, Regulates Microtubule Dynamics and Dendrite Morphogenesis. *Neuron*, 2016; 90(3):551-63. doi: 10.1016/j.neuron.2016.03.027.

Pang W. and Hu F. Cellular and physiological functions of C9ORF72 and implications for ALS/FTD. *Journal of Neurochemistry*. 2020, Volume 157, Issue 3, pages 334-350. doi: 10.1111/jnc.15255.

Pannese E. Neurocytology: fine structure of neurons, nerve processes, and neuroglial cells. *Springer*, 2015. DOI:10.1007/978-3-319-06856-5.

Panzer J. A., Gibbs S. M., Dosch R. Wagner D., Mullins M. C., Granato M., Gordon R. j. B. Neuromuscular synaptogenesis in wild-type and mutant zebrafish. *Developmental Biology*, 2005; Volume 285, Issue 2, pages 340-357. doi: 10.1016/j.ydbio.2005.06.027.

Passemard S., Perez F., Gressens P., El Ghouzzi V. Endoplasmic reticulum and Golgi stress in microcephaly. *Cell Stress*, 2019;3(12):369-384. doi: 10.15698/cst2019.12.206.

Patton E.E., Zon L.I., Langenau D.M. Zebrafish disease models in drug discovery: from preclinical modelling to clinical trials. *Nature Reviews Drug Discovery*, 2021;20(8):611-628. doi: 10.1038/s41573-021-00210-8.

Parichy D. M. Advancing biology through a deeper understanding of zebrafish ecology and evolution. *Elife*. 2015;4:e05635. doi: 10.7554/eLife.05635.

Peris L., Thery M., Fauré J., Saoudi Y., Lafanecherè L., Chilton J. K., Gordon-Weeks P., Galjart N., Bornens M., Wordman L., Wehland J., Andrieux A., Job D. Tubulin tyrosination is a major factor affecting the recruitment of CAP-Gly proteins at microtubule plus end. *Journal of Cell Biology*, 2006; Volume 174, Number 6, pages 839-849. doi: 10.1083/jcb.200512058.

Perez-Lanzon M., Kroemer G., Maiuri M. C. Chapter Two – Organoids for Modeling Genetic Diseases. *International Review of Cell and Molecular Biology*. 2018, Volume 337, pages 49-81. doi: 10.1016/bs.ircmb.2017.12.006.

Picton L. D., Bertuzzi M., Pallucchi I., Fontanel P., Dahlberg E., Björnfors E. R., Iacoviello F., Shearing P. R., El Manira A. A spinal organ of proprioception for integrated motor action feedback. *Neuron*, 2021;109(7):1188-1201.e7. doi: 10.1016/j.neuron.2021.01.018.

Pinto C.S., Mishima M., Sampath, K. Tools of the trade: studying actin in zebrafish. *Histochemistry and Cell Biology*, 154, 481–493 (2020). doi: 10.1007/s00418-020-01932-3.

Pode-Shakked B., Barash H., Ziv L., Gripp K. W., Flex E., Barel O., Carvalho K. S., Scavina M., Chillemi G., Niceta M., Eyal E., Kol N., Ben-Zeev B., Bar-Yosef O., Marek-Yagel D., Bertini E., Duker A. L., Anikster Y., Tartaglia M., Raas-Rothschild A. Microcephaly, intractable seizures and developmental delay caused by biallelic variants in TBCD: further delineation of a new chaperone-mediated tubulinopathy. *Clinical Genetics*, 2017; 91(5):725-738. doi: 10.1111/cge.12914.

Prokop A. Cytoskeletal organization of axons in vertebrates and invertebrates. *Journal of Cell Biology*, 2020; 219 (7): e201912081. doi: 10.1083/jcb.201912081.

Ragagnin A. M. G., Shadfar S., Vidal M., Jamali M. S., Atkin J. D. Motor Neuron Susceptibility in ALS/FTD. Frontiers in Neuroscience. 2019, 13:532. doi: 10.3389/fnins.2019.00532.

Rao A. N., Patil A., Black M. M., Craig E. M., Myers K. A., Yeung H. T., Baas P. W. Cytoplasmic dynein transports axonal microtubules in a polarity-sorting manner. *Cell Reports*, 2017; 19, 2210–2219. doi: 10.1016/j.celrep.2017.05.064.

Rasika S., Passemard S., Verloes A., Gressens P., El Ghouzzi V. Golgipathies in Neurodevelopment: A New View of Old Defects. *Developmental Neuroscience*, 2019; 40(5-6):39-416. doi: 10.1159/000497035.

Rocha M., Singh N., Ahsan K., Bieriger A., Prince V. E. Neural crest development: insights from the zebrafish. *Developmental Dynamics*, 2019; Volume 249, Issue 1: Part Two, Stem Cells & Tissue Engineering in Development, Disease and Repair Special Issue, pages 88-111. doi: 10.1002/dvdy.122.

Roll-Mecak A. Intrinsically disordered tubulin tails: complex tuners of microtubule functions? *Seminars in Cell & Developmental Biology*. 2015; Volume 37, pages 11-19. DOI: 10.1016/j.semcdb.2014.09.026.

Romaniello R., Arrigoni F., Fry A. E., Bassi M. T., Rees M. I., Borgatti R., Pliz D. T., Cushion T. D. Tubulin genes and malformations of cortical development.

European Journal of Medical Genetics, 2018; Volume 61, Issue 12, pages 744-754. DOI: 10.1016/j.ejmg.2018.07.012.

Roymahapatra G., Sinha C. Birth of 'Nanoscope' and 'Chemistry Nobel-2014'. Conference: 4th International Conference, World Science Congress, 2014 (WSC-2014), 16th - 18th December, 2014. At: Jadvpur University, Kolkata, India. doi:10.13140/2.1.4536.3529.

Ruggeri P., Farina A. R., Cappabianca L., Di Ianni N., Ragone M., Merolle S., Gulino A., Mackay A. R. Neurotrophin and Neurotrophin Receptor Involvement in Human Neuroblastoma [Internet]. *Neuroblastoma*. InTech; 2013. DOI: 10.5772/55536.

Sakakibara A., Ando R., Sapir T., Tanaka T. Microtubule dynamics in neuronal morphogenesis. *Open Biology*, 2013, Volume 3, Issue 7. doi: 10.1098/rsob.130061.

Sandve S. R., Rohlfs R. V., Hvidsten T. R. Subfunctionalization versus neofunctionalization after whole-genome duplication. *Nature Genetics*, 2018; 50, 908–909 (2018). doi: 10.1038/s41588-018-0162-4.

Santos D., Monteiro S.M., Luzio A. General Whole-Mount Immunohistochemistry of Zebrafish (Danio rerio) Embryos and Larvae Protocol. Eds: Félix L. Teratogenicity Testing. *Methods in Molecular Biology*, 2018; Volume l797. Humana Press, New York, NY. doi: 10.1007/978-1-4939-7883-0_19.

Sau D., Rusmini P., Crippa V., Onesto E., Bolzoni E., Ratti A., Poletti A. Dysregulation of axonal transport and motorneuron diseases. *Biology of the Cell*., 2011; 103, 87-107. doi: 10.1042/BC20100093.

Schieppati A., Henter J-I., Daina E., Aperia A. Why rare diseases are an important medical and social issue. *Lancet*, 2008; 371: 2039-2041. doi: 10.1016/S0140-6736(08)60872-7.

Schindelin J., Arganda-Carreras I., Frise E., Kaynig V., Longair M., Pietzsch T., Preibisch S., Rueden C., Saalfeld S., Schmid B., Tinevez J-V., White D.J., Hartenstein V., Eliceiri K., Tomancak P., Cardona A. (2012). Fiji: an open-source platform for biological-image analysis. *Nature Methods* 9, 676–682 (2012). doi: 10.1038/nmeth.2019.

Schmidt R., Strähle U., Scholpp S. Neurogenesis in zebrafish – from embyo to adult. *Neural Development*, 2013; 8, 3. doi: 10.1186/1749-8104-8-3.

Seifert W., Kühnisch J., Maritzen T., Horn D., Haucke V., Hans C.H. Cohen syndrome-associated protein, COH1, is a novel, giant Golgi matrix protein required for Golgi integrity. *Journal of Biological Chemistry*, 2011; 286, 37665–37675. doi: 10.1074/jbc.M111.267971.

Semmler S., Gagné M., Garg P., Pickles S. R., Baudouin C., Hamon-Keromen E., Destroismaisons L., Khalfallah Y., Chaineau M., Caron E., Bayne A. N., Trempe J-F., Cashman N. R., Star A. T., Haqqani A. S., Durcan T. M., Meiering E. M., Robertson J., Grandvaux N., Plotkin S. S., McBride H. M., Vande Velde C. TNF receptor–associated factor 6 interacts with ALS-linked misfolded superoxide dismutase 1 and promotes aggregation. *Molecular Bases of Disease*, 2020, Volume 295, Issue 12, pages 3808-3825. doi: 10.1074/jbc.RA119.011215.

Seredick S. D., Van Ryswyk L., Hutchinson S. A., Eisen J. S. Zebrafish Mnx proteins specify one motorneuron subtype and suppress acquisition of interneuron characteristics. *Neural Development*, 2012; 7, 35. doi: 10.1186/1749-8104-7-35.

Seredick S. D., Hutchinson S. A., Van Ryswyk L., Talbot J. C., Eisen J. S. Lhx3 and Lhx4 suppress Kolmer–Agduhr interneuron characteristics within zebrafish axial motoneurons. *Development*, 2014; 141 (20): 3900–3909. doi: 10.1242/dev.105718.

Serna M., Carranza G. Martin-Benito J., Janowski R., Canals A., Coll M., Zabala J.C, Valpuesta J.M. The structure of the complex between α-tubulin, TBCE and TBCB reveals a tubulin dimer dissociation mechanism. *Journal of Cell Science*, 23 Apr 2015, 128(9):1824-1834. doi: 10.1242/jcs.167387.

Sertori R., Trengove M., Basheer F., Ward A. C., Liongue C. Genome editing in zebrafish: a practical overview. *Briefings in Functional Genomics*, 2016; 15(4):322-30. doi: 10.1093/bfgp/elv051.

Sferra A., Nicita F., Bertini E. Microtubule Dysfunction: A Common Feature of Neurodegenerative Diseases. *International Journal of Molecular Sciences*, 2020; 21(19): 7354. doi: 10.3390/ijms21197354.

Sferra A., Fattori F., Rizza T., Flex E., Bellacchio E., Bruselles A., Petrini S., Cecchetti S., Teson M., Restaldi F., Ciolfi A., Santorelli F.M., Zanni G., Barresi S., Castiglioni C., Tartaglia M., Bertini E. Defective kinesin binding of TUBB2A causes progressive spastic ataxia syndrome resembling sacsinopathy. *Human Molecular Genetics*, 2018, Volume 27, Issue 11, 01 June 018, Pages 1892–1904. doi: 10.1093/hmg/ddy096.

Sferra A, Baillat G, Rizza T, et al. TBCE Mutations Cause Early-Onset Progressive Encephalopathy with Distal Spinal Muscular Atrophy. *American Journal of Human Genetics*. 2016; 99(4):974-983. doi: 10.1016/j.ajhg.2016.08.006.

Shamseldin H. E., Bennett A. H., Alfadhel M., Gupta V., Alkuraya F.S. GOLGA2, encoding a master regulator of Golgi apparatus, is mutated in a patient with a neuromuscular disorder. *Human Genetics*, 2016; 135, 245–251. doi: 10.1007/s00439-015-1632-8.

Shaw P. J. Molecular and cellular pathways of neurodegeneration in motor neurone disease. *Journal of Neurology, Neurosurgery, and Psychiatry*. 2005 Aug;76(8):1046-57. doi: 10.1136/jnnp.2004.048652.

Sheffer I. E and Liao Jianxiang. Deciphering the concepts behind “Epileptic encephalopathy” and “Developmental and epileptic encephalopathy”. *European Journal of Pediatric Neurology*, 2020, Volume 24, pages 11-14. doi: 10.1016/j.ejpn.2019.12.023.

Simon C. M., Van Alstyne M., Lotti F., Bianchetti E., Tisdale S., Watterson D. M., Mentis G. Z., Pellizzoni L. Stasimon Contributes to the Loss of Sensory Synapses and Motor Neuron Death in a Mouse Model of Spinal Muscular Atrophy. *Cell Reports*, 2019;29(12):3885-3901.e5. doi: 10.1016/j.celrep.2019.11.058.

Singh J., Patten S. A. Modeling neuromuscular disease in zebrafish. *Frontiers in Molecular Neuroscience*, 2022; 15:1054573. doi: 10.3389/fnmol.2022.1054573.

Sirajuddin M., Rice L. M., Vale R.D. Regulation of microtubule motors by tubulin isotypes and post-translational modifications. *Nature Cell Biology*, 2014;16(4):335-44. doi: 10.1038/ncb2920.

Sivanesan S., Howell M. D., Didonato C. J., Singh R. N. Antisense oligonucleotide mediated therapy of spinal muscular atrophy. *Translational Neuroscience*. 2013 Mar, 4(1):10.2478/s13380-013-0109-2. doi: 10.2478/s13380-013-0109-2.

Slanzi A., Iannoto G., Rossi B., Zenaro E., Constantin G. In vitro Models of Neurodegenerative Diseases. *Frontiers in Cell and Developmental Biology*. 2020; 8:328. doi: 10.3389/fcell.2020.00328.

Slatko B. E., Gardner A.F., Ausubel F. M. Overview of Next Generation Sequencing Technologies. *Current Protocol in Molecular Biology*. 2018; 122(1): e59. DOI: 10.1002/cpmb.59.

Smith B. N., Ticozzi N., Fallini C., Gkazi A. S., Topp S., Kenna K. P., Scotter E. L., Kost J., Keagle P., Miller J. W., Calini D., Vance C., Danielson E.W., Troakes C., Tiloca C., Al-Sarraj S., Lewis E. A., King A., Colombrita C., Pensato V., Castellotti B., de Belleroche J., Baas F., ten Asbroek A. L., Sapp P. C., McKenna-Yasek D., McLaughlin R. L., Polak M., Asress S., Esteban-Pérez J., Muñoz-Blanco J. L., Simpson M.; SLAGEN Consortium; van Rheenen W., Diekstra F. P., Lauria G., Duga S., Corti S., Cereda C., Corrado L., Sorarù G., Morrison K. E., Williams K. L., Nicholson G. A., Blair I. P., Dion P. A., Leblond C. S., Rouleau G. A., Hardiman O., Veldink J. H., van den Berg L. H., Al-Chalabi A., Pall H., Shaw P. J., Turner M. R., Talbot K., Taroni F., García-Redondo A., Wu Z., Glass J. D., Gellera C., Ratti A., Brown R. H. Jr, Silani V., Shaw C. E., Landers J. E. Exome-wide rare variant analysis identifies TUBA4A mutations associated with familial ALS. *Neuron*, 2014;84(2):324-31. doi: 10.1016/j.neuron.2014.09.027.

Spence R., Gerlach G., Lawrence C., Smith C. The behaviour and ecology of the zebrafish, *Danio rerio*. *Biological Reviews of the Cambridge Philosophical Society,* 2008; 83(1), 13–34. doi: 10.1111/j.1469-185X.2007.00030.x.

Sperry R.W. Chemoaffinity in the orderly growth of nerve fiber patterns and connections. *Proceedings of the National Academy of Science of the United States of America*, 1963; 50, pages 703-710. doi: 10.1073/pnas.50.4.703.

Spoto. G., Valentini G., Saia M. C., Butera A., Amore G., Sapietro V., Nicotera A. G., Di Rosa G. Synaptopathies in Developmental and Epileptic

Encephalopathies: A Focus on Pre-synaptic Dysfunction. *Frontiers in Neurology*, 2022; 8;13:826211. doi: 10.3389/fneur.2022.826211.

Spring A. M., Raimer A. C., Hamilton C. D., Schillinger M. J., Matera A. G. Comprehensive Modeling of Spinal Muscular Atrophy in *Drosophila melanogaster*. *Frontiers in Molecular Neuroscience*, 2019; 12:113. doi: 10.3389/fnmol.2019.00113.

Stainier D. Y. R., Raz E., Lawson N. D., Ekker S. C., Burdine R. D., Eisen J. S., Ingham P. W., Schulte-Merker S., Yelon D., Weinstein B. M., Mullins M. C., Wilson S. W., Ramakrishnan L., Amacher S. L., Neuhauss S. C. F., Meng A., Mochizuki N., Panula P., Moens C. B. Guidelines for morpholino use in zebrafish. *PLoS Genetics*, 2017; 13(10):e1007000. doi: 10.1371/journal.pgen.1007000.

Steinborn K., Maulbetsch C., Priester B., Trautmann S., Pacher T., Geiges B., Kuttner F., Lepiniec L., Stierhof Y. D., Schwarz H. *et al*. The Arabidopsis PILZ group genes encode tubulin-folding cofactor orthologs required for cell division but not cell growth. *Genes&Development*, 2002; 16,959-971. doi: 10.1101/gad.221702.

Stifani N. Motor neurons and the generation of spinal motor neuron diversity. *Frontiers in Cellular Neuroscience*, 2014; 8:293. doi: 10.3389/fncel.2014.00293.

Suter D. M, Forscher P. An emerging link between cytoskeletal dynamics and cell adhesion molecules in growth cone guidance. *Current Opinion in Neurobiology*, 1998; 8(1):106-16. doi: 10.1016/s0959-4388(98)80014-7.

Stoeckli E. T. Understanding axon guidance: are we nearly there yet? *Development*, 2018; 145(10):dev151415. doi: 10.1242/dev.151415.

Tarrade, A., Fassier, C., Courageot, S., Charvin, D., Vitte, J., Peris, L., Thorel A., Mouisel E., Fonknechtne N., Roblot N., Seilhean D., Dierich A., Hauw J. J., Melki J. A mutation of spastin is responsible for swellings and impairment of transport in a region of axon characterized by changes in microtubule composition. *Human Molecular Genetics*, 2006; 15, 3544–3558. doi: 10.1093/hmg/ddl431.

Tartaglia M., Gelb B. D., Zenker M. Noonan syndrome and clinically related disorders. *Best Practise & Research Clinical Endocrinology & Metabolism.* 2011; Volume 25, Issue 1, pages 161-179. doi: 10.1016/j.beem.2010.09.002.

Tay S.H., Ellieyana E.N., Le Y., Sarusie M.V., Grimm C., Ohmer J., Mathuru A.S., Fischer U., Winkler C. A novel zebrafish model for intermediate type spinal muscular atrophy demonstrates importance of Smn for maintenance of mature motor neurons, *Human Molecular Genetics*, Volume 30, Issue 24, 15 December 2021, Pages 2488–2502. doi: 10.1093/hmg/ddab212.

Teoh H. L., Carey K., Sampaio H., Mowat D., Roscioli T., Farrar M. Inherited Paediatric Motor Neuron Disorders: Beyond Spinal Muscular Atrophy. *Neural Plasticity*, 2017; 2017:6509493. doi: 10.1155/2017/6509493.

Tessier-Lavigne M., Goodman C. S. The molecular biology of axon guidance. *Science*, 1996; 274:1123-1133. doi: 10.1126/science.274.5290.1123.

Theisen A., Shaffer L.G. Disorders caused by chromosome abnormalities. *The Application of Clinical Genetics*. 2010; 3:159-174. doi: 10.2147/TACG.S8884. Print 2010.

Thomas A. X., Link N., Robak L. A., Demmler-Harrison G., Pao E. C., Squire A. E., Michels S., Cohen J. S., Comi A., Prontera P., Verrotti di Pianella A., Di Cara G., Garavelli L., Caraffi S. G., Fusco C., Zuntini R., Parks K. C., Sherr E. H., Hashem M. O., Maddirevula S., Alkuraya F. S., Cantractar I. A. F., Neil J. E., Walsh C. A., Bellen H. J., Chao H-T., Clark R. D., Mirzaa G. M. ANKLE2-related microcephaly: A variable microcephaly syndrome resembling Zika infection. *Annals of Clinical and Translational Neurology*. 2022, Volume 9, Issue 8, pages 1276-1288. doi: 10.1002/acn3.51629.

Thomas S., Maynard N., Gill J. DNA library construction using Gibson Assembly®. *Nature Methods* 12, i–ii (2015). https://doi.org/10.1038/nmeth.f.384.

Tian D., Rizwan K., Liu Y., Kang L., Yang Y., Mao X., Shu L. Biallelic pathogenic variants in TBCD-related neurodevelopment disease with mild clinical features. *Neurological Sciences*, 2019; 40(11):2325-2331. doi: 10.1007/s10072-019-03979-0.

Tian G., Bhamidipati A., Cowan N.J., Lewis S. A. Tubulin folding cofactors as GTPase-activating proteins. GTP hydrolysis and the assembly of the alpha/beta-tubulin heterodimer. *Journal of Biological Chemistry*. 1999, 274(34):24054-8. doi: 10.1074/jbc.274.34.24054.

Tran S., Facciol A., Gerlai R. T. Chapter 21 - Behavioral genetics of embryonic ethanol exposure in zebrafish: a model for FASD. *Behavioral and Neural Genetics of Zebrafish*. Academic Press, 2020, pages 343-362, ISBN 9780128175286. DOI:10.1016/b978-0-12-817528-6.00021-8.

Van Schoor E., Strubbe D., Braems E., Weishaupt J., Ludolph A. C., Van Damme P., Thal D. R., Bercier V., Van Den Bosch L. TUBA4A downregulation as observed in ALS post-mortem motor cortex causes ALS-related abnormalities in zebrafish. *Frontiers in Cellular Neuroscience*, 2024; 18:1340240. doi: 10.3389/fncel.2024.1340240.

Varshney G. K, Raman S., Burgess S. Understanding and Editing the Zebrafish Genome. *Advances in Genetics*, 2015; 92:1-52. doi: 10.1016/bs.adgen.2015.09.002.

Vaz R., Hofmeister W., Lindstrand A. Zebrafish Models of Neurodevelopmental Disorders: Limitations and Benefits of Current Tools and Techniques. *International Journal of Molecular Sciences*, 2019;20(6):1296. doi: 10.3390/ijms20061296.

Veldman M. B., Lin S. Zebrafish as a developmental model organism for pediatric research. *Pediatric Research,* 2008; 64(5):470-6. doi: 10.1203/PDR.0b013e318186e609.

Verhey K. J., Gaertig J. The tubulin code. *Cell Cycle,* 2007; 6(17):2152-60. doi: 10.4161/cc.6.17.4633.

Vicidomini G., Bianchini P., Diaspro A., Fioretto D. STED super-resolved microscopy. *Nature Methods*, 2013, 10(4), 331-332. doi: 10.1038/nmeth.4593.

Vinograd-Byk H., Sapir T., Cantarero L., Lazo. P. A., Zeligson S., Lev D., Lerman-Sagie T., Renbaum P., Reiner O., Levy-Lahad E. The spinal muscular atrophy with pontocerebellar hypoplasia gene VRK1 regulates neuronal migration through an amyloid-beta precursor protein-dependent mechanism. *The Journal of Neuroscience*. 2015;35(3):936-942. doi: 10.1523/JNEUROSCI.1998-14.2015.

Walhout R., Verstraete E., van den Heuvel M. P., Veldink J. H., van den Berge L. H. Patterns of symptom development in patients with motor neuron

disease. *Amyotrophic Lateral Sclerosis and Frontotemporal Degeneration*., 2018, Volume 19, Issue 1-2, pages 21-28. doi: 10.1080/21678421.2017.1386688.

Walton R. T., Christie K. A., Whittaker M. N., Kleinstiver B. P. Unconstrained genome targeting with near-PAMless engineered CRISPR-Cas9 variants. *Science*, 2020;368(6488):290-296. doi: 10.1126/science.aba8853.

Watchon M., Yuan K. C., Mackovski N., Svahn A. J., Cole N. J., Goldsbury C., Rinkwitz S., Becker T. S., Nicholson G. A., Laird A. S. Calpain Inhibition Is Protective in Machado-Joseph Disease Zebrafish Due to Induction of Autophagy. *The Journal of Neuroscience,* 2017;37(32):7782-7794. doi: 10.1523/JNEUROSCI.1142-17.2017.

Weber T., Köster R. Genetic tools for multicolor imaging in zebrafish larvae. *Methods,* 2013;62(3):279-91. doi: 10.1016/j.ymeth.2013.07.028.

Wen H. L., Lin Y. T., Ting C. H., Lin-Chao S., Li H., Hsieh-Li H. M. Stathmin, a microtubule-destabilizing protein, is dysregulated in spinal muscular atrophy. *Human Molecular Genetics*, 2010; 19(9):1766-78. doi: 10.1093/hmg/ddq058.

Werner T. Next generation sequencing in functional genomics. *Briefings in Bioinformatics*, Volume 11, Issue 5, September 2010, Pages 499–511. doi: 10.1093/bib/bbq018.

Westerfield M. (2000). The Zebrafish Book. A Guide for the Laboratoraty Use of Zebrafish (*Danio rerio*). *4th edition, University of Oregon Press, Eugene*.

Wishart T. M., Parson S. H., Gillingwater T. H. Synaptic vulnerability in neurodegenerative disease. *Journal of Neuropathology and Experimental Neurology,* 2006;65(8):733-9. doi: 10.1097/01.jnen.0000228202.35163.c4.

Wood J. D., Landers J. A., Bingley M., McDermott C. J., Thomas-McArthur V., Gleadall L. J., Shaw P. J. Cunliffe V. T. The microtubule-severing protein Spastin is essential for axon outgrowth in the zebrafish embryo. *Human Molecular Genetics*, 2006; Vol. 15, No. 18 2763–2771. doi: 10.1093/hmg/ddl212.

Xu Y., Li Z. CRISPR-Cas systems: Overview, innovations and applications in human disease research and gene therapy. *Computational and Structural Biotechnology Journal*, 2020;18:2401-2415. doi: 10.1016/j.csbj.2020.08.031.

Yamamoto S., Jaiswal M., Charng W-L, Gambin T., Karaca E., Mirzaa G., Wiszniewski W., Sandoval H., Haelterman N. A., Xiong B., Zhang K., Bayat V., David G., Li T., Chen K., Gala U., Harel T., Pehlivan D., Penney S., Vissers L. E. L. M., de Ligt J., Jhangiani S. N., Xie Y., Tsang S. H., Parman Y., Sivaci M., Battaloglu E., Munzy D., Wan Y-W., Liu Z., Lin-Moore A. T., Clark R. D., Curry C. J., Link N., Schulze K. L., Boerwinkle E., Dobyns W. B., Allikmets R., Gibbs R. A., Chen R., Lupski J. R., Wangler M. F., Bellen H. J. Drosophila genetic resource of mutants to study mechanisms underlying human genetic diseases. *Cell*, 2014; 159: 200-214. doi: 10.1016/j.cell.2014.09.002.

Yaron A., Schuldiner O. Common and Divergent Mechanisms in Developmental Neuronal Remodeling and Dying Back Neurodegeneration. *Current Biology*, 2016; Volume 26, Issue 13, pages 628-639. doi: 10.1016/j.cub.2016.05.025.

Ye X., Qiu Y., Gao Y., Wan D., Zhu H. A Subtle Network Mediating Axon Guidance: Intrinsic Dynamic Structure of Growth Cone, Attractive and Repulsive Molecular Cues, and the Intermediate Role of Signaling Pathways. *Neuronal Plasticity*., 2019; 2019:1719829. doi: 10.1155/2019/1719829.

Yu I., Garnham C.P., Roll-Mecak A. Writing and Reading the Tubulin Code. *The Journal of biological chemistry*, 2015;290(28):17163-72. doi: 10.1074/jbc.R115.637447.

Yu W., Cook C., Sauter C., Kuriyama R., Kaplan P. L., Baas, P. W. Depletion of a microtubule-associated motor protein induces the loss of dendritic identity. *Journal of Neuroscience*, 2000; 20, 5782–5791. doi: 10.1523/JNEUROSCI.20-15-05782.2000.

Zenker M., Edouard T., Blair J. C., Cappa M. Noonan syndrome: improving recognition and diagnosis. *Archives of Disease in Childhood*. 2022;107(12):1073-1078. doi: 10.1136/archdischild-2021-322858.

Zhang Y., Zhang L., Zhou S. Developmental Regression and Epilepsy of Infancy with Migrating Focal Seizures Caused by TBCD Mutation: A Case Report and Review of the Literature. *Neuropediatrics,* 202; 51(1):68-71. doi: 10.1055/s-0039-1698423.